ADVANCES IN RESOURCE ALLOCATION OPTIMIZATION FOR MULTIUSER WIRELESS SYSTEMS WITH JOINT ENERGY AND INFORMATION TRANSFER

LIU LIANG

NATIONAL UNIVERSITY OF SINGAPORE

2014

ADVANCES IN RESOURCE ALLOCATION OPTIMIZATION FOR MULTIUSER WIRELESS SYSTEMS WITH JOINT ENERGY AND INFORMATION TRANSFER

LIU LIANG

(*B. Eng. Tianjin University*)

A THESIS SUBMITTED
FOR THE DEGREE OF DOCTOR OF PHILOSOPHY
DEPARTMENT OF ELECTRICAL AND COMPUTER ENGINEERING
NATIONAL UNIVERSITY OF SINGAPORE

2014

Declaration

I hereby declare that this thesis is my original work and it has been written by me in its entirety.

I have duly acknowledged all the sources of information which have been used in the thesis.

This thesis has also not been submitted for any degree in any university previously.

_____

Liu Liang

31 July 2014

Acknowledgements

First of all, I want to express my sincere gratitude and appreciation to my main supervisor Dr. Rui Zhang for his great support and guidance throughout the past four years. I have benefitted tremendously from his unique blend of solid knowledge on optimization and MIMO, constructive criticism, boundless energy, broad vision, practical sensitivity, and devotion to his students. Without his continual advice and encouragement, this thesis would certainly not be possible. He has been and will be the role model for me in both my future career and my personal lives.

I am also very grateful to my co-supervisor Prof. Kee-Chaing Chua. He has always been a wonderful reference and supporter for my research. I deeply appreciate his valuable advice on my research and future career.

I thank all the current and past group members, including Jie Xu, Hyungsik Ju, Yong Zeng, Suzhi Bi, Shixin Luo, Xun Zhou, Mohammad Reza, Katayoun Rahbar, Yinghao Guo, Seunghyun Lee, Shuowen Zhang, Reuben Stephen, Chuan Huang, Nguyen Duy Hieu, Yueling Che, and Hong Xing, with whom I have had the good fortune to work. Our research group is like a big family. I will miss the fun and intellectually stimulating environment in the weekly group meeting with them and Dr. Rui Zhang. I also thank my colleagues in the communication lab, including Yu Wang, Tong Wu, Yi Yu, Gaofeng Wu, Chenlong Jia, Tianyu Song, Qian Wang, Mingwei Wu, and many others, for making the years so enjoyable.

At last, but at most, I wish to express my heartfelt thankfulness to my parents, Xiujun Liu and Yulan Liu, for their unselfish love. They are always there to support me throughout years, no matter what.

Table of Contents

Summary

As radio signals carry information as well as energy at the same time, a new wireless system with simultaneous wireless information and power transfer (a.k.a. SWIPT) has drawn significant attention recently. This thesis is devoted to investigating various interference management strategies and their corresponding resource allocation optimizations in the SWIPT system with multiple users.

This thesis starts with addressing a special case of the SWIPT system with only information transmissions of the users. We thus consider a multi-user Gaussian interference channel (GIC) model where multiple mutually interfering wireless links communicate simultaneously over a shared band. A pragmatic approach to characterize the fundamental limits of GIC is by maximizing the weighted sum-rate (WSR) of the users achievable with the mutual interference treated as additional Gaussian noise at the receivers. However, due to the coupled interference among users, such a problem is in general non-convex and how to find its globally optimal solution has been open for decades. By utilizing the technique of "monotonic optimization" together with a novel idea called "rate profile", in the first part of this thesis we propose a new optimization framework to achieve the global optimality of the non-convex WSR maximization problem for various types of GICs with multi-antenna transmitters and/or receivers, which provides a valuable performance upper bound for other heuristic algorithms in the literature.

Then, we study the wireless system for SWIPT. We start by considering the basic setup of a point-to-point wireless link over the flat-fading channel subject to time-varying co-channel interference. Different from the case of conventional wireless communication system in which interference is an undesired phenomenon,

interference is beneficial from the perspective of wireless power transfer since it is an additional energy source. To exploit this new role of interference, we propose a novel opportunistic energy harvesting scheme where the receiver switches between information decoding and energy harvesting over time based on the instantaneous power of the direct-link channel as well as that of the interfering channel. By applying convex optimization techniques, we derive the optimal receiver mode switching rule to achieve various information/power transfer trade-offs. Moreover, for the case that the channel state information is known at the transmitter, joint optimization of transmitter power control and receiver mode switching is solved.

Lastly, we study a multi-user SWIPT system consisting of one multi-antenna transmitter, one single-antenna information receiver (IR), and multiple single-antenna energy receivers (ERs). The SWIPT system is concerned with a potential security issue since the ERs are in general deployed in more proximity to the transmitter than the IR for effective energy reception and as a result could easily eavesdrop the information sent to the IR. To achieve desired wireless power transfer to the ERs and yet prevent them from overhearing the information for the IR, we propose a new transmission scheme where a certain fraction of the transmit power is allocated to send artificially generated interference signal called artificial noise (AN). AN serves as energy signal for achieving wireless power transfer to the ERs, and at the same time reduces the capability of the ERs to decode the information for the IR. Under this scheme, we propose efficient algorithms to obtain the optimal and suboptimal transmit power control and beamforming solutions to balance between the achievable secrecy rate of the IR and the harvested energy of the ERs.

List of Tables

List of Figures

List of Abbreviations

ADC	Analog-to-Digital Converter
ADP	Asynchronous Distributed Pricing
AP	Access Point
APC	Average Power Constraint
AWGN	Additive White Gaussian Noise
BC	Broadcast Channel
CSI	Channel State Information
CSIT	Channel State Information at the Transmitter
DC	Difference of Convex Functions
DOF	Degree of Freedom
DSL	Digital Subscriber Line
EH	Energy Harvesting
ER	Energy Receiver
EVD	Eigenvalue Decomposition
FDMA	Frequency-Division-Multiple-Access
GIC	Gaussian Interference Channel
GP	Geometric Programming
IA	Interference Alignment
ICI	Inter-Cell Interference
ID	Information Decoding
i.i.d.	Independent and Identically Distributed
IR	Information Receiver
KKT	Karush-Kuhn-Tucker

LPF	Low Pass Filter
MAC	Multiple-Access Channel
MIMO	Multiple-Input Multiple-Output
MIMO-IC	Multiple-Input Multiple-Output Gaussian Interference Channel
MISO	Multiple-Input Single-Output
MISO-IC	Multiple-Input Single-Output Gaussian Interference Channel
MMSE	Minimum-Mean-Square-Error
MRC	Maximum Ratio Combining
MRT	Maximum Ratio Transmission
O-E	Outage-Rate
OFDMA	Orthogonal-Frequency-Division-Multiple-Access
PDF	Probability Density Function
PPC	Peak Power Constraint
PS	Power Splitting
QCQP	Quadratically Constrained Quadratic Program
R-E	Rate-Energy
RF	Radio Frequency
RV	Random Variable
Rx	Receiver
SCALE	Successive Convex Approximation for Low complExity
SDP	Semidefinite Program
SDR	Semidefinite Relaxation
SIMO	Single-Input Multiple-Output
SIMO-IC	Single-Input Multiple-Output Gaussian Interference Channel
SINR	Signal-to-Interference-Plus-Noise Ratio
SISO	Single-Input Single-Output
SISO-IC	Single-Input Single-Output Gaussian Interference Channel
SNR	Signal-to-Noise Ratio
SOCP	Second-Order Cone Program

SP	Signomial Programming
SVD	Singular Value Decomposition
SWIPT	Simultaneous Wireless Information and Power Transfer
TDMA	Time-Division-Multiple-Access
TS	Time Switching
Tx	Transmitter
WIT	Wireless Information Transmission
W/O	Without
WPCN	Wireless Powered Communication Network
WPT	Wireless Power Transfer
WSR	Weighted Sum-Rate
ZF	Zero-Forcing

List of Symbols

Throughout this thesis, scalars are denoted by lower-case letters, vectors denoted by bold-face lower-case letters, and matrices denoted by bold-face upper-case letters. Also, we define the following symbols:

$\boldsymbol{I}$	an Identity Matrix with Appropriate Dimension
$\mathbf{0}$	an All-Zero Matrix with Appropriate Dimension
$\boldsymbol{S}^{-1}$	the Inverse of the Square Full-Rank Matrix $\boldsymbol{S}$
$\mathrm{Tr}(\boldsymbol{S})$	the Trace of the Square Matrix $\boldsymbol{S}$
$\boldsymbol{S} \succeq \mathbf{0}$	$\boldsymbol{S}$ is Positive Semi-Definite
$\boldsymbol{S} \preceq \mathbf{0}$	$\boldsymbol{S}$ is Negative Semi-Definite
$\boldsymbol{S} \succ \mathbf{0}$	$\boldsymbol{S}$ is Positive Definite
$\boldsymbol{S} \prec \mathbf{0}$	$\boldsymbol{S}$ is Negative Definite
$\boldsymbol{M}^H$	the Conjugate Transpose of $\boldsymbol{M}$
$\boldsymbol{M}^T$	the Transpose of $\boldsymbol{M}$
$\rho(\boldsymbol{M})$	the Spectral Radius of $\boldsymbol{M}$
$\mathrm{rank}(\boldsymbol{M})$	the Rank of $\boldsymbol{M}$
$\mathrm{Diag}(\boldsymbol{X}_1, \cdots, \boldsymbol{X}_K)$	a Block Diagonal Matrix with the Diagonal Matrices Given by $\boldsymbol{X}_1, \cdots, \boldsymbol{X}_K$
$\mathcal{CN}(\boldsymbol{x}, \boldsymbol{\Sigma})$	the Distribution of a CSCG Random Vector with Mean Vector $\boldsymbol{x}$ and Covariance Matrix $\boldsymbol{\Sigma}$
$\sim$	"Distributed As"
$\mathbb{C}^{x \times y}$	the Space of $x \times y$ Complex Matrices
$\mathbb{R}$	the Real Number Space
$\mathbb{R}^x$	the $x \times 1$ Real Vector Space

$\mathbb{R}_+^x$	the Non-Negative Orthants of the $x \times 1$ Real Vector Space
$\|\boldsymbol{x}\|$	the Euclidean Norm of a Complex Vector $\boldsymbol{x}$
$\boldsymbol{e}_k$	a Vector with its kth Component Being 1, and all Other Components Being 0
$\boldsymbol{x} \geq \boldsymbol{y}$	$\boldsymbol{x}$ is Greater than or Equal to $\boldsymbol{y}$ in a Component-Wise Manner
$A \backslash B$	the Set $\{x \| x \in A \text{ and } x \notin B\}$
$\|A\|$	the Cardinality of the Set A
$[x]_a^b$	$\max(\min(x, b), a)$

Chapter 1

Introduction

In wireless communication systems, radio frequency (RF) signals are used as a carrier to convey information over the air. Recently, an interesting new application of RF signals arises for achieving wireless power transfer (WPT) thanks to the advent of more efficient hardware circuits for RF energy harvesting. Many promising applications of RF-based WPT can be envisaged, especially for powering a large number of communication nodes (e.g., sensors) freely located in wide areas. Compared with traditional battery-powered wireless communication system in which the operation is often interrupted due to the need of manually replacing/recharging the batteries, RF-based WPT provides a more cost-effective solution to provide truly perpetual energy supply to the communication nodes. As a result, RF-based WPT is envisioned as a key enabling technique for the next generation energy-constrained wireless networks. For the historic development and applications of WPT via leveraging RF signals or other means, please refer to [1].

Since RF signals carry information as well as energy at the same time, a unified study of RF-based simultaneous wireless information and power transfer (SWIPT) has recently drawn significant attention, which is not only theoretically intricate but also practically appealing for simultaneously enabling both the wireless data and wireless energy access to the users with the same transmitted signals. This thesis is devoted to investigating the optimal resource (such as power, time, bandwidth, and antenna beam) allocation schemes in multi-user SWIPT systems to achieve desired performance trade-offs in wireless power versus information transmission.

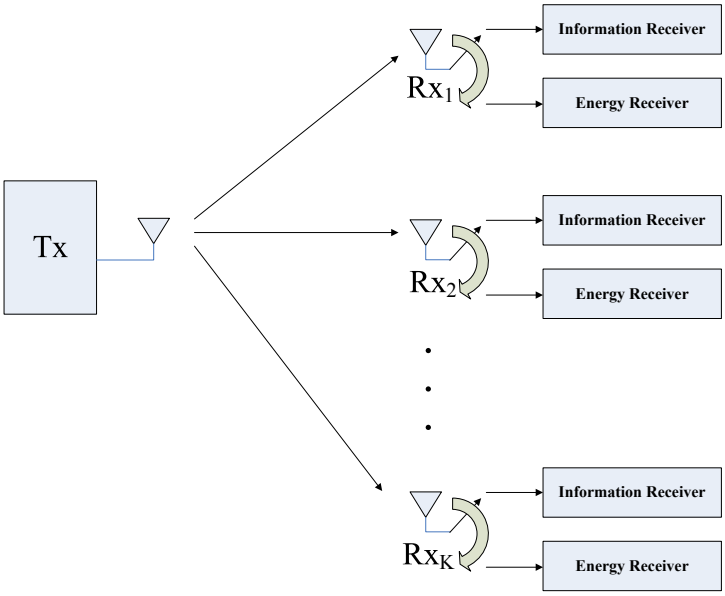

Figure 1.1: A BC-based SWIPT system.

1.1 Multi-User SWIPT System

In a typical multi-user SWIPT system, one or more transmitters (Txs) each equipped with a stable power supply coordinate wireless information and energy transmissions to a set of distributed receivers (Rxs) that need to replenish energy from the received signals. In such systems, there is generally a practical circuit limitation that each Rx cannot decode the information and harvest the energy from the same received signal independently. In the pioneer work [2], a practical "time switching (TS)" Rx is proposed to implement SWIPT using off-the-shelf circuits that are designed for information decoding (ID) and RF energy harvesting (EH), respectively. Specifically, the Rx is connected to either the ID circuit or the EH circuit at any time such that it can switch between the two operation modes of ID and EH from one time to another.

In Fig. 1.1, a point-to-multipoint SWIPT system with TS Rxs is depicted, where one Tx broadcasts multiple data streams to different Rxs simultaneously, and each Rx decides to either decode information or harvest energy from its received

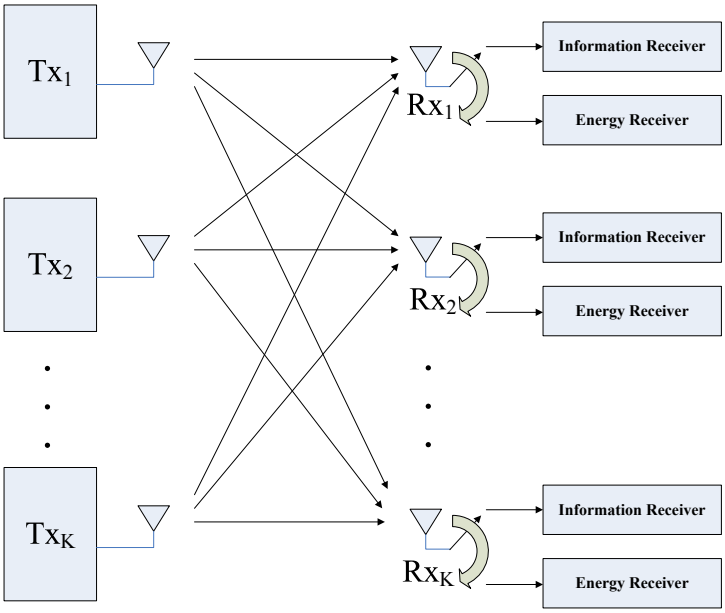

Figure 1.2: A GIC-based SWIPT system.

signal. If a Rx connects to the information receiver (IR), it decodes its desired message in the received signal subject to possible inter-user interference. On the other hand, if the Rx connects to the energy receiver (ER), it harvests energy from both of its intended signal as well as the interference. Accordingly, the point-to-multipoint SWIPT system shown in Fig. 1.1 can be viewed as an extension of the conventional broadcast channel (BC) in wireless communication with the Tx for SWIPT sending both the information and energy to the Rxs in general.

In Fig. 1.2, a multipoint-to-multipoint SWIPT system with TS Rxs is depicted, where distributed Txs send independent messages to their respective Rxs over the same frequency band at the same time. Different from the point-to-multipoint SWIPT system shown in Fig. 1.1, each Tx in this setup has its intended message to send to only one Rx in wireless information transmission (WIT). However, for WPT, each Rx can harvest energy from the signals from its desired Tx as well as all other interfering Txs. As a result, the multipoint-to-multipoint SWIPT system shown in Fig. 1.2 can be viewed as a generalization of the traditional Gaussian interference channel (GIC) in wireless communication with joint information and

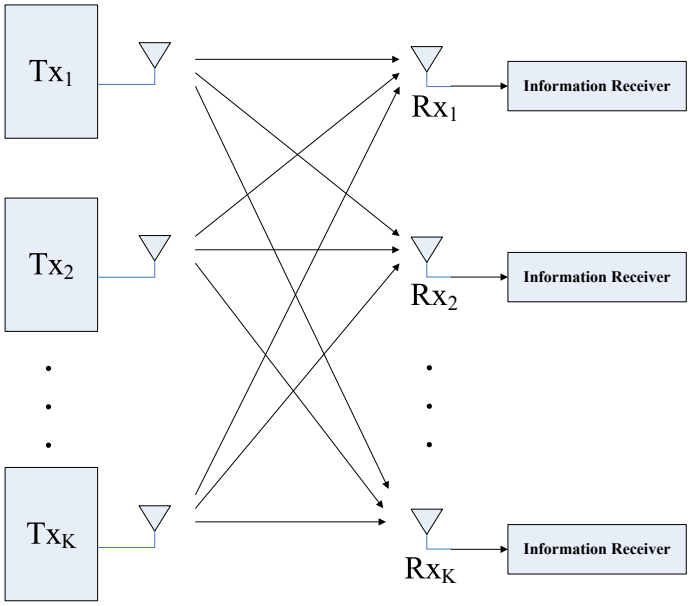

Figure 1.3: Multi-user interference channel.

energy transfer.

1.2 Motivation

In this section, we present three key challenges each in one special application based on the general multi-user SWIPT system models in Figs. 1.1 or 1.2, namely "interference mitigation in GIC", "joint information and energy scheduling in point-to-point SWIPT", and "security issue in multi-user SWIPT".

1.2.1 Interference Mitigation in GIC

We start with addressing the multi-user SWIPT system with WIT only, where the Rxs only intend to decode their desired information from received signals. Under this setup, Fig. 1.2 reduces to the classic multi-user GIC, as depicted in Fig. 1.3. A general GIC is composed of multiple pairs of Txs and Rxs, where each Tx has its intended messages to send to one Rx and each Rx receives the desired signal from its Tx as well as interfering signals from the other Txs at the same time.

One important application of the GIC is the multi-cell cellular network. Traditionally, most of the studies on cellular networks focused on the single-cell setup, while the inter-cell interference (ICI) experienced by a Rx in one cell caused by the Txs in other cells is minimized by means of frequency reuse, which avoids the same frequency band from being used by adjacent cells. However, future wireless systems advocate to reduce the cell size by increasing the frequency reuse factor and even allowing it to be one or so-called "universal frequency reuse", due to which the issue of ICI becomes more crucial. Consequently, joint resource allocation and user scheduling across neighboring cells becomes a practically appealing approach for mitigating the ICI. If the users in each cell are separated for transmission in frequency via orthogonal frequency-division multiple-access (OFDMA) or in time via time-division multiple-access (TDMA), then the scheduled links in different cells transmitting at the same frequency tone or in the same time slot will interfere with each other, which is modeled by a GIC.

In GIC, the key issue is how to mitigate the effect of interference on system throughput by proper resource allocation schemes. In the literature, the weighted sum-rate (WSR) maximization problem in GIC with interference treated as additional Gaussian noise has been investigated for decades. However, due to the mutual interference among users, this problem is non-convex and thus how to efficiently achieve its global optimality still remains open in general.

1.2.2 Joint Information and Energy Scheduling in Point-to-Point SWIPT

Consider the multi-user SWIPT system in Fig. 1.2 where the users design their transmissions independently for the ease of implementation. Then, only one pair of Tx and Rx needs to be considered, where the other Txs' signals can be treated as an aggregate interference. As a result, Fig. 1.2 reduces to a point-to-point wireless link subject to a co-channel interference, as shown in Fig. 1.4. In a fading environment, there exists a non-trivial trade-off for the information and energy scheduling over

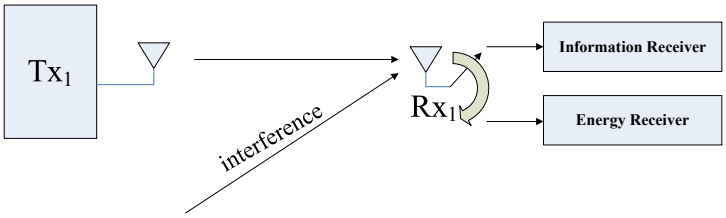

Figure 1.4: Point-to-point SWIPT with co-channel interference.

different fading states of the channel, since both WIT and WPT can improve their respective performance if more fading states are allocated. To balance between the performances of WIT and WPT, it is important to investigate the optimal mode switching rule at the Rx, i.e., how should the Rx decide to operate in an ID or EH mode based on the instantaneous power of the direct-link channel as well as that of the aggregate interference. Moreover, in the case with the channel state information (CSI) known at the Tx (CSIT), we can further improve the WIT and WPT performance trade-off by jointly optimizing the power control at Tx and the mode switching at Rx.

1.2.3 Security Issue in Multi-User SWIPT

Consider the multiuser SWIPT system in Fig. 1.1 with separated IRs and ERs, i.e., each Rx only decodes information or harvests energy from its received signal based on its own application. Then, Fig. 1.1 reduces to a BC with multiple IRs and ERs, as shown in Fig. 1.5. Note that in general practical IRs and ERs operate with very different power requirements or sensitivity, e.g., -60dBm for the IR versus -10dBm for the ER. To meet this practical requirement, ERs are generally deployed in closer proximity to the Tx than IRs for receiving higher power. However, the above "near-far" based energy and information transmission scheme gives rise to a more challenging information security issue since ERs, which are closer to the Tx and thus have better channels than IRs, can more easily eavesdrop the information for IRs. Therefore, in addition to achieving efficient WPT to ERs, a secure information

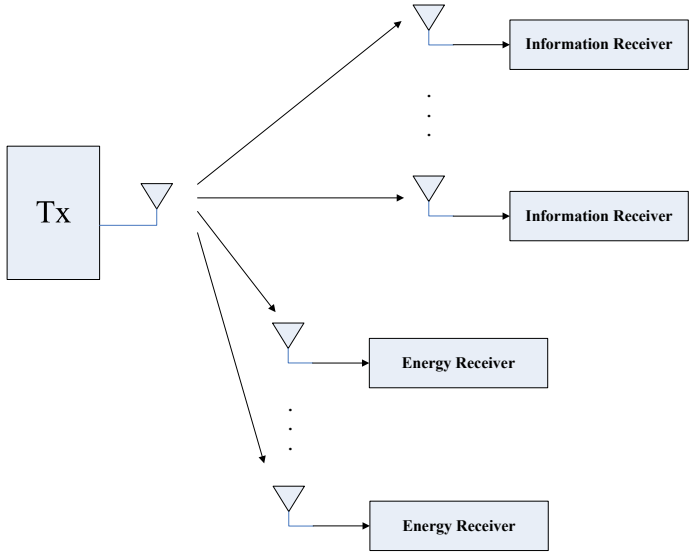

Figure 1.5: A multi-user SWIPT system with separate IRs and ERs.

transmission to IRs should be ensured by a proper design of resource allocation at the Tx.

1.3 Objective and Organization of the Thesis

Motivated by the above discussions, in this thesis we focus our study on solving three important resource allocation problems in wireless communication system or SWIPT system: WSR maximization in GIC, joint wireless information and energy scheduling in point-to-point fading channel subject to co-channel interference, and physical-layer security in multi-user SWIPT system. The thesis is organized as follows.

Chapter 1 presents the motivation, objective, and major contributions of the thesis.

Chapter 2 studies the WSR maximization problem in the single-input single-output (SISO) GIC, termed as SISO-IC, single-input multiple-output (SIMO) GIC, termed as SIMO-IC, and multiple-input single-output (MISO) GIC, termed as MISO-IC. A novel optimization approach is proposed and developed to achieve the

globally optimal solutions under the above GIC setups.

Chapter 3 introduces the TS scheme for a point-to-point single-antenna flat fading channel subject to time-varying co-channel interference and investigates how the Rx should switch between ID and EH based on the powers of the direct channel and the interference to balance between minimizing the outage probability or maximizing the ergodic capacity for WIT versus maximizing the average harvested energy for WPT. In the case with CSIT, power control at the Tx is jointly optimized. The extension of TS scheme to the SIMO SWIPT system is also discussed.

Chapter 4 studies the physical-layer security problem in a MISO SWIPT system consisting of one multi-antenna Tx, one single-antenna IR, and multiple single-antenna ERs. To prevent ERs from eavesdropping the information sent to the IR, two secrecy beamforming design problems are considered. In the first problem, the secrecy rate of the IR is maximized subject to individual harvested energy constraints of ERs, while in the second problem, the weighted sum-energy transferred to ERs is maximized subject to a secrecy rate constraint for the IR. Both optimal and suboptimal algorithms are proposed to solve these two problems.

Lastly, Chapter 5 concludes this thesis and discusses about future work.

1.4 Major Contributions of the Thesis

The major contributions of this thesis are summarized as follows.

1.4.1 Three New Approaches to Interference Management

Interference management is a long-standing research problem in multi-user wireless communications and has been investigated for decades. The first contribution of this thesis is to provide answers to the following fundamental questions: in the new wireless system with joint WIT and WPT, what is the role that interference plays compared with that in conventional wireless systems with WIT only, and how should we deal with or even utilize interference?

1. Interference Coordination for WIT

In Chapter 2, we study the optimal interference management strategy in conventional GIC with WIT only, as shown in Fig. 1.3. In this scenario, interference is undesired since it limits the system throughput. To fully mitigate the effect of interference on the achievable WSR in GIC, sophisticated multi-user encoding and decoding techniques are in general required, which are difficult to implement in practice. In Chapter 2, we consider a practical interference coordination approach to tackle the interference, where the interference is treated as additional Gaussian noise at each Rx, and the Txs optimally allocate their resources, e.g., transmit power and/or antenna beams, to minimize the system performance loss due to the interference.

2. Interference as Energy Source for WPT

In Chapter 3, we investigate a new role of interference in SWIPT system over a point-to-point fading channel with time-varying co-channel interference, as shown in Fig. 1.4. In this scenario, interference is harmful for WIT but is beneficial for WPT since the Rx can harvest energy from interference if it operates in an EH mode. This implies that for designing a wireless system with joint WIT and WPT, we should take a fundamental paradigm shift from mitigating the interference as in conventional WIT to opportunistically utilizing it for WPT. In Chapter 3, we investigate this new design principle by deriving the optimal policy for the Rx to switch between ID and EH based on the channel and interference conditions.

3. Interference as Both Energy Source and Artificial Noise in Secure SWIPT

In a SWIPT system with secure information transmission as shown in Fig. 1.5, there are two conflicting goals for the design of the transmit signal. On the one hand, to minimize the information leakage to ERs, the power of the received signal at each ER should be kept as small as possible. On the other hand, to maximize

the harvested energy at ERs, the power of the received signal at each ER is desired to be as large as possible. In Chapter 4, we propose a novel idea to fulfil these two conflicting goals at the same time. Specifically, besides the information signal intended to the IR, we split a certain fraction of the transmit power to generate interference signal known as artificial noise (AN) [3]. From the perspective of secrecy information transmission, the AN signal reduces the information rate that can be decoded by ERs, while from the perspective of WPT, it also delivers energy to ERs. With the above novel design, the challenging security issue in SWIPT systems can be efficiently solved from a physical-layer approach.

1.4.2 Optimal Resource Allocation Schemes

It is worth noting that due to the existence of interference, the above three interference management schemes in general result in non-convex resource allocation optimization problems, which are difficult to be solved by conventional convex optimization techniques. The second contribution of this thesis is to present the globally optimal solutions to these non-convex problems by exploiting their specific structures, where the solutions also provide key insights to the design of SWIPT systems in practice.

1. New Algorithms for Solving WSR Maximization in GIC

In Chapter 2, based on an optimization technique called monotonic optimization [4], we propose new algorithms to optimally solve the WSR maximization problems in SISO-IC, SIMO-IC and MISO-IC, respectively. It is worth noting that our proposed algorithms are the first in the literature which globally optimally solve the problems of WSR maximization in SIMO-IC and MISO-IC, while a similar algorithm is reported in [5] for the special case of SISO-IC. One important application of our proposed algorithms is to provide an exact performance upper bound for many heuristic algorithms reported in the literature which may have faster computation time but in general only guarantee a local optimality. This is especially important

in the case of MISO-IC where the globally optimal solution by exhaustive search is hardly feasible when the number of antennas at each Tx becomes large.

2. Key Insights from Joint Information and Energy Scheduling Optimization

In Chapter 3, based on an optimization technique named dual decomposition [6], we solve the optimal EH/ID mode switching rule at the Rx to achieve various performance trade-offs between WIT and WPT in the case without CSIT, and the optimal transmit power control, information and energy transfer scheduling, jointly with the Rx's mode switching in the case with CSIT. Some insightful results are obtained. For example, when the interference is strong but the direct channel is weak, the Rx should switch to EH instead of ID mode to harvest more energy from the strong interference. More interestingly, we show that when the direct channel is sufficiently stronger than the interference, i.e., the case with high signal-to-interference-plus-noise ratio (SINR), the optimal operation mode for the Rx is still EH rather than ID, which is due to the fact that EH gains more than ID with increasing SINR, as the harvested energy scales linearly with the increased total power of signal and interference while the information rate scales only logarithmically with the increased SINR.

3. Fundamental Design Principle for Secure SWIPT

In Chapter 4, we formulate the optimization problems for designing transmit power control and beamforming with AN-based energy signal as non-convex quadratically constrained quadratic programs (QCQPs), and apply the celebrated semidefinite relaxation (SDR) optimization technique [7] to obtain the optimal solutions. We show that with the proposed scheme where the transmit signal is the superposition of information and energy/AN signals, secrecy information transmission can be effectively achieved without compromising the energy transmission performance notably.

Chapter 2

WSR Maximization in GIC

2.1 Introduction

GIC is a fundamental model that characterizes many real-life interference-limited communication systems, e.g., multi-cell cellular networks and bundled digital subscriber lines (DSLs) communication. As a result, characterizing the global maximum of WSR for the K-user GIC, with the interference treated as additional Gaussian noise at Rxs, is a key problem that is however not yet completely solved. Due to the users' coupled transmission with interference, the resulted WSR maximization problem is in general non-convex and thus cannot be solved directly by conventional convex optimization techniques. In this chapter, we present a new optimization framework to obtain the globally optimal power control and/or beamforming solutions to WSR maximization problems for the SISO-IC, SIMO-IC and MISO-IC, respectively. This novel framework is based on two essential techniques: *monotonic optimization* and *rate profile*. The proposed optimal algorithms can provide performance upper bounds for other existing heuristic algorithms in the literature.

2.2 Literature Review

2.2.1 Information-Theoretic Study on GIC

The information-theoretic study on GIC has a long history, but the capacity region of the GIC, which is defined as the set of rate-tuples for all Tx-Rx pairs that can be simultaneously achieved, still remains unknown in general, even for the simplest two-user case. The best achievable rate region for the two-user GIC to date is established by Han and Kobayashi in [8], which utilizes rate splitting at Txs, joint decoding at Rxs, and time sharing among codebooks. This achievable rate region is proved to be within 1-bit of the capacity region of the GIC in [9].

For the general K-user GIC, two well-known interference mitigation techniques are, respectively, decoding the interference and treating the interference as noise at Rxs. In the case of very strong interference [10] or strong interference [8, 11], it is known that the capacity achieving strategy at the Rxs is to decode and subtract the interference prior to decoding the desired message. On the other hand, treating interference as noise in the case of weak interference is shown to be optimal from an information-theoretic perspective in [9, 12–14].

Recently, another approach, namely "interference alignment (IA)", is proposed [15], where interference signals are properly aligned in a certain subspace of the received signal at each Rx to achieve the maximum degrees of freedom (DoF) for the sum-rate. This approach is shown to be capacity-achieving when the signal-to-noise ratio (SNR) of all users goes to infinity. Inspired by the work [15], substantial research has been done on characterizing the DoF in GIC for different scenarios, such as constant channels without symbol extension [16, 17], delayed CSIT [18–20], no CSIT [21, 22], etc. Moreover, IA also helps advance our understanding of GIC. For example, [23] shows that proper Gaussian signalling is not generally optimal in GIC, which motivates subsequent work [24, 25] to investigate the improper Gaussian signalling optimization in GIC from a signal processing perspective. Furthermore, different from Gaussian parallel point-to-point channels, multiple-access channels

(MACs) and BCs where separate encoding over the parallel channels is optimal, [26] shows that joint encoding over the parallel channels is in general necessary to achieve the maximum DoF in parallel GICs.

2.2.2 WSR Maximization in GIC: State-of-the-Art

The aforementioned capacity-approaching techniques in general require non-linear multi-user encoding and decoding, which may not be suitable for practical systems. A more pragmatic approach that leads to suboptimal achievable rates in GIC is by considering only single-user encoding and decoding by treating the interference from all other unintended users as additive Gaussian noise. For this approach, the key design challenge lies in how to optimally allocate transmission resources such as power, bandwidth, and antenna beams among different users to maximize their WSR. Due to the coupled interference with transmission, the WSR maximization problem in GIC is in general NP-hard, which motivates extensive studies to seek various efficient algorithms to achieve suboptimal or locally optimal solutions.

Specifically, for the WSR maximization in SISO-IC, many efficient power control schemes are studied [6, 27–33]. It is shown in [27] that in the two-user GIC the optimal power allocation to maximize the sum-rate is "binary", i.e., either one user transmits with full power and the other user shuts down, or both users transmit with full power. [27] also extends the binary power control concept to the general case when the number of users is more than two, which, however, is not always optimal. Based on game theory, an "asynchronous distributed pricing (ADP)" algorithm is proposed in [28] whereby each user iteratively updates its power level based on the prices that reflect the interference levels it causes to other users. In [29], the WSR maximization problem is transformed into a signomial programming (SP) problem, which is efficiently solved by constructing a series of geometric programming (GP) problems through the approach of successive convex approximation. As for the case of parallel SISO-ICs, [30] proposes an iterative water-filling algorithm by viewing

the spectrum management problem as a non-cooperative Nash game. In [31], an algorithm called "Successive Convex Approximation for Low complExity (SCALE)" is proposed, where the non-convex WSR maximization problem in parallel SISO-ICs is transformed into a series of convex problems by utilizing the technique of convex relaxation. Furthermore, frequency-division-multiple-access (FDMA) is shown to be the optimal spectrum sharing strategy in the case of strong interference in [32], where several suboptimal distributed algorithms are also proposed based on FDMA. Last, the authors in [6], [33] show that the duality gap for the WSR maximization problem is zero when the number of parallel GICs becomes asymptotically large. As a result, the Lagrange duality method can be applied to decouple the problem into parallel sub-problems in the dual domain, a technique termed as dual decomposition. However, the power optimization in each sub-problem for a given GIC is still non-convex.

For WSR maximization in multi-antenna GICs, the optimality of transmit beamforming in MISO-IC is proved in [34, 35]. Moreover, an iterative beamforming algorithm is proposed in [36] from an egotistic versus altruistic viewpoint, but in general it cannot achieve the global WSR maximum for MISO-IC. As for the more general case of multiple-input multiple-output (MIMO) GIC, termed as MIMO-IC, various iterative suboptimal algorithms are studied in the literature [37–42]. Based on the gradient projection method, both centralized and distributed algorithms are proposed in [37] to obtain the suboptimal transmit covariance solutions. Motivated by an interesting equivalence between the WSR maximization problem in MIMO BC and weighted sum minimum-mean-square-error (MMSE) minimization problem with some properly selected weight matrices shown in [38], an iterative algorithm is proposed in [39] where each user updates its weight matrix and transmit covariance matrix in each iteration. Moreover, [40, 41] extend the ADP algorithm in [28] to the MIMO-IC and prove its convergence. An iterative algorithm is also proposed in [42] based on the well-known uplink-downlink duality [43–46].

Recently, based on the advanced non-convex optimization techniques, e.g.,

outer polyblock approximation and branch-and-bound, the globally optimal solution to the WSR maximization problem in GIC is obtained in [5, 47–50]. Based on outer polyblock approximation algorithm [4] and the generalized linear fractional programming [51], [5] solves the WSR maximization problem in SISO-IC in the SINR domain. In [47], the outer polyblock approximation algorithm is applied to obtain the optimal beamforming solution in the special case of two-user MISO-IC by leveraging a prior result in [52] that the optimal transmit beamforming vector to achieve any Pareto-boundary rate-pair can be expressed as a linear combination of the zero-forcing (ZF) and maximal ratio transmission (MRT) beamformers. Moreover, in [48] and [49], branch and bound methods combined with difference of convex functions (DC) programming [53] are proposed to obtain the globally optimal power solution to the WSR maximization problem in SISO-IC, while a generalized branch and bound method applicable to problems in which the objective function cannot be expressed in the form of DC, is proposed in [50]. Branch and bound method is also used in [54] to solve the WSR maximization problem in MISO-IC. Although the convergence of the above mentioned optimal algorithms is generally slow especially when the number of users becomes large, they provide useful performance benchmarks to other more efficient but suboptimal algorithms for WSR maximization in GIC.

2.2.3 Achievable Rate Region in GIC

Besides WSR maximization, another line of research on GIC with interference treated as noise is aimed to characterize the achievable rate region, which constitutes all the rate-tuples simultaneously achievable by all the users under a given set of transmit-power constraints. The rate region is characterized in [55] for the SISO-IC, and in [34, 35, 52, 56] for the MISO-IC. Recently, some new results are reported in [57–59] for the characterization of the rate region in MIMO-IC.

It is worth noting that the achievable rate region of GIC can be specified by its Parato boundary, which consists of all the rate-tuples for each of which it is

impossible to improve one user's rate without decreasing the rate of at least one of the other users. Since the rate region of GIC is in general a non-convex set, the well-known WSR maximization approach is not directly applicable to characterize the complete Parato boundary. One general method to characterize the Parato boundary of even non-convex achievable rate regions is the so-called "rate profile" approach, which results in solving a sequence of SINR feasibility problems. It is worth noting that rate profile is first proposed in [60] as an alternative method to WSR maximization for characterizing the Pareto boundary of the capacity region for the multi-antenna Gaussian MAC, which is a convex set. This method is later applied to characterize the Pareto boundary of non-convex rate regions for the MISO-IC in [34] and the two-way multi-antenna relay channel in [61].

2.3 System Model

In this chapter, we consider a K-user GIC, in which K mutually interfering wireless links communicate simultaneously over a common bandwidth, as shown in Fig. 2.1. Firstly, consider the case where all Txs and Rxs are each equipped with one single antenna, as shown in Fig. 2.1 (a). The system is thus modeled as SISO-IC, for which the discrete-time baseband signal received at the kth Rx is given by

$$y_k = h_{k,k}\sqrt{p_k}x_k + \sum_{j\neq k} h_{k,j}\sqrt{p_j}x_j + z_k, \quad k = 1, \cdots, K, \tag{2.1}$$

where $h_{k,j}$ denotes the complex channel gain from the jth Tx to the kth Rx, p_k denotes the transmit power of the kth Tx, x_k denotes the transmitted signal from the kth Tx, and z_k denotes the background noise at the kth Rx. It is assumed that $z_k \sim \mathcal{CN}(0, \sigma_k^2)$, $\forall k$, and all z_k's are independent.

We assume independent encoding across different Txs and thus x_k's are independent over k. It is also assumed that the Gaussian codebook is used and

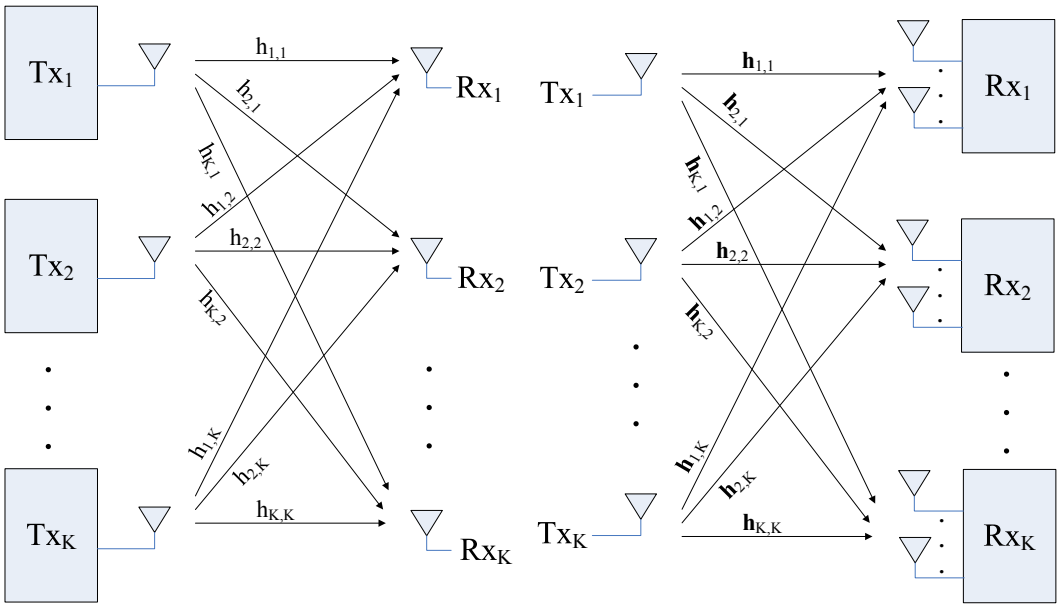

(a) SISO-IC

(b) SIMO-IC

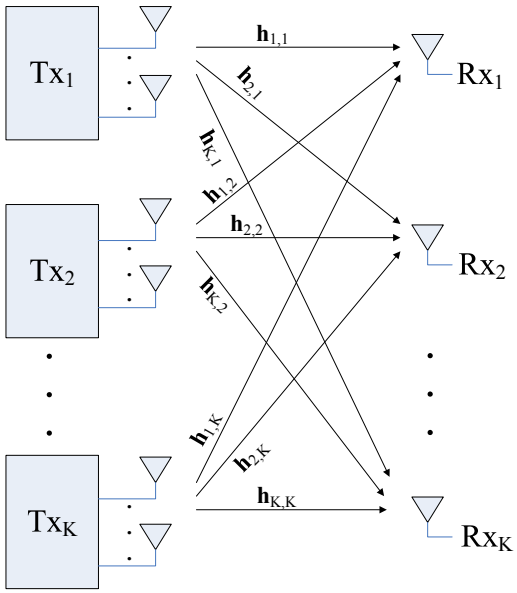

(c) MISO-IC

Figure 2.1: System model for the K-user SISO-IC, SIMO-IC and MISO-IC.

thus $x_k \sim \mathcal{CN}(0,1)$. Accordingly, the SINR of the kth Rx is expressed as

$$\gamma_k^{\text{SISO-IC}} = \frac{\|h_{k,k}\|^2 p_k}{\sum\limits_{j\neq k} \|h_{k,j}\|^2 p_j + \sigma_k^2}. \tag{2.2}$$

Secondly, consider the case where all Txs are each equipped with one single antenna but each Rx is equipped with multiple antennas, i.e., SIMO-IC, as shown in Fig. 2.1 (b). Assuming that the kth Rx is equipped with $M_k > 1$ antennas, its discrete-time baseband received signal is given by

$$y_k = \boldsymbol{w}_k^H (\boldsymbol{h}_{k,k}\sqrt{p_k}x_k + \sum_{j\neq k} \boldsymbol{h}_{k,j}\sqrt{p_j}x_j + \boldsymbol{z}_k), \quad \forall k, \tag{2.3}$$

where $\boldsymbol{w}_k^H \in \mathbb{C}^{1\times M_k}$ is the receive beamforming vector for the kth Rx, $\boldsymbol{h}_{k,j} \in \mathbb{C}^{M_k\times 1}$ is the channel vector from the jth Tx to the kth Rx, and $\boldsymbol{z}_k \in \mathbb{C}^{M_k\times 1}$ is the noise vector at the kth Rx. It is assumed that $\boldsymbol{z}_k \sim \mathcal{CN}(\boldsymbol{0}, \sigma_k^2 \boldsymbol{I})$. Thus, the SINR of the kth Rx can be expressed as

$$\gamma_k^{\text{SIMO-IC}} = \frac{p_k \|\boldsymbol{w}_k^H \boldsymbol{h}_{k,k}\|^2}{\boldsymbol{w}_k^H (\sum\limits_{j\neq k} p_j \boldsymbol{h}_{k,j}\boldsymbol{h}_{k,j}^H + \sigma_k^2 \boldsymbol{I})\boldsymbol{w}_k}. \tag{2.4}$$

Thirdly, consider the MISO-IC case in which all Txs are each equipped with multiple antennas while each Rx is equipped with one single antenna, as shown in Fig. 2.1 (c). Assume that the kth Tx is equipped with $N_k > 1$ antennas. The discrete-time baseband signal at the kth Rx is then given by

$$y_k = \boldsymbol{h}_{k,k}^H \boldsymbol{v}_k x_k + \sum_{j\neq k} \boldsymbol{h}_{k,j}^H \boldsymbol{v}_j x_j + z_k, \quad \forall k, \tag{2.5}$$

where $\boldsymbol{v}_k \in \mathbb{C}^{N_k\times 1}$ is the transmit beamforming vector at the kth Tx, and $\boldsymbol{h}_{k,j}^H \in \mathbb{C}^{1\times N_j}$ denotes the channel vector from the jth Tx to the kth Rx. Accordingly, the

SINR of the kth Rx can be expressed as

$$\gamma_k^{\text{MISO-IC}} = \frac{\|\boldsymbol{h}_{k,k}^H \boldsymbol{v}_k\|^2}{\sum\limits_{j \neq k} \|\boldsymbol{h}_{k,j}^H \boldsymbol{v}_j\|^2 + \sigma_k^2}. \tag{2.6}$$

With γ_k defined in (2.2), (2.4) or (2.6), the achievable rate of the kth Rx can be formulated as

$$R_k(\gamma_k) = \log_2(1 + \gamma_k), \quad k = 1, \cdots, K. \tag{2.7}$$

Next, we define the achievable rate region for each type of GIC, which constitutes all the rate-tuples simultaneously achievable by all the users under a given set of transmit-power constraints denoted by $P_1^{\max}, \cdots, P_K^{\max}$:

$$\mathcal{R}^{\text{SISO-IC}} \triangleq \bigcup_{\{p_k\}: 0 \leq p_k \leq P_k^{\max},\ \forall k} \left\{(r_1, \ldots, r_K) : 0 \leq r_k \leq R_k(\gamma_k^{\text{SISO-IC}}), \forall k\right\}, \tag{2.8}$$

$$\mathcal{R}^{\text{SIMO-IC}} \triangleq \bigcup_{\{p_k\}, \{\boldsymbol{w}_k\}: 0 \leq p_k \leq P_k^{\max},\ \forall k} \left\{(r_1, \ldots, r_K) : 0 \leq r_k \leq R_k(\gamma_k^{\text{SIMO-IC}}), \forall k\right\}, \tag{2.9}$$

$$\mathcal{R}^{\text{MISO-IC}} \triangleq \bigcup_{\{\boldsymbol{v}_k\}: 0 \leq \|\boldsymbol{v}_k\|^2 \leq P_k^{\max},\ \forall k} \left\{(r_1, \ldots, r_K) : 0 \leq r_k \leq R_k(\gamma_k^{\text{MISO-IC}}), \forall k\right\}. \tag{2.10}$$

The upper-right boundary of each defined rate region is called the *Pareto boundary*, constituted by rate-tuples for each of which it is impossible to improve one particular user's rate without decreasing the rate of at least one of the other users.

2.4 Problem Formulation

The WSR maximization problems for SISO-IC, SIMO-IC and MISO-IC are then formulated as (P1.1)-(P1.3) as follows.

$$\text{(P1.1)}: \quad \underset{\boldsymbol{p}}{\texttt{Maximize}} \quad U(\boldsymbol{p}) := \sum_{k=1}^{K} \mu_k R_k(\gamma_k^{\text{SISO-IC}})$$
$$\texttt{Subject to} \quad 0 \le p_k \le P_k^{\max}, \ \forall k,$$

$$\text{(P1.2)}: \quad \underset{\boldsymbol{W},\boldsymbol{p}}{\texttt{Maximize}} \quad U(\boldsymbol{W},\boldsymbol{p}) := \sum_{k=1}^{K} \mu_k R_k(\gamma_k^{\text{SIMO-IC}})$$
$$\texttt{Subject to} \quad 0 \le p_k \le P_k^{\max}, \ \forall k,$$

$$\text{(P1.3)}: \quad \underset{\boldsymbol{V}}{\texttt{Maximize}} \quad U(\boldsymbol{V}) := \sum_{k=1}^{K} \mu_k R_k(\gamma_k^{\text{MISO-IC}})$$
$$\texttt{Subject to} \quad \|\boldsymbol{v}_k\|^2 \le P_k^{\max}, \forall k,$$

where $\boldsymbol{p} = (p_1, \cdots, p_K)$ denotes the transmit power vector, $\boldsymbol{W} = (\boldsymbol{w}_1, \cdots, \boldsymbol{w}_K)$ and $\boldsymbol{V} = (\boldsymbol{v}_1, \cdots, \boldsymbol{v}_K)$ constitute the receive and transmit beamforming vectors, respectively, and μ_k is the non-negative rate weight for user k. Since the objective functions are all non-concave with respect to the power values or beamforming vectors due to the coupled interference, all the WSR maximization problems in (P1.1)-(P1.3) are non-convex and thus cannot be solved globally optimally by conventional convex optimization techniques.

2.5 Proposed Approach

In this section, we solve the formulated WSR maximization problems in (P1.1)-(P1.3) globally optimally by a new approach based on the outer polyblock

approximation and rate profile techniques.

2.5.1 WSR Maximization in Rate Region

Traditionally, problems (P1.1)-(P1.3) are solved in the domain of power allocation and/or beamforming vectors, resulting in non-convex optimization problems. In this subsection, we study the WSR maximization problem based on a new formulation, which maximizes the WSR directly in the achievable rate region.

If the achievable rate vector $\boldsymbol{r} = (R_1, \cdots, R_K)$ is treated as the design variable, where R_k is the achievable rate of user k defined in (2.7), the WSR maximization problems (P1.1)-(P1.3) can be unified in the following form.

$$\text{(P2)}: \quad \underset{\boldsymbol{r}}{\texttt{Maximize}} \quad U(\boldsymbol{r}) := \sum_{k=1}^{K} \mu_k R_k$$
$$\texttt{Subject to} \quad \boldsymbol{r} \in \mathcal{R},$$

where the rate region $\mathcal{R}$ is defined in (2.8), (2.9) or (2.10) for SISO-IC, SIMO-IC or MISO-IC.

Next, we will show that problem (P2) belongs to one special class of optimization problems: monotonic optimization over a "normal" set. Two useful definitions are given first as follows.

Definition 2.5.1. *A function $f : \mathbb{R}^n \to \mathbb{R}$ is said to be strictly increasing on $\mathbb{R}^n_+$ if for any $\boldsymbol{x}', \boldsymbol{x} \in \mathbb{R}^n_+$, $\boldsymbol{x}' \geq \boldsymbol{x}$ and $\boldsymbol{x}' \neq \boldsymbol{x}$ imply that $f(\boldsymbol{x}') > f(\boldsymbol{x})$.*

Definition 2.5.2. *A set $\mathcal{D} \in \mathbb{R}^n_+$ is called normal if given any point $\boldsymbol{x} \in \mathcal{D}$, all the points $\boldsymbol{x}'$ with $\mathbf{0} \leq \boldsymbol{x}' \leq \boldsymbol{x}$ satisfy that $\boldsymbol{x}' \in \mathcal{D}$.*

Based on the above definitions, we declare the following two facts regarding problem (P2), which can be easily verified to be true.

Fact 1. *The objective function of problem (P2) is a strictly increasing function with respect to $\boldsymbol{r}$.*

Fact 2. *The achievable rate region defined in (2.8), (2.9) or (2.10) is a normal set.*

Facts 1 and 2 imply that problem (P2) maximizes a strictly increasing function over a normal set. In [4], the "outer polyblock approximation" algorithm is proposed to achieve the global optimality for this type of problems. In the following, we apply this algorithm to solve problem (P2).

2.5.2 Outer Polyblock Approximation Algorithm

In this subsection, we introduce the outer polyblock approximation algorithm to solve problem (P2). First, two definitions are given as follows.

Definition 2.5.3. *Given any vector* $\boldsymbol{v} \in \mathbb{R}_+^n$*, the hyper rectangle* $[\mathbf{0}, \boldsymbol{v}] = \{\boldsymbol{x} | \mathbf{0} \leq \boldsymbol{x} \leq \boldsymbol{v}\}$ *is referred to as a box with vertex* $\boldsymbol{v}$*.*

Definition 2.5.4. *A set is called a polyblock if it is the union of a finite number of boxes.*

Next, we show one important property of the polyblock in the following proposition.

Proposition 2.5.1. *The maximum of a strictly increasing function* $f(\boldsymbol{x})$ *over a polyblock is achieved at one of the vertices of the polyblock.*

Proof. Suppose that $\boldsymbol{x}^*$ is the globally optimal solution over the polyblock, and it is not a vertex. Then, there exists at least one vertex $\boldsymbol{x}'$ satisfying $\boldsymbol{x}' \geq \boldsymbol{x}^*$ but $\boldsymbol{x}' \neq \boldsymbol{x}^*$. Since $f(\boldsymbol{x})$ is a strictly increasing function, $f(\boldsymbol{x}^*) < f(\boldsymbol{x}')$ must hold, which contradicts to the presumption. The proof is thus completed. □

According to Proposition 2.5.1, the maximum of an increasing function over a polyblock can be obtained efficiently by enumeration of the vertices of that polyblock. Consequently, we can construct a sequence of polyblocks to approximate the rate region $\mathcal{R}$ with the increasing accuracy for problem (P2). In other words, we

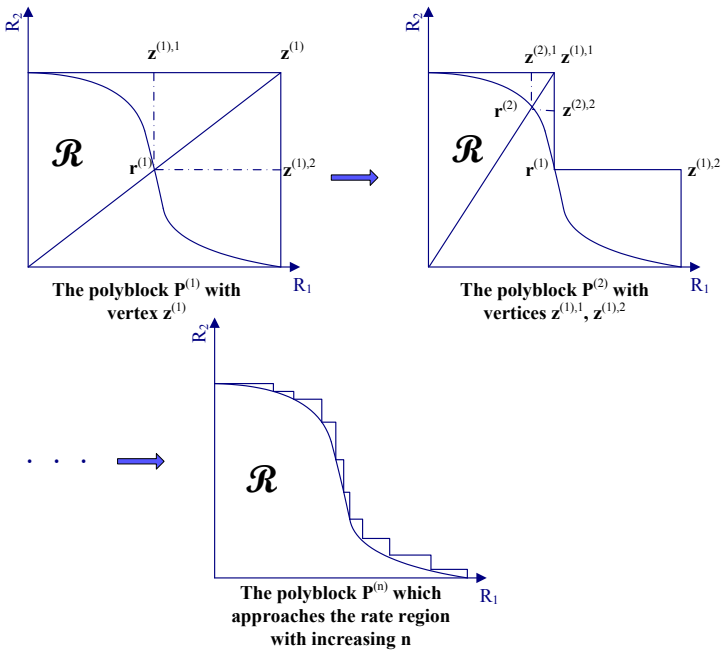

Figure 2.2: Illustration of the procedure for constructing new polyblocks.

need to find an iterative method to generate a sequence of polyblocks of shrinking sizes such that

$$P^{(1)} \supset P^{(2)} \supset \cdots \supset \mathcal{R}, \tag{2.11}$$

$$\lim_{n\to\infty} [\max_{\boldsymbol{r}\in P^{(n)}} U(\boldsymbol{r})] = \max_{\boldsymbol{r}\in\mathcal{R}} U(\boldsymbol{r}), \tag{2.12}$$

where $P^{(n)}$ denotes the polyblock generated at the nth iteration.

Next, we present one method to generate the polyblocks satisfying (2.11) and (2.12). Let $\mathcal{Z}^{(n)}$ denote the set containing all the vertices of the polyblock $P^{(n)}$. The vertex that achieves the maximum WSR in polyblock $P^{(n)}$ can be formulated as

$$\tilde{\boldsymbol{z}}^{(n)} = \arg\max_{\boldsymbol{z}\in\mathcal{Z}^{(n)}} U(\boldsymbol{z}). \tag{2.13}$$

Define $\delta\tilde{\boldsymbol{z}}^{(n)}$ as the line that connects the two points $\mathbf{0}$ and $\tilde{\boldsymbol{z}}^{(n)}$, and $\boldsymbol{r}^{(n)}$ as the intersection point on the Pareto boundary with the line $\delta\tilde{\boldsymbol{z}}^{(n)}$. The following

method can be used to generate K new vertices adjacent to $\tilde{\boldsymbol{z}}^{(n)}$:

$$\boldsymbol{z}^{(n),i} = \tilde{\boldsymbol{z}}^{(n)} - (\tilde{z}_i^{(n)} - r_i^{(n)})\boldsymbol{e}_i, \quad i = 1, \cdots, K, \tag{2.14}$$

where $\boldsymbol{z}^{(n),i}$ denotes the ith new vertex generated at the nth iteration; $\tilde{z}_i^{(n)}$ and $r_i^{(n)}$ denote the ith element of vectors $\tilde{\boldsymbol{z}}^{(n)}$ and $\boldsymbol{r}^{(n)}$, respectively. Then, the new vertex set can be expressed as

$$\mathcal{Z}^{(n+1)} = \mathcal{Z}^{(n)} \backslash \tilde{\boldsymbol{z}}^{(n)} \bigcup \{\boldsymbol{z}^{(n),1}, \cdots, \boldsymbol{z}^{(n),K}\}. \tag{2.15}$$

Each vertex in the set $\mathcal{Z}^{(n+1)}$ defines a box, and thus the new polyblock $P^{(n+1)}$ is the union of all these boxes. An illustration about the above procedure to generate polyblocks for the case of two-user rate region is given in Fig. 2.2. In the following proposition, we show the feasibility of the above polyblock generation method.

Proposition 2.5.2. *If the rate region $\mathcal{R}$ is a normal set (as we have already shown), the polyblocks generated by (2.15) satisfy (2.11).*

Proof. Please refer to [4]. □

Proposition 2.5.2 ensures that the above polyblock generation method can be used to approximate the rate region from the outside with increasing accuracy. Let $\boldsymbol{r}^* = (R_1^*, \cdots, R_K^*)$ denote the optimal solution to problem (P2). Based on the above method, in the following we present an algorithm to find $\boldsymbol{r}^*$ in the rate region $\mathcal{R}$. It is worth noting that $\boldsymbol{r}^*$ must be on the Pareto boundary of the rate region; thus, we only need to search over the Pareto boundary to find $\boldsymbol{r}^*$.

The outer polyblock approximation algorithm works iteratively as follows. In the nth iteration, the optimal vertex $\tilde{\boldsymbol{z}}^{(n)}$ is first obtained by (2.13). According to Proposition 2.5.1, in the polyblock $P^{(n)}$ the maximum WSR is $U(\tilde{\boldsymbol{z}}^{(n)})$. Since Proposition 2.5.2 implies that $P^{(n)}$ always contains the rate region $\mathcal{R}$, $U(\tilde{\boldsymbol{z}}^{(n)})$ is an upper bound of $U(\boldsymbol{r}^*)$. Then, the intersection point $\boldsymbol{r}^{(n)}$ on the Pareto boundary with the line $\delta\tilde{\boldsymbol{z}}^{(n)}$ is obtained. Define the best intersection point up to the nth

iteration as

$$\tilde{\boldsymbol{r}}^{(n)} = \arg\max\{U(\boldsymbol{r}^{(n)}), U(\tilde{\boldsymbol{r}}^{(n-1)})\}. \tag{2.16}$$

Consequently, $U(\tilde{\boldsymbol{r}}^{(n)})$ is the tightest lower bound of $U(\boldsymbol{r}^*)$ by the nth iteration. Next, we can compute the value of $U(\tilde{\boldsymbol{z}}^{(n)}) - U(\tilde{\boldsymbol{r}}^{(n)})$, which is the difference between the upper and lower bounds of the optimal value of problem (P2) at the nth iteration. If this difference is less than η (a small positive number), the algorithm can terminate and $\tilde{\boldsymbol{r}}^{(n)}$ is at least an η-optimal solution to problem (P2) because

$$U(\boldsymbol{r}^*) - U(\tilde{\boldsymbol{r}}^{(n)}) < U(\tilde{\boldsymbol{z}}^{(n)}) - U(\tilde{\boldsymbol{r}}^{(n)}) < \eta. \tag{2.17}$$

Otherwise, we construct a new polyblock $P^{(n+1)}$ by the above polyblock generation method. We repeat the above procedure until an η-optimal solution is found.

The above algorithm, denoted as Algorithm 2.1, is summarized in Table 2.1. It is worth noting that in Algorithm 2.1, $\tilde{\boldsymbol{z}}^{(n)}$ is obtained by enumeration in the set $\mathcal{Z}_\epsilon^{(n)}$ rather than $\mathcal{Z}^{(n)}$. This is because in [4] it is shown that if the optimal solution lies in a strip defined by $\{\boldsymbol{r}^* | 0 \leq R_k^* \leq \epsilon\}$ with arbitrary k and a small value $\epsilon > 0$, then as $\tilde{\boldsymbol{z}}^{(n)}$ approaches this strip, the algorithm converges very slowly. Consequently, ϵ is chosen to balance the tradeoff between the accuracy and complexity of Algorithm 2.1. With ϵ, Algorithm 2.1 solves the following problem

$$\begin{aligned} (\text{P2}-\text{A}): \quad & \underset{\boldsymbol{r}}{\texttt{Maximize}} \quad U(\boldsymbol{r}) := \sum_{k=1}^{K} \mu_k R_k \\ & \texttt{Subject to} \quad \boldsymbol{r} \in \mathcal{R}^\epsilon, \end{aligned}$$

where $\mathcal{R}^\epsilon$ is defined as

$$\mathcal{R}^\epsilon = \mathcal{R} \cap \{(r_1, \cdots, r_K) : r_k \geq \epsilon, \forall k\}. \tag{2.19}$$

Thus, the corresponding solution is called an (ϵ, η)-optimal solution to problem (P2).

Table 2.1: **Algorithm 2.1**: Outer Polyblock Approximation Algorithm for Solving problem (P2)

---

a) Initialize: Set $n = 1$, $\mathcal{Z}^{(1)} = \{\boldsymbol{z}^{(1)}\}$;

b) **While** (ϵ, η)-accuracy is not reached, **do**

1) Find the optimal vertex $\tilde{\boldsymbol{z}}^{(n)}$ that maximizes the WSR in the set $\mathcal{Z}_{\epsilon}^{(n)}$ based on

$$\tilde{\boldsymbol{z}}^{(n)} = \arg \max_{\boldsymbol{z} \in \mathcal{Z}_{\epsilon}^{(n)}} U(\boldsymbol{z}), \tag{2.18}$$

where ϵ is a small positive number and $\mathcal{Z}_{\epsilon}^{(n)} = \{\boldsymbol{z} \in \mathcal{Z}^{(n)} | z_k \geq \epsilon, \ \forall k\}$;

2) Compute the intersection point $\boldsymbol{r}^{(n)}$ on the Pareto boundary of the rate region $\mathcal{R}$ with the line $\delta\tilde{\boldsymbol{z}}^{(n)}$;

3) Update the best intersection point until the nth iteration $\tilde{\boldsymbol{r}}^{(n)}$ according to (2.16);

4) **If** $U(\tilde{\boldsymbol{z}}^{(n)}) - U(\tilde{\boldsymbol{r}}^{(n)}) \leq \eta$, **then**

Stop and $\tilde{\boldsymbol{r}}^{(n)}$ is an (ϵ, η)-optimal solution to problem (P2);

5) **else**

Compute K new vertices that are adjacent to $\tilde{\boldsymbol{z}}^{(n)}$ by (2.14) and update the vertex set $\mathcal{Z}^{(n+1)}$ by (2.15);

6) **end**

7) $n = n + 1$;

c) **end**

Next, we address the convergence issue of Algorithm 2.1. According to Proposition 2.5.2, $P^{(n)} \supset P^{(n+1)}$ always holds. Moreover, the optimal vertex $\tilde{\boldsymbol{z}}^{(n)}$ is removed from $\mathcal{Z}_{\epsilon}^{(n+1)}$ after each iteration. Thus, $U(\tilde{\boldsymbol{z}}^{(n+1)}) < U(\tilde{\boldsymbol{z}}^{(n)})$ also holds. Furthermore, the lower bound $U(\tilde{\boldsymbol{r}}^{(n)})$ is non-decreasing. Consequently, the value of $U(\tilde{\boldsymbol{z}}^{(n)}) - U(\tilde{\boldsymbol{r}}^{(n)})$ will decrease after each iteration. It is shown in [4] that as n increases, the difference between the upper and lower bounds can be reduced to an arbitrary small positive number in a finite number of iterations. Thus, Algorithm 2.1 converges given small positive values ϵ and η. More details about the selection

of the values of ϵ and η will be given later in Section 2.7.2.

Last, we explain how to obtain an initial vertex $\boldsymbol{z}^{(1)} = (z_1^{(1)}, \cdots, z_K^{(1)})$ for the first iteration of Algorithm 2.1. Since the box $[\mathbf{0}, \boldsymbol{z}^{(1)}]$ needs to contain the rate region $\mathcal{R}$, for any user k, $z_k^{(1)}$ can be obtained when all other users switch off their transmission (thus no interference exists for user k), and user k transmits its maximum power $P_k^{\max}$. More specifically, for SISO-IC,

$$z_k^{(1)} = \log_2(1 + \frac{P_k^{\max}\|h_{k,k}\|^2}{\sigma_k^2}),\ \forall k. \tag{2.20}$$

Since for MISO-IC,

$$\begin{aligned}\gamma_k^{\text{MISO-IC}} &= \frac{\|\boldsymbol{h}_{k,k}^H \boldsymbol{w}_k\|^2}{\sum\limits_{j\neq k}\|\boldsymbol{h}_{k,j}^H \boldsymbol{w}_j\|^2 + \sigma_k^2} < \frac{\|\boldsymbol{h}_{k,k}^H \boldsymbol{w}_k\|^2}{\sigma_k^2} \\ &\overset{(a)}{\leq} \frac{\|\boldsymbol{w}_k\|^2\|\boldsymbol{h}_{k,k}\|^2}{\sigma_k^2} \leq \frac{P_k^{\max}\|\boldsymbol{h}_{k,k}\|^2}{\sigma_k^2},\ \forall k,\end{aligned} \tag{2.21}$$

where (a) is due to the Cauchy-Schwarz inequality, $z_k^{(1)}$ can thus be set as

$$z_k^{(1)} = \log_2(1 + \frac{P_k^{\max}\|\boldsymbol{h}_{k,k}\|^2}{\sigma_k^2}),\ \forall k. \tag{2.22}$$

The initial vertex for SIMO-IC can be obtained similar to (2.22), and is thus omitted for brevity.

To summarize, the only challenge that remains unaddressed in Algorithm 2.1 is on how to compute the intersection point $\boldsymbol{r}^{(n)}$ on the Pareto rate boundary with the line $\delta\tilde{\boldsymbol{z}}^{(n)}$ at the nth iteration, which will be addressed next.

2.5.3 Finding Intersection Points by "Rate Profile" Technique

In this subsection, we show how to obtain the intersection point on the Pareto boundary of the rate region with the line $\delta\tilde{\boldsymbol{z}}^{(n)}$, to complete Algorithm 2.1. Let

$R_{\text{sum}} = \sum_{k=1}^{K} R_k$ denote the sum-rate of all the users, $\boldsymbol{\alpha} = \tilde{\boldsymbol{z}}^{(n)} / \sum_{k=1}^{K} \tilde{z}_k^{(n)}$ denote the slope of the line $\delta\tilde{\boldsymbol{z}}^{(n)}$. Consequently, the intersection point at the nth iteration can be expressed as $\boldsymbol{r}^{(n)} = R_{\text{sum}}^{*}\boldsymbol{\alpha}$, where R_{sum}^{*} is the optimal value of the following problem:

$$\begin{aligned} \texttt{Maximize} \quad & R_{\text{sum}} \\ \texttt{Subject to} \quad & R_{\text{sum}}\boldsymbol{\alpha} \in \mathcal{R}. \end{aligned} \tag{2.23}$$

The above approach to find the intersection point on the Pareto boundary of the rate region is known as *rate profile* [34, 60, 61]. In the following, we solve Problem (2.23) to obtain the intersection point $\boldsymbol{r}^{(n)}$ on the Pareto boundary with a given $\delta\tilde{\boldsymbol{z}}^{(n)}$.

Problem (2.23) is solvable via solving a sequence of feasibility problems shown as follows. Given a target sum-rate $\bar{R}_{\text{sum}}$, the feasibility problems for SISO-IC, SIMO-IC and MISO-IC can be expressed in the following problems (P3.1)-(P3.3), respectively.

$$\begin{aligned} \text{(P3.1)}: \ \texttt{Find} \quad & \{p_k\} \\ \texttt{Subject to} \quad & \log_2(1+\gamma_k^{\text{SISO-IC}}) \geq \alpha_k \bar{R}_{\text{sum}}, \ \forall k \\ & p_k \leq P_k^{\max}, \ \ \forall k. \end{aligned}$$

$$\begin{aligned} \text{(P3.2)}: \ \texttt{Find} \quad & \{\boldsymbol{w}_k\}, \ \{p_k\} \\ \texttt{Subject to} \quad & \log_2(1+\gamma_k^{\text{SIMO-IC}}) \geq \alpha_k \bar{R}_{\text{sum}}, \ \forall k \\ & p_k \leq P_k^{\max}, \ \ \forall k. \end{aligned}$$

$$\begin{aligned} \text{(P3.3)}: \ \texttt{Find} \quad & \{\boldsymbol{v}_k\} \\ \texttt{Subject to} \quad & \log_2(1+\gamma_k^{\text{MISO-IC}}) \geq \alpha_k \bar{R}_{\text{sum}}, \ \forall k \\ & \|\boldsymbol{v}_k\|^2 \leq P_k^{\max}, \ \forall k. \end{aligned}$$

If any of Problems (P3.1), (P3.2) and (P3.3) is feasible, it follows that $R_{\text{sum}}^* \geq \bar{R}_{\text{sum}}$; otherwise, $R_{\text{sum}}^* < \bar{R}_{\text{sum}}$. Hence, R_{sum}^* can be obtained for problem (2.23) by applying a simple bisection method [62], for which the detail is omitted for brevity.

The remaining challenge is on solving the feasibility problems (P3.1)-(P3.3), which is addressed next. Let $\bar{\gamma}_k = 2^{\alpha_k \bar{R}_{\text{sum}}} - 1$, $\forall k$. Then, the first constraint of each feasibility problem can be re-expressed as

$$\gamma_k \geq \bar{\gamma}_k, \quad \forall k. \tag{2.24}$$

Therefore, given any sum-rate target $\bar{R}_{\text{sum}}$, the feasibility problems (P3.1)-(P3.3) are equivalent to finding whether a corresponding SINR target vector $\bar{\boldsymbol{\gamma}} = (\bar{\gamma}_1, \cdots, \bar{\gamma}_K)$ is achievable. In the next section, we will propose efficient algorithms to solve these SINR feasibility problems.

Remark 2.5.1. *In the case where a set of minimum rate constraints $R_k \geq R_k^{\min}$, $\forall k$, are added to the WSR maximization problem (P2), where $R_k^{\min}$ is the minimum rate required for user k, we can solve this new problem by modifying Algorithm 2.1 as follows. Since the new rate region $\mathcal{R}'$ is the intersection of the original rate region with the set $\{(r_1, \cdots, r_K) : r_k \geq R_k^{\min}, \ \forall k\}$, we should change the initial point from $\mathbf{0}$ to $\boldsymbol{r}^{\min}$ in Algorithm 2.1, where $\boldsymbol{r}^{\min} = (R_1^{\min}, \cdots, R_K^{\min})$ is the rate constraint vector. Thus, at each iteration we need to compute the intersection point on the Pareto boundary with the line passing through the optimal vertex $\tilde{\boldsymbol{z}}^{(n)}$ and the point $\boldsymbol{r}^{\min}$ (instead of $\mathbf{0}$ in Algorithm 2.1). In addition, any point $\boldsymbol{r}$ on this line with $R_{\text{sum}} = \sum_{k=1}^K R_k$ can be rewritten as*

$$\boldsymbol{r} = \boldsymbol{r}^{\min} + \boldsymbol{\alpha}(R_{\text{sum}} - \sum_{k=1}^K R_k^{\min}), \tag{2.25}$$

where the rate profile $\boldsymbol{\alpha}$ is obtained by $\boldsymbol{\alpha} = \frac{\tilde{\boldsymbol{z}}^{(n)} - \boldsymbol{r}^{\min}}{\sum_{k=1}^K \tilde{z}_k^{(n)} - \sum_{k=1}^K R_k^{\min}}$.

2.6 Solutions to SINR Feasibility Problems

In this section, we solve problems (P3.1)-(P3.3) subject to the equivalent SINR constraints given in (2.24) for SISO-IC, SIMO-IC and MISO-IC, respectively.

2.6.1 The SISO-IC Case

We first study the feasibility problem (P3.1) for SISO-IC. Given a SINR target vector $\bar{\boldsymbol{\gamma}} = (\bar{\gamma}_1, \cdots, \bar{\gamma}_K)$ with $\bar{\gamma}_k = 2^{\alpha_k \bar{R}_{\text{sum}}} - 1$, we check whether it is achievable under users' individual power constraints as follows.

Let $\boldsymbol{G}$ denote the $K \times K$ normalized channel gain matrix given by

$$G_{k,j} = \begin{cases} \frac{\bar{\gamma}_k \|h_{k,j}\|^2}{\|h_{k,k}\|^2}, & k \neq j \\ 0, & k = j, \end{cases} \tag{2.26}$$

and $\boldsymbol{\eta}$ denote the $K \times 1$ normalized noise vector given by

$$\eta_k = \frac{\bar{\gamma}_k \sigma_k^2}{\|h_{k,k}\|^2}, \quad \forall k. \tag{2.27}$$

To achieve the SINR target, the transmit power vector for users is given by

$$\boldsymbol{p} = (\boldsymbol{I} - \boldsymbol{G})^{-1} \boldsymbol{\eta}. \tag{2.28}$$

Let $\rho(\boldsymbol{B})$ denote the spectral radius (defined as the maximum eigenvalue in absolute value) of the non-negative matrix $\boldsymbol{B}$. The following propositions are shown in [63], which play important roles in solving Problem (P3.1).

Proposition 2.6.1. *The power allocation $\boldsymbol{p}$ given by (2.28) satisfies $\boldsymbol{p} \geq \boldsymbol{0}$ if and only if $\rho(\boldsymbol{G}) < 1$.*

Proposition 2.6.2. *If $\rho(\boldsymbol{G}) < 1$, the power allocation $\boldsymbol{p}$ given by (2.28) is component-wise minimum in the sense that any other power allocation $\boldsymbol{p}'$ that satisfies (2.24) needs to satisfy $\boldsymbol{p}' \geq \boldsymbol{p}$.*

Propositions 2.6.1 and 2.6.2 imply that a SINR target vector $\bar{\boldsymbol{\gamma}}$ is feasible if and only if: (1) $\rho(\boldsymbol{G}) < 1$, and (2) the power solution obtained by (2.28) satisfies $p_k \leq P_k^{\max}$, $\forall k$. Consequently, we propose Algorithm 2.2 in Table 2.2 to solve Problem (P3.1).

Table 2.2: **Algorithm 2.2**: Algorithm for Solving Problem (P3.1)

a) Given any SINR target vector $\bar{\boldsymbol{\gamma}} = (\bar{\gamma}_1, \cdots, \bar{\gamma}_K)$, compute the spectrum radius of matrix $\boldsymbol{G}$. If it is larger than 1, conclude that there is no feasible power allocation to meet the SINR target and exit the algorithm; otherwise, go to step *b*);
b) Compute the power allocation $\boldsymbol{p}$ by (2.28), and check for any user k, whether the power constraint $p_k \leq P_k^{\max}$ is satisfied. If so, conclude that the SINR target is feasible; otherwise, the SINR target is not feasible.

Remark 2.6.1. *It is worth comparing Algorithm 2.1 with the MAPEL algorithm proposed in [5]. MAPEL solves Problem (P1.1) for SISO-IC in the SINR region (as opposed to the rate region in our approach) due to the fact that the problem to characterize the Pareto boundary of the SINR region for SISO-IC can be transformed into a generalized linear fractional programming problem and thus efficiently solved by Dinkelbach-type algorithm [64]. However, this transformation does not work for SIMO-IC or MISO-IC if the beamforming vectors are involved. Consequently, MAPEL cannot be extended to the GIC with multiple antennas. As comparison, in this chapter we solve the WSR maximization problem in the rate region directly because the Pareto boundary can be characterized completely by the rate profile approach, as along as the associated SINR feasibility problem can be solved. Thus, our proposed algorithm is more applicable than MAPEL in solving the WSR maximization problems for SIMO-IC and MISO-IC, as shown next.*

2.6.2 The SIMO-IC Case

The feasibility of Problem (P3.2) can be checked by using the optimal value of the following SINR balancing problem:

$$\begin{aligned} \texttt{Maximize} \quad & \min_{1\le k\le K} \frac{\gamma_k}{\bar{\gamma}_k} \\ \texttt{Subject to} \quad & p_k \le P_k^{\max},\ \forall k. \end{aligned} \tag{2.29}$$

If the optimal value of Problem (2.29) is no smaller than 1, then the SINR target vector $\bar{\boldsymbol{\gamma}} = (\bar{\gamma}_1, \cdots, \bar{\gamma}_K)$ is achievable; otherwise, this SINR target cannot be achieved.

In [65], an efficient algorithm is proposed to solve a SINR balancing problem similar to Problem (2.29), where only one sum-power constraint is imposed. However, the algorithm in [65] cannot be directly applied to solve Problem (2.29) due to multiple users' individual power constraints. To utilize the algorithm proposed in [65], we decouple Problem (2.29) into K sub-problems, with the ith sub-problem formulated as:

$$\begin{aligned} \texttt{Maximize} \quad & \min_{1\le k\le K} \frac{\gamma_k}{\bar{\gamma}_k} \\ \texttt{Subject to} \quad & p_i \le P_i^{\max}. \end{aligned} \tag{2.30}$$

Therefore, for the ith sub-problem only the ith user's power constraint is considered. Next, we show how to solve Problem (2.30) by extending the algorithm in [65], and then reveal an important relationship between problems (2.29) and (2.30), based upon which we further propose an efficient algorithm to solve Problem (2.29).

- Solution to Problem (2.30)

In this part, we extend the algorithm proposed in [65] to solve Problem (2.30) for a given i.

One important property of the SINR balancing problem in (2.30) is that given any receive beamforming vectors $\bar{\boldsymbol{W}} = (\bar{\boldsymbol{w}}_1, \cdots, \bar{\boldsymbol{w}}_K)$, the corresponding optimal

power allocation $\bar{\boldsymbol{p}}$ must satisfy the following two conditions:

$$\frac{\gamma_k(\bar{\boldsymbol{W}}, \bar{\boldsymbol{p}})}{\bar{\gamma}_k} = C(\bar{\boldsymbol{W}}),\ \forall k, \tag{2.31}$$

$$\bar{p}_i = P_i^{\max}, \tag{2.32}$$

where $C(\bar{\boldsymbol{W}})$ is the maximum SINR balancing value for all users given $\bar{\boldsymbol{W}}$.

We justify the above conditions as follows. (2.31) can be shown by contradiction. Supposing that the SINR balancing values are not the same for all the users, then we select the user with the highest SINR balancing value and decrease its transmit power by a small amount such that its new SINR balancing value is still above $\min_k \frac{\gamma_k}{\bar{\gamma}_k}$. Since the other users' SINR balancing values will increase, the minimum SINR balancing value among all the users will increase accordingly. Thus, whenever the SINR balancing values are not the same for all users, we can proceed as above to improve the optimal value. Hence, (2.31) must hold. Similarly to show (2.32) by contradiction, suppose $\bar{p}_i < P_i^{\max}$. With $\alpha = \frac{P_i^{\max}}{\bar{p}_i} > 1$, we can multiply the transmit power values of each user by α, and the SINRs of all users will be increased accordingly. Hence, (2.32) must hold.

We can express (2.31) for all k's in the following matrix form:

$$\bar{\boldsymbol{p}}\frac{1}{C(\bar{\boldsymbol{W}})} = \boldsymbol{D}\boldsymbol{\Psi}(\bar{\boldsymbol{W}})\bar{\boldsymbol{p}} + \boldsymbol{D}\boldsymbol{\sigma}, \tag{2.33}$$

where $\boldsymbol{D} = \mathrm{Diag}\{\frac{\bar{\gamma}_1}{\|\bar{\boldsymbol{w}}_1^H \boldsymbol{h}_{1,1}\|^2}, \cdots, \frac{\bar{\gamma}_K}{\|\bar{\boldsymbol{w}}_K^H \boldsymbol{h}_{K,K}\|^2}\}$, $\boldsymbol{\sigma} = [\sigma_1^2\|\bar{\boldsymbol{w}}_1\|^2, \cdots, \sigma_K^2\|\bar{\boldsymbol{w}}_K\|^2]^T$, and the $K \times K$ non-negative matrix $\boldsymbol{\Psi}(\bar{\boldsymbol{W}})$ is a function of $\bar{\boldsymbol{W}}$ defined as

$$[\Psi(\bar{\boldsymbol{W}})]_{k,j} = \begin{cases} \|\bar{\boldsymbol{w}}_k^H \boldsymbol{h}_{k,j}\|^2, & k \neq j \\ 0, & k = j. \end{cases} \tag{2.34}$$

By multiplying both sides of (2.33) by $\boldsymbol{e}_i^T$, we obtain

$$\boldsymbol{e}_i^T \bar{\boldsymbol{p}}\frac{1}{C(\bar{\boldsymbol{W}})} = \frac{P_i^{\max}}{C(\bar{\boldsymbol{W}})} = \boldsymbol{e}_i^T \boldsymbol{D}\boldsymbol{\Psi}(\bar{\boldsymbol{W}})\bar{\boldsymbol{p}} + \boldsymbol{e}_i^T \boldsymbol{D}\boldsymbol{\sigma}. \tag{2.35}$$

Therefore, by combining (2.33) and (2.35), it follows that

$$\frac{1}{C(\bar{\boldsymbol{W}})}\bar{\boldsymbol{p}}_{\text{ext}} = \boldsymbol{A}_i(\bar{\boldsymbol{W}})\bar{\boldsymbol{p}}_{\text{ext}}, \tag{2.36}$$

where $\bar{\boldsymbol{p}}_{\text{ext}} = \begin{pmatrix} \bar{\boldsymbol{p}} \\ 1 \end{pmatrix}$ and

$$\boldsymbol{A}_i(\bar{\boldsymbol{W}}) = \begin{pmatrix} \boldsymbol{D}\boldsymbol{\Psi}(\bar{\boldsymbol{W}}) & \boldsymbol{D}\boldsymbol{\sigma} \\ \frac{1}{P_i^{\max}}\boldsymbol{e}_i^T\boldsymbol{D}\boldsymbol{\Psi}(\bar{\boldsymbol{W}}) & \frac{1}{P_i^{\max}}\boldsymbol{e}_i^T\boldsymbol{D}\boldsymbol{\sigma} \end{pmatrix}. \tag{2.37}$$

Next, we show one important property for (2.36) in the following lemma.

Lemma 2.6.1. *Given any fixed $\bar{\boldsymbol{W}}$, there exists a unique solution $(\bar{\boldsymbol{p}}, C(\bar{\boldsymbol{W}}))$ to the equation in (2.36).*

Proof. Please refer to Appendix A. □

According to Perron-Frobenius theory [66], for any nonnegative matrix, there is at least one positive eigenvalue and the spectral radius of the matrix is equal to the largest positive eigenvalue. Furthermore, according to Lemma 2.6.1, there is only one strictly positive eigenvalue to matrix $\boldsymbol{A}_i(\bar{\boldsymbol{W}})$. Accordingly, it follows from (2.36) that given $\bar{\boldsymbol{W}}$, the inverse of the optimal SINR balancing value $1/C(\bar{\boldsymbol{W}})$ is the spectral radius of $\boldsymbol{A}_i(\bar{\boldsymbol{W}})$. Consequently, the maximum SINR balancing solution to Problem (2.30) is obtained as

$$C^* = \frac{1}{\min\limits_{\boldsymbol{W}} \rho(\boldsymbol{A}_i(\boldsymbol{W}))}. \tag{2.38}$$

Next, by defining a cost function as

$$\Upsilon(\boldsymbol{W}, \boldsymbol{p}_{\text{ext}}) = \max_{\boldsymbol{x}>0} \frac{\boldsymbol{x}^T\boldsymbol{A}_i(\boldsymbol{W})\boldsymbol{p}_{\text{ext}}}{\boldsymbol{x}^T\boldsymbol{p}_{\text{ext}}}, \tag{2.39}$$

then the min-max characterization of the spectral radius of $\boldsymbol{A}_i(\boldsymbol{W})$ can be expressed

as [65], [67]

$$\rho(\boldsymbol{A}_i(\boldsymbol{W})) = \min_{\boldsymbol{p}_{\text{ext}}} \Upsilon(\boldsymbol{W}, \boldsymbol{p}_{\text{ext}}). \tag{2.40}$$

Taking (2.40) into (2.38), it follows that

$$\frac{1}{C^*} = \min_{\boldsymbol{W}} \min_{\boldsymbol{p}_{\text{ext}}} \Upsilon(\boldsymbol{W}, \boldsymbol{p}_{\text{ext}}). \tag{2.41}$$

Similar to [65], we can solve Problem (2.41) via the alternating optimization shown as follows. First, given $\bar{\boldsymbol{W}}$, we find the optimal power allocation for $\boldsymbol{p}_{\text{ext}}$. Let $\bar{\boldsymbol{p}}_{\text{ext}}$ denote the dominant eigenvector corresponding to the spectral radius of $\boldsymbol{A}_i(\bar{\boldsymbol{W}})$. It then follows that

$$\frac{\boldsymbol{x}^T \boldsymbol{A}_i(\bar{\boldsymbol{W}}) \bar{\boldsymbol{p}}_{\text{ext}}}{\boldsymbol{x}^T \bar{\boldsymbol{p}}_{\text{ext}}} = \rho(\boldsymbol{A}_i(\bar{\boldsymbol{W}})) = \min_{\boldsymbol{p}_{\text{ext}}} \Upsilon(\bar{\boldsymbol{W}}, \boldsymbol{p}_{\text{ext}}). \tag{2.42}$$

Thus, $\bar{\boldsymbol{p}}_{\text{ext}}$ is the optimal power allocation given $\bar{\boldsymbol{W}}$.

Furthermore, we know that given any power allocation $\boldsymbol{p}_{\text{ext}}$, the optimal receive beamformer in $\boldsymbol{W}$ to maximize the SINR is MMSE based for each of the users. Therefore, we propose an iterative algorithm in Table 2.3, denoted as Algorithm 2.3, to solve Problem (2.30).

The convergence of Algorithm 2.3 can be shown in the following way. Since given any power allocation $\boldsymbol{p}_{\text{ext}}^{(n)}$ for the nth iteration, $\boldsymbol{W}^{(n+1)}$ minimizes $\Upsilon(\boldsymbol{W}, \boldsymbol{p}_{\text{ext}}^{(n)})$, i.e.,

$$\Upsilon(\boldsymbol{W}^{(n+1)}, \boldsymbol{p}_{\text{ext}}^{(n)}) \leq \Upsilon(\boldsymbol{W}^{(n)}, \boldsymbol{p}_{\text{ext}}^{(n)}) = \rho^{(n)}. \tag{2.43}$$

Moreover, given $\boldsymbol{W}^{(n+1)}$, $\boldsymbol{p}_{\text{ext}}^{(n+1)}$ minimizes $\Upsilon(\boldsymbol{W}^{(n+1)}, \boldsymbol{p}_{\text{ext}})$ as

$$\rho^{(n+1)} = \Upsilon(\boldsymbol{W}^{(n+1)}, \boldsymbol{p}_{\text{ext}}^{(n+1)}) \leq \Upsilon(\boldsymbol{W}^{(n+1)}, \boldsymbol{p}_{\text{ext}}^{(n)}). \tag{2.44}$$

Hence, we can guarantee $\rho^{(n+1)} \leq \rho^{(n)}$ after each iteration. Since ρ is lower-bounded

Table 2.3: **Algorithm 2.3**: Algorithm for Solving Problem (2.30)

a) Initialize: $n = 0$, $\boldsymbol{p}^{(0)} = [0, \cdots, 0]^T$ and $\rho^{(0)} = \infty$;

b) **repeat**

1) $n = n + 1$;

2) Update $\boldsymbol{W}^{(n)}$ by $\boldsymbol{w}_k^{(n)} = (\sum_{j \neq k} p_j^{(n-1)} \mathbf{h}_{k,j} \mathbf{h}_{k,j}^H + \sigma_k^2 \mathbf{I})^{-1} \mathbf{h}_{k,k}, \quad \forall k$;

3) Update $\boldsymbol{p}_{\text{ext}}^{(n)}$ as the dominant eigenvector of the matrix $\boldsymbol{A}_i(\boldsymbol{W}^{(n)})$;

4) $\rho^{(n)} = \rho(\boldsymbol{A}_i(\boldsymbol{W}^{(n)}))$ and $C^{(n)} = \frac{1}{\rho^{(n)}}$;

c) **until** $\rho^{(n-1)} - \rho^{(n)} < \epsilon$.

by 0, Algorithm 2.3 thus converges.

Finally, the convergence of Algorithm 2.3 to the global optimality of Problem (2.30) can be proven similarly as Section IV.A in [65], and the proof is thus omitted for brevity. After convergence, $C^{(n)}\bar{\boldsymbol{\gamma}}$ is the maximum achievable SINR vector and $\boldsymbol{p}^{(n)}$, $\boldsymbol{W}^{(n)}$ are the optimal power and receive beamforming vectors to achieve this SINR vector, respectively.

- Solution to Problem (2.29)

Next, we show that Problem (2.29) can be efficiently solved via solving Problem (2.30) for all i's. Let $\boldsymbol{W}^*$ and $\boldsymbol{p}^*$ denote the optimal beamforming vectors and power allocation for Problem (2.29), respectively. Let $\boldsymbol{W}_i^*$ and $\boldsymbol{p}_i^*$ denote the optimal beamforming vectors and power allocation for the ith sub-problem in (2.30), respectively. Next, we provide a theorem to reveal the relationship between the optimal solutions to problems (2.29) and (2.30).

Theorem 2.6.1. *For all sub-problems in (2.30) with $i = 1, \cdots, K$, there exists one and only one sub-problem for which the optimal power solution satisfies all users' individual power constraints of Problem (2.29). Furthermore, let i^* denote the index of the corresponding sub-problem in (2.30), then it holds that $\boldsymbol{W}^* = \boldsymbol{W}_{i^*}^*$, and*

$\boldsymbol{p}^* = \boldsymbol{p}_{i^*}^*$.

Proof. Please refer to Section IV.B in [68]. □

Theorem 2.6.1 reveals that Problem (2.29) can be solved as follows. First, we apply Algorithm 2.3 to solve Problem (2.30) in the order of $i = 1, \cdots, K$. If the optimal power solution to any of these problems satisfies all users' individual power constraints, the algorithm terminates, and the obtained optimal power and beamforming solutions to Problem (2.30) are also those to Problem (2.29). The above algorithm, denoted by Algorithm 2.4, is summarized in Table 2.4.

Table 2.4: **Algorithm 2.4**: Algorithm for Solving Problem (2.29)

a) Initialize: $i = 0$;

b) **repeat**

1) $i = i + 1$;

2) Solve the ith sub-problem in (2.30) by Algorithm 2.3, and find the optimal beamforming solution $\boldsymbol{W}_i^*$ and power solution $\boldsymbol{p}_i^*$;

3) Check whether $\boldsymbol{p}_i^*$ satisfies all power constraints of Problem (2.29). If so, exit the algorithm and set $\boldsymbol{W}_i^*$ and $\boldsymbol{p}_i^*$ as the optimal solution to Problem (2.29); otherwise, continue the algorithm;

c) **until** $i = K$.

2.6.3 The MISO-IC Case

In this subsection, we show how to solve the feasibility problem (P3.3) for MISO-IC under the equivalent SINR constraints given by (2.24). It is shown in [34] that this problem can be transformed into a second-order cone programming (SOCP) problem, which is briefly described as follows for the sake of completeness. The SINR

constraints in Problem (P3.3) can be rewritten as

$$(1+\frac{1}{\bar{\gamma}_k})\|\boldsymbol{h}_{k,k}^H\boldsymbol{v}_k\|^2 \geq \sum_{j=1}^{K}\|\boldsymbol{h}_{k,j}^H\boldsymbol{v}_j\|^2+\sigma_k^2, \quad \forall k. \tag{2.45}$$

Without loss of generality, we can assume that $\boldsymbol{h}_{k,k}^H\boldsymbol{v}_k$ is a positive real number, $\forall k$. Thus we can reformulate the above SINR constraints as

$$\sqrt{1+\frac{1}{\bar{\gamma}_k}}\boldsymbol{h}_{k,k}^H\boldsymbol{v}_k \geq \sqrt{\sum_{j=1}^{K}\|\boldsymbol{h}_{k,j}^H\boldsymbol{v}_j\|^2+\sigma_k^2}, \quad \forall k. \tag{2.46}$$

Denote $\boldsymbol{x}=[\boldsymbol{v}_1^T,\cdots,\boldsymbol{v}_K^T,0]^T$ of dimension $(K^2+1)\times 1$, $\boldsymbol{n}_k=[0,\cdots,0,\sigma_k]^T$ of dimension $(K+1)\times 1$, and $\boldsymbol{E}_k=\mathrm{Diag}(\boldsymbol{h}_{k,1}^H,\cdots,\boldsymbol{h}_{k,K}^H,0)$ of dimension $(K+1)\times(K^2+1)$, $\forall k$. We further define $\boldsymbol{L}_k$ as

$$\boldsymbol{L}_k=\Big[\underbrace{\boldsymbol{0}^{K\times K},\cdots,\boldsymbol{0}^{K\times K}}_{k-1},\boldsymbol{I}^{K\times K},\underbrace{\boldsymbol{0}^{K\times K},\cdots,\boldsymbol{0}^{K\times K}}_{K-k},\boldsymbol{0}^{K\times 1}\Big], \tag{2.47}$$

where $\boldsymbol{0}^{K\times K}$ and $\boldsymbol{0}^{K\times 1}$ denote the $K\times K$ all-zero matrix and $K\times 1$ all-zero vector, respectively, and $\boldsymbol{I}^{K\times K}$ denotes the $K\times K$ identity matrix. Thus, (2.46) can be reformulated as

$$\|\boldsymbol{E}_k\boldsymbol{x}+\boldsymbol{n}_k\| \leq \sqrt{1+\frac{1}{\bar{\gamma}_k}}\boldsymbol{h}_{k,k}^H\boldsymbol{L}_k\boldsymbol{x}, \quad \forall k. \tag{2.48}$$

Moreover, we can reformulate the power constraints as

$$\|\boldsymbol{L}_k\boldsymbol{x}\| \leq \sqrt{P_k^{\max}}, \quad \forall k. \tag{2.49}$$

Using (2.48) and (2.49), Problem (P3.3) can be transformed into a SOCP feasibility problem over $\boldsymbol{x}$ and efficiently solvable by existing software [69].

Remark 2.6.2. *It is worth comparing our proposed algorithm with that in [47] for solving the WSR maximization problem (P1.3) for MISO-IC. The algorithm in [47]*

is based on a prior result in [52] that for the special case of two-user MISO-IC, any point on the Pareto boundary of the rate region can be achieved by transmit beamforming vectors that are obtained by linearly combining the ZF and MRT beamformers. In [47], the outer polyblock approximation algorithm is applied to find the optimal beamformer combining coefficients. However, since this result does not hold for MISO-IC with more than two users, the algorithm in [47] cannot be extended to the general K-user MISO-IC with $K > 2$. In contrast, our proposed algorithm can be applied to MISO-IC with arbitrary number of users.

2.7 Numerical Results

In this section, we provide numerical results to validate the proposed algorithms in this chapter. We assume that $\mu_k = 1, \forall k$, i.e., the sum-rate maximization problem is considered. We also assume that $P_k^{\max} = 3, \forall k$. For SIMO-IC and MISO-IC, we further assume that $M_k = 2$ and $N_k = 2$, respectively, $\forall k$. The numerical results with related discussions are presented in the following subsections.

2.7.1 Achievable Rate Region

First, we study the convexity of the achievable rate region of the GIC. In the following, we provide a numerical example to show the rate region of the SISO-IC defined in (2.8) obtained by the rate profile approach presented in Section 2.6.2. Specifically, a 2-user SISO-IC is considered, i.e., $K = 2$, for which the channel is given as

$$\boldsymbol{H} = \begin{bmatrix} 1 & \alpha \\ \alpha & 1 \end{bmatrix}, \tag{2.50}$$

with each element denoting the power of the corresponding channel gain, i.e., $H_{k,j} = |h_{k,j}|^2$. Figs. 2.3 (a) and (b) show the resulted rate regions with $\alpha = 0.5$, i.e., weak interference, and $\alpha = 2$, i.e., strong interference, respectively. It is observed that in

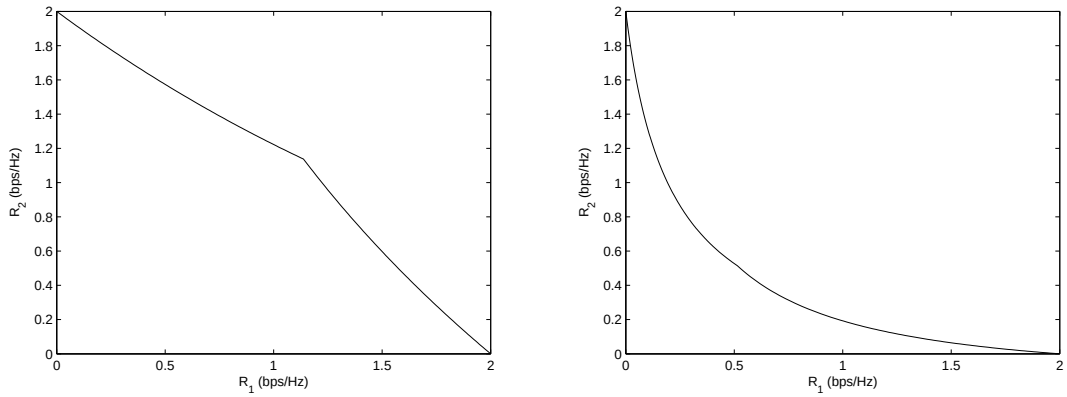

(a) $\alpha = 0.5$ (b) $\alpha = 2$

Figure 2.3: Achievable rate region of 2-user SISO-IC.

the case of weak interference, i.e., $\alpha = 0.5$, the rate region is convex, while in the case of strong interference, i.e., $\alpha = 2$, the rate region is non-convex. As a result, it is necessary to solve problem (P2) using the proposed outer polyblock approximation algorithm, since the rate region in problem (P2) in general cannot be guaranteed to be convex.

2.7.2 Convergence Performance

Next, we study the convergence performance of Algorithm 2.1 for SISO-IC. We assume that there are 4 users, i.e., $K = 4$, and there is a minimum rate constraint for each user with $R_k^{\min} = 0.5$, $\forall k$. We set the parameters to control the accuracy of Algorithm 2.1 as $\epsilon = 0.01$ and $\eta = 0.5$. We consider the following matrix:

$$\boldsymbol{H} = \begin{bmatrix} 0.4310 & 0.0022 & 0.0105 & 0.0042 \\ 0.0200 & 0.4102 & 0.0180 & 0.0035 \\ 0.0210 & 0.0200 & 0.5162 & 0.0112 \\ 0.0210 & 0.0021 & 0.0063 & 0.3634 \end{bmatrix}, \tag{2.51}$$

with each element denoting the power of the corresponding channel gain, i.e., $H_{k,j} = \|h_{k,j}\|^2$.

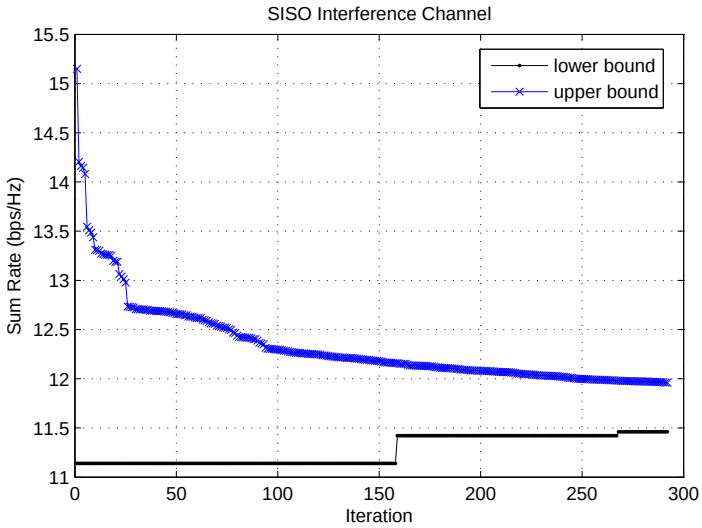

Figure 2.4: Convergence performance of Algorithm 2.1 for SISO-IC with weak interference channel gains.

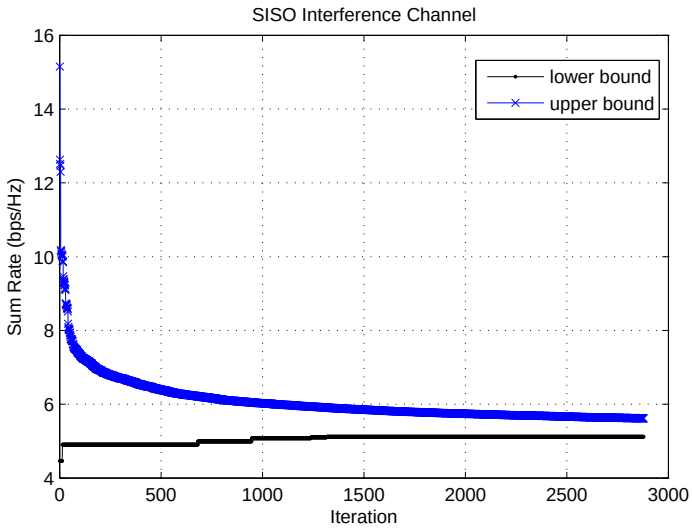

Figure 2.5: Convergence performance of Algorithm 2.1 for SISO-IC with strong interference channel gains.

Fig. 2.4 shows the convergence of Algorithm 2.1 under the above channel setup. It is observed that this algorithm takes about 300 iterations to converge. The converged sum-rate is 11.4605 with users' individual rates given by $[3.1982, 2.6297, 2.8441, 2.7884]$. To verify that the global sum-rate maximum is achieved, we compare the obtained maximum sum-rate with that by an exhaustive search, which is equal to 11.5349. Thus, Algorithm 2.1 does achieve the global optimality of sum-rate maximization within a guaranteed error $11.5349 - 11.4605 = 0.0744$, which is smaller than the set threshold $\eta = 0.5$.

Next, we consider a SISO-IC with stronger cross-user interference channel gains than those given in (2.51) by keeping all diagonal elements of $\boldsymbol{H}$ unchanged, but scaling all off-diagonal elements by 10 times. As shown in Fig. 2.5, for this new channel setup, Algorithm 2.1 takes about 2900 iterations to converge. The converged sum-rate in this case is 5.1184 with users' individual rates given by $[0.5408, 1.9119, 0.5060, 2.1597]$, while that obtained by the exhaustive search is 5.1392. Thus, as compared to the previous case with weaker interference channel gains, the global optimality for sum-rate maximization is achieved in this case with a much slower convergence. The reason is as follows. With stronger interference channel gains, the optimal power allocation for sum-rate maximization is more likely to render some users transmit at their minimum required rates (e.g., user 1 and user 3 in this example). Hence, the corresponding optimal rate values will lie in the strip defined by $\{\boldsymbol{r}^* | R_k^{\min} \leq R_k^* \leq R_k^{\min} + \epsilon\}$ for some k's. Since in Algorithm 2.1 each new polyblock is generated from the previous one by cutting off some unfit portions, the cuts become shallower and shallower as $\tilde{\boldsymbol{z}}^{(n)}$ approaches the above strip. This can be observed from Fig. 2.5 that after the 1300th iteration, the best intersection point $\tilde{\boldsymbol{r}}^{(n)}$ has never changed. However, to make $U(\tilde{\boldsymbol{z}}^{(n)}) - U(\tilde{\boldsymbol{r}}^{(n)}) \leq \eta$ hold, another 1700 iterations are taken just to reduce the value of $U(\tilde{\boldsymbol{z}}^{(n)})$. Since this reduction becomes very inefficient near the strip, the algorithm converges much more slowly to the desired accuracy with the increasing of interference channel gains. From this observation, we infer that the values of ϵ and η need to be properly set to balance

Table 2.5: Selection of ϵ on the Performance of the Proposed Algorithm

Value of ϵ	Number of iterations	Converged WSR
0.05	8183	4.7625
0.10	3498	4.7438
0.15	2212	4.7275
0.20	1642	4.6942
0.25	1396	4.6825
0.30	1148	4.6620
0.35	1029	4.6350
0.40	866	4.6165
0.45	651	4.5880

between the accuracy and convergence speed of our proposed algorithm.

Next, we give another example to illustrate the important role of parameter ϵ in balancing between the accuracy and convergence speed of our proposed algorithm. We assume that $K = 3$, and there are no minimum rate requirements for the users. We consider the following channel matrix:

$$\boldsymbol{H} = \begin{bmatrix} 0.4310 & 0.0187 & 0.0893 \\ 0.1700 & 0.4102 & 0.1530 \\ 0.1785 & 0.1700 & 0.5162 \end{bmatrix}, \tag{2.52}$$

with $H_{k,j} = \|h_{k,j}\|^2$. By an exhaustive search, the optimal sum-rate is obtained as 4.8079 with users' individual rates given by $[3.2146, 1.5933, 0]$.

Table 2.5 shows the convergence speed and the converged sum-rate of our proposed algorithm for different values of ϵ with $\eta = 0.2$. We observe that as ϵ increases, the algorithm convergence speed improves rapidly, but the converged sum-rate decreases. When $\epsilon = 0.45$, the difference between the optimal sum-rate and converged sum-rate is $4.8079 - 4.5880 = 0.2199$, which is even larger than $\eta = 0.2$. This is because that as we show in Section 2.5.2, with non-zero ϵ, we are in fact solving Problem (P2-A) instead of the original problem (P2). Consequently, the proposed algorithm can only guarantee that the difference between the maximum

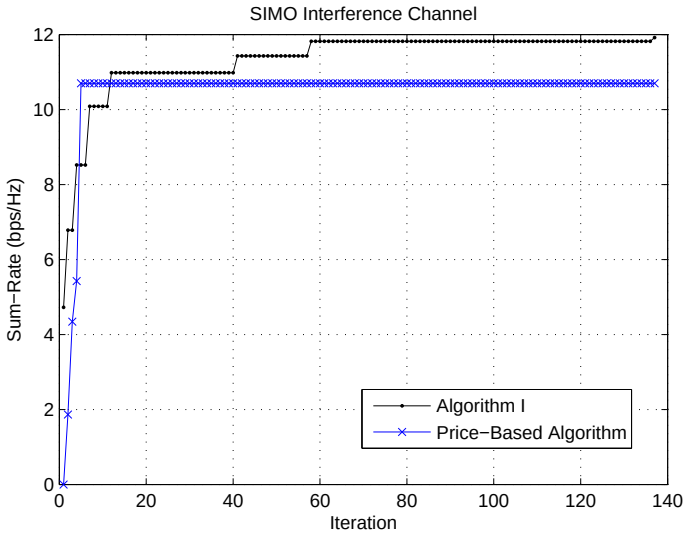

Figure 2.6: Performance comparison for Algorithm 2.1 versus the price-based algorithm in SIMO-IC.

sum-rate of Problem (P2-A) and the converged sum-rate is less than η, but not necessarily for Problem (P2). Thus, if the value of ϵ is selected to be too large such that all the η-optimal solutions lie in the excluded strips, the difference of the converged sum-rate and the maximum sum-rate of Problem (P2) will be larger than η. Therefore, the value of ϵ should be carefully selected based on the value of η. In this numerical example, we can select $\epsilon = 0.40$ such that the η-optimal solution is still guaranteed and also the converged speed is reasonably fast.

2.7.3 Performance Comparison

A key application of our proposed algorithm is to provide performance upper bounds for other heuristic algorithms designed for WSR maximization in the GIC, especially in the case of MISO-IC where the globally optimal solution by exhaustive search is hardly feasible as the number of transmit antennas per user becomes large. In the following, we provide an example to show how to utilize our proposed algorithm to evaluate the performance of other suboptimal algorithms for WSR maximization in MISO-IC and SIMO-IC.

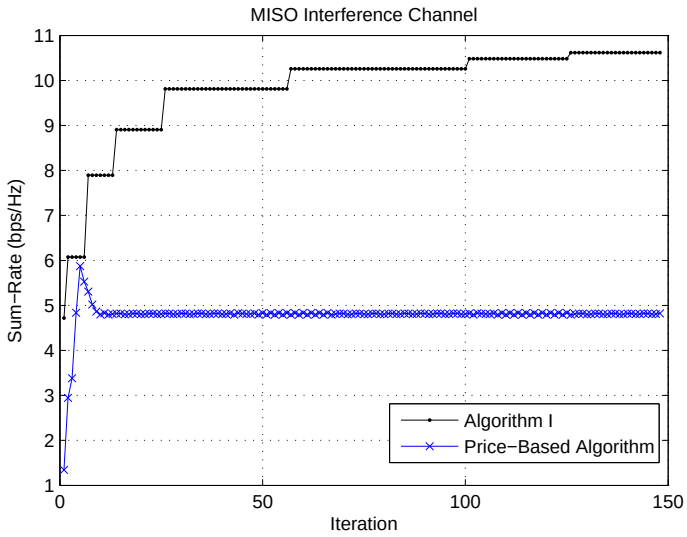

Figure 2.7: Performance comparison for Algorithm 2.1 versus the price-based algorithm in MISO-IC.

We consider the "price-based" suboptimal algorithm, e.g., the ADP algorithm, which is proposed in [28] as an efficient distributed algorithm for WSR maximization in SISO-IC. We provide the details for extensions of ADP to SIMO-IC and MISO-IC in Appendix B.

Figs. 2.6 and 2.7 show the achievable sum-rates by the price-based algorithm versus Algorithm 2.1 for 4-user SIMO-IC and MISO-IC, respectively, without the minimum rate constraints. Each element in all channel vectors involved is randomly generated by the CSCG distribution with zero mean and unit variance. We set the parameters to control the accuracy of Algorithm 2.1 as $\epsilon = 0.01$ and $\eta = 0.5$. In Fig. 2.6, the price-based algorithm converges to the sum-rate of 10.6989 in SIMO-IC, while the maximum sum-rate achieved by Algorithm 2.1 is 11.9182. In Fig. 2.7, the price-based algorithm converges to the sum-rate of 4.8216 (although it has reached almost 6 before convergence) in MISO-IC, while Algorithm 2.1 achieves the maximum sum-rate of 10.6193. Based on these results as well as other numerical examples (not shown here due to the space limitation), we infer that in general the price-based algorithm for SIMO-IC performs better than MISO-IC, as both

compared with our proposed algorithm that achieves the global sum-rate maximum. Moreover, the price-based algorithm for MISO-IC does not converge under certain channel setups, while even when the algorithm converges, the resulted sum-rate can be far from the global maximum. In contrast, for SIMO-IC, the price-based algorithm usually achieves the sum-rate very close to the global maximum, and even converges to it under certain channel setups.

2.8 Chapter Summary

In this chapter, we proposed a new optimization framework to achieve the global optimality of WSR maximization problems in SISO-IC, SIMO-IC, and MISO-IC, respectively, with the interference treated as Gaussian noise. Although the studied problems are non-convex with respect to the power allocation and/or beamforming vectors, we showed that they belong to the class of monotonic optimization over a normal set by reformulating them for maximizing the WSR in the achievable rate regions directly. Therefore, the outer polyblock approximation algorithm can be applied to achieve the global WSR maximum. Furthermore, by utilizing the technique of rate profile, at each iteration of the proposed algorithm, the updated intersection point on the Pareto boundary of the achievable rate region was efficiently obtained via solving a sequence of SINR feasibility problems. It is worth noting that although the developed framework in this chapter is aimed to solve the WSR maximization problem for the GIC, it can be similarly applied to other multiuser communication systems with non-convex rate regions provided that the problem of characterizing the intersection Pareto boundary point with an arbitrary rate-profile vector can be efficiently solved. Finally, the proposed algorithm can be applied to provide upper-bound performance benchmarks for other heuristic algorithms that usually converge faster but only guarantee suboptimal solutions.

Chapter 3

Joint Energy and Information Scheduling in SWIPT

3.1 Introduction

In the previous section, we investigate how to mitigate interference in WIT systems. In this section, we propose a novel approach so-called "opportunistic energy harvesting", to manage interference in SWIPT systems, where the interference can be used for energy harvesting when it is sufficiently strong. In such a SWIPT system, we investigate two practical receiver schemes, namely TS and power splitting (PS). We first consider TS in a point-to-point SWIPT link over a narrowband flat-fading channel subject to time-varying co-channel interference. We assume a single-antenna receiver that can only decode information or harvest energy at any time due to the practical circuit limitation. Therefore, it is important to investigate when the receiver should switch between the two modes of ID and EH, based on the instantaneous channel and interference conditions. We investigate the optimal mode switching rule at the receiver to achieve various performance trade-offs between WIT versus WPT in the case without CSIT, and the joint optimization of transmit power control, information and energy transfer scheduling, and the receiver's mode switching in the case with CSIT. Besides TS, we also briefly discuss the joint information and energy scheduling problem in SWIPT with the PS receiver. Last, we extend the optimal TS and PS schemes from SISO to SIMO SWIPT systems. Our results provide important guidelines for designing SWIPT systems over practical wireless channels subject to both fading and co-channel interference.

3.2 Literature Review

3.2.1 RF Signal Enabled WPT

In conventional energy-constrained wireless networks such as sensor networks, the lifetime of the network is an important performance indicator since sensors are usually equipped with fixed energy supplies, e.g., batteries, which are of limited operation time. Recently, EH has become an appealing solution to prolong the lifetime of wireless networks. Unlike battery-powered networks, energy-harvesting wireless networks potentially have an unlimited energy supply from the environment. Consequently, the research of wireless networks powered by renewable energy has recently drawn a great deal of attentions (see e.g. [70] and references therein).

In addition to other commonly used energy sources such as solar and wind, ambient RF signals can be a viable new source for EH [71–76]. Note that EH from the environment is very susceptible to the availability of environmental energy sources, which are not dedicated to EH, and thus cannot be controlled. As a result, the best strategy for designing conventional EH based communication systems is via optimizing the transmissions and corresponding power consumptions over time based on the intermittent and random harvested energy from the environment [77–79]. In contrast, EH via RF-enabled WPT from dedicated energy sources (power nodes) is stable and controllable. As a result, in RF powered communication systems, we can optimize the amount of energy transferred to each node to improve the network performance, which provides a new design paradigm. It is worth noting that RF based WPT is becoming a more mature technology recently. It is reported in [72] that 3.5mW and 1uW amount of power is harvested at a distance of 0.6 meter and 11 meters, respectively, by using the Powercast EH receivers operating at 915MHz. More information for practical products of RF based WPT can be found at the company website of Powercast (http://www.powercastco.com/).

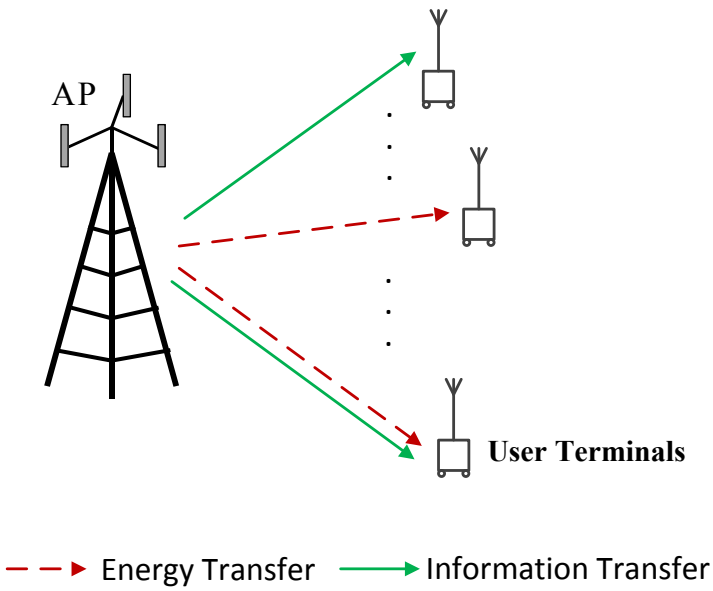

Figure 3.1: Simultaneous wireless information and power transfer (SWIPT).

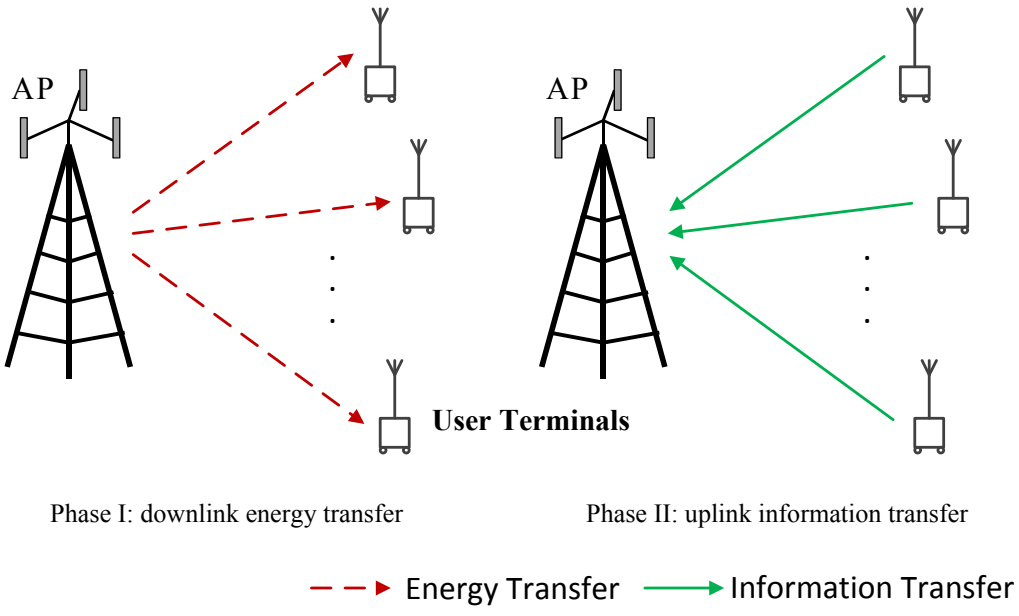

Figure 3.2: Wireless powered communication network (WPCN).

3.2.2 A Unified Study on RF-based WIT and WPT

Due to the recent advancement in RF based WPT, a unified study on WIT and WPT has recently drawn significant attentions. In the literature, there are two main directions of research on this subject, namely "SWIPT", as shown in Fig. 3.1, and "wireless powered communication network (WPCN)", as shown in Fig. 3.2. In a SWIPT system, a fixed access point (AP) with constant power supply broadcasts wireless signals to a set of distributed user terminals, among which some intend to decode information from the received signal, some are interested in harvesting the signal energy, while the others in general aim to decode information and also harvest energy from the same received signal. In such a system, the key design challenge is to find the optimal transmitter and receiver strategies to achieve desired rate-energy performance trade-offs between WIT versus WPT [2]. In a WPCN, on the other hand, the AP coordinates the wireless energy transfer to the users in the downlink, as well as their information transmissions in the uplink using the RF energy harvested in the downlink. For example, a "harvest-then-transmit" protocol is proposed in [80] where the users first harvest energy from the signals broadcast by one single-antenna AP in the downlink, and then use their harvested energy to send independent information to the AP in the uplink based on TDMA. Then, the orthogonal time allocations for the downlink energy transfer and uplink information transmissions of all users are jointly optimized to maximize the network throughput. WCPN is also studied in [81, 82] with a multi-antenna AP.

It is worth pointing out that among the above two promising directions, we focus our study on the SWIPT systems in this thesis.

3.2.3 SWIPT with Ideal Receiver

Two pioneer works on SWIPT are [83, 84], both assuming the ideal receivers that are able to simultaneously harvest and decode the same signal without any loss. In [83], Varshney first proposes the capacity-energy function to characterize the fundamental performance limits of communication channels used

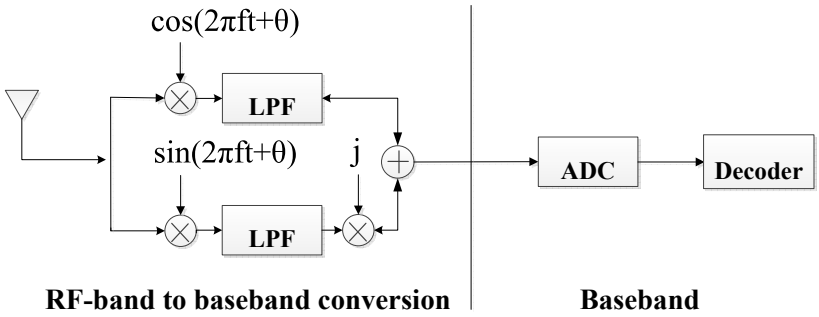

(a) information receiver (IR)

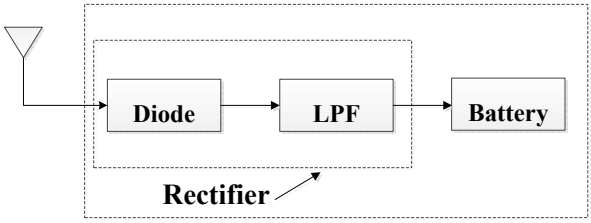

(b) energy receiver (ER)

Figure 3.3: An illustration of the IR and ER.

for both information and energy transfer. For the SISO additive white Gaussian noise (AWGN) channel with amplitude-constrained input, [83] shows that there exist non-trivial trade-offs in maximizing the information rate versus energy simultaneously transferred by optimizing the input signal distribution. However, if the average power constraint is considered, then the above trade-offs do not exist since Gaussian input signal is optimal for both information and power transfer. Furthermore, the authors in [84] extend the results in [83] to a frequency-selective AWGN channel with average power constraint. They show that there exist non-trivial trade-offs in power allocation over frequency domain to maximize the information rate versus energy transferred.

3.2.4 TS and PS Schemes

In [83, 84], the ideal Rx is assumed to be able to decode the information and harvest the energy independently from the same signal. However, due to the existing circuit limitations, this cannot be realizable yet in practical SWIPT systems. To

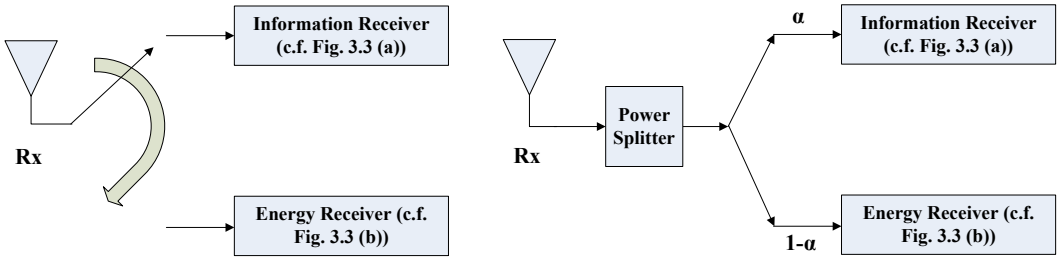

(a) TS Rx (b) PS Rx

Figure 3.4: An illustration of time switching (TS) and power splitting (PS) receivers.

illustrate this, Figs. 3.3 (a) and (b) show the architectures of the state-of-the-art IR and ER, respectively. For the IR, the received RF band signal is first converted to a complex baseband signal and then sampled and digitalized by the analog-to-digital converter (ADC) for further decoding, while for the ER, the received signal is converted to a direct current by a rectifier, which is comprised of a diode and a passive low-pass filter (LPF), and then the direct current is used to charge a rechargeable battery. Clearly, the operations of the IR and ER are very different.[1]

One pioneering work that proposes to study SWIPT with practical receivers is [2]. To tackle the challenge that a practical Rx cannot decode the information and harvest the energy independently from the same signal, two receiver schemes, namely TS and PS, are proposed in [2]. As shown in Fig. 3.4 (a), with a TS receiver, at each time the received signal is either switched to the IR for decoding information or ER for harvesting energy, while in Fig. 3.4 (b), with a PS receiver, $0 \leq \alpha \leq 1$ portion of the received signal power is split to the IR for decoding information and the remaining $1 - \alpha$ portion of signal power is for harvesting energy. It is worth noting that theoretically TS can be regarded as a special case of PS with only on-off power switching, and thus in general PS achieves better rate-energy transmission trade-offs than TS. However, in practice TS is much easier for implementation than PS since the former only requires a switcher at the Rx while the latter needs a more sophisticated power splitter in the RF band [86].

[1]For more details about the operations of the IR and ER, please refer to [85].

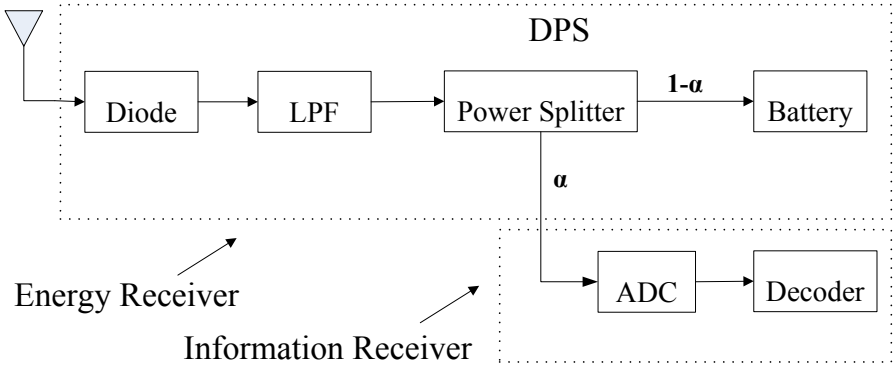

Figure 3.5: Architecture for the integrated information and energy Rx.

Based upon the TS and PS schemes proposed in [2], one simple practical Rx architecture for SWIPT is the so-called separated information and energy receivers, as shown in Fig. 3.4. With separated information and energy receivers, the received signal is split into two signal streams with different power levels, which are fed to the conventional information and energy Rxs shown in Fig. 3.3. In contrast, [85] proposes an interesting new structure for SWIPT with integrated information and energy receivers, as shown in Fig. 3.5. The novelty of this design lies in that the information is modulated onto the energy signal by varying its power levels over time, thus achieving continuous information transfer without degrading the power transfer efficiency. This receiver design integrates the front-end components of the separated information and energy receivers, thus also achieving a smaller form factor. However, the separated receivers shown in Fig. 3.4 are relatively easier for implementation since the off-the-shelf commercially available circuits that are separately designed for ID and EH can be directly applied with only a switcher or a power splitter added. As a result, in the rest of this chapter, we focus our study on the case of separated information and energy receivers.

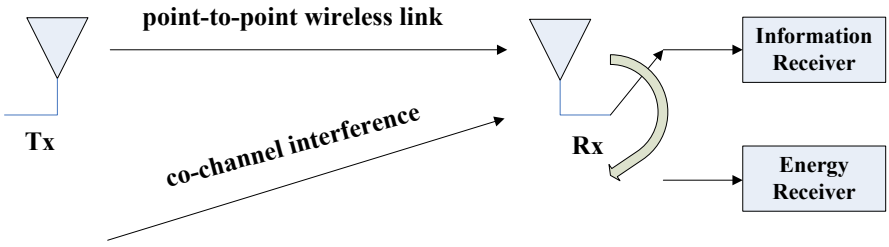

Figure 3.6: System model.

3.3 System Model

As shown in Fig. 3.6, in this chapter we consider a wireless point-to-point link consisting of one pair of single-antenna Tx and Rx over the flat-fading channel. It is assumed that there is an aggregate interference at Rx, which is in the same band as the transmitted signal from Tx, and changes over time. For convenience, we assume that the channel from Tx to Rx follows a block-fading model [87]. Since the coherence time for the time-varying interference is in general different from the channel coherence time, we choose the block duration to be sufficiently small as compared to the minimum coherence time of the channel and interference such that they can both be assumed to be constant during each block transmission. It is worth noting that the above model is an example of the "block interference" channel introduced in [88]. The channel power gain and the interference power at Rx for one particular fading state are denoted by $h(\nu)$ and $I(\nu)$, respectively, where ν denotes the joint fading state. It is assumed that $h(\nu)$ and $I(\nu)$ are two random variables (RVs) with a joint probability density function (PDF) denoted by $f_\nu(h, I)$. At any fading state ν, $h(\nu)$ and $I(\nu)$ are assumed to be perfectly known at Rx. In addition, the additive noise at Rx is assumed to be a CSCG RV with zero mean and variance σ^2.

We consider block-based transmissions at Tx and the TS scheme [2] at Rx for decoding information or harvesting energy at each fading state. Next, we elaborate the encoding and decoding strategies for our system of interest in the following two cases based on the availability of CSI at Tx: Case I: $h(\nu)$ and $I(\nu)$ are unknown at

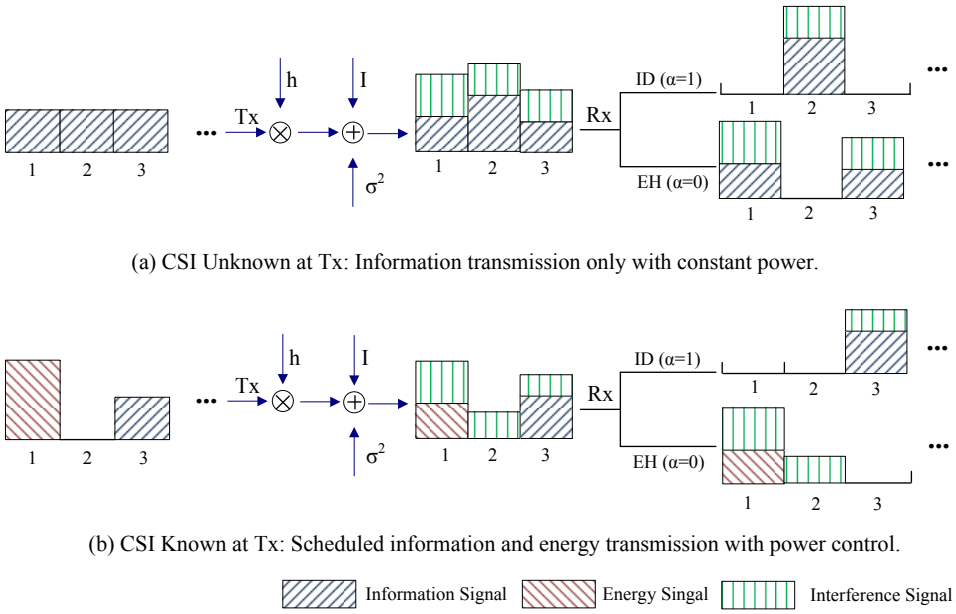

Figure 3.7: Encoding and decoding strategies for wireless information transfer with opportunistic EH (via Rx mode switching). The height of the block shown in the figure denotes the signal power.

Tx for all the fading states of ν, referred to as *CSI Unknown at Tx*; and Case II: $h(\nu)$ and $I(\nu)$ are perfectly known at Tx at each fading state ν, referred to as *CSI Known at Tx* (CSIT).

First, consider the case of CSI Unknown at Tx. As shown in Fig. 3.7 (a), in this case Tx transmits information continuously with constant power P for all the fading states due to the lack of CSIT. At each fading state ν, Rx decides whether to decode the information or harvest the energy from the received signal based on $h(\nu)$ and $I(\nu)$. For example, as shown in Fig. 3.7 (a), time slots 1 and 3 are switched to EH mode at Rx, while time slot 2 is switched to ID mode. For convenience, we define an indicator function to denote the Rx's mode switching at any given ν as follows:

$$\alpha(\nu) = \begin{cases} 1, & \text{ID mode is active} \\ 0, & \text{EH mode is active.} \end{cases} \tag{3.1}$$

Next, we consider the other case with CSIT, i.e., the channel gain $h(\nu)$ and interference power $I(\nu)$ are known at Tx for each fading state ν. In this case, Tx is able to schedule transmission for information and energy transfer to Rx based on the instantaneous CSI. As shown in Fig. 3.7 (b), Tx allocates time slot 1 for energy transfer, time slot 3 for information transfer, and transmits no signals in time slot 2. Accordingly, Rx will be in EH mode (i.e., $\alpha(\nu) = 0$) to harvest energy from the received signal (including the interference) in time slot 1 or solely from the received interference in time slot 2, but in ID mode (i.e., $\alpha(\nu) = 1$) to decode the information in time slot 3. In addition to transmission scheduling, Tx can implement power control based on the CSI to further improve the information/energy transmission efficiency. Let $p(\nu)$ denote the transmit power of Tx at fading state ν. In this chapter, we consider two types of power constraints on $p(\nu)$, namely *average power constraint* (APC) and *peak power constraint* (PPC) [87]. The APC limits the average transmit power of Tx over all the fading states,i.e., $E_\nu[p(\nu)] \leq P_{\text{avg}}$, where $E_\nu[\cdot]$ denotes the expectation over ν. In contrast, the PPC constrains the instantaneous transmit power of Tx at each of the fading states, i.e., $p(\nu) \leq P_{\text{peak}}$, $\forall \nu$. Without loss of generality, we assume $P_{\text{avg}} \leq P_{\text{peak}}$. For convenience, we define the set of feasible power allocation as

$$\mathcal{P} \triangleq \left\{p(\nu) : E_\nu[p(\nu)] \leq P_{\text{avg}}, p(\nu) \leq P_{\text{peak}}, \forall \nu\right\}. \tag{3.2}$$

3.4 WIT and WPT Performance Trade-offs in Fading Channels with TS-based SWIPT

In this chapter, we consider three performance measures at Rx, which are the outage probability and the ergodic capacity for WIT and the average harvested energy for WPT. For delay-limited information transmission, outage probability is a relevant performance indicator. Assuming that the interference is treated as additive Gaussian noise at Rx and the transmitted signal is Gaussian distributed, the

instantaneous mutual information for the Tx-Rx link at fading state ν is expressed as [89]

$$r(\nu) = \log\left(1 + \frac{\alpha(\nu)h(\nu)p(\nu)}{I(\nu) + \sigma^2}\right). \tag{3.3}$$

Note that $r(\nu) = 0$ if Rx switches to EH mode (i.e., $\alpha(\nu) = 0$). Thus, considering a delay-limited transmission with constant rate r_0, following [90] the outage probability at Rx can be expressed as

$$\varepsilon = Pr\left\{r(\nu) < r_0\right\}, \tag{3.4}$$

where $Pr\{\cdot\}$ denotes the probability. For information transfer without CSIT, the Rx-aware outage probability is usually minimized with a constant transmit power, i.e., $p(\nu) = P_{\text{avg}} \triangleq P$, $\forall\nu$ [90], whereas in the case with CSIT, the Tx-aware outage probability can be further minimized with the "truncated channel inversion" based power allocation [91], [89].

Next, consider the case of no-delay-limited information transmission for which the ergodic capacity is a suitable performance measure expressed as

$$R = E_\nu[r(\nu)]. \tag{3.5}$$

For information transfer, if CSIT is not available, the ergodic capacity can be achieved by a single Gaussian codebook with constant transmit power over all different fading states [92]; however, with CSIT, the ergodic capacity can be further maximized by the "water-filling" based power allocation [89].

On the other hand, the amount of energy (normalized to the transmission block duration) that can be harvested at Rx at fading state ν is expressed as $Q(\nu) = \zeta\big(1 - \alpha(\nu)\big)\big(h(\nu)p(\nu) + I(\nu) + \sigma^2\big)$, where ζ is a constant that accounts for the loss in the energy transducer for converting the harvested energy to electrical energy to be stored; for convenience, it is assumed that $\zeta = 1$ in this chapter unless stated

otherwise. Moreover, since the background thermal noise has constant power σ^2 for all the fading states and σ^2 is typically a very small amount for EH, we may ignore it in the expression of $Q(\nu)$. Thus, in the rest of this chapter, we assume

$$Q(\nu) = \big(1 - \alpha(\nu)\big)\big(h(\nu)p(\nu) + I(\nu)\big). \tag{3.6}$$

The average energy that can be harvested at Rx is then given by

$$Q_{\text{avg}} = E_\nu[Q(\nu)]. \tag{3.7}$$

It is easy to see that there exist non-trivial trade-offs in assigning the Rx mode $\alpha(\nu)$ and/or transmit power $p(\nu)$ (in the case of CSIT) to balance between minimizing the outage probability or maximizing the ergodic capacity for WIT versus maximizing the average harvested energy for WPT. To characterize such trade-offs, for the case when information transmission is delay-limited, we introduce a so-called *Outage-Energy* (O-E) region (defined below) that consists of all the achievable non-outage probability (defined as $\delta = 1 - \varepsilon$ with outage probability ε given in (3.4)) and average harvested energy pairs for a given set of transmit power constraints, while for the case when information transmission is not delay-limited, we use another *Rate-Energy* (R-E) region (defined below) that consists of all the achievable ergodic capacity and average harvested energy pairs. More specifically, in the case without (w/o) CSIT, the corresponding O-E region is defined as

$$\begin{aligned}\mathcal{C}_{\text{O-E}}^{\text{w/o CSIT}} \triangleq \bigcup_{\alpha(\nu)\in\{0,1\},\forall\nu} \Big\{ &(\delta, Q_{\text{avg}}) : \\ &\delta \le Pr\left\{r(\nu) \ge r_0\right\}, Q_{\text{avg}} \le E_\nu\left[Q(\nu)\right] \Big\},\end{aligned} \tag{3.8}$$

while in the case with CSIT, the O-E region is defined as

$$\mathcal{C}_{\text{O-E}}^{\text{with CSIT}} \triangleq \bigcup_{p(\nu)\in\mathcal{P},\alpha(\nu)\in\{0,1\},\forall\nu} \Big\{(\delta, Q_{\text{avg}}) : \delta \leq Pr\left\{r(\nu) \geq r_0\right\}, Q_{\text{avg}} \leq E_\nu\left[Q(\nu)\right]\Big\}. \tag{3.9}$$

On the other side, in the case without CSIT, the R-E region is defined as

$$\mathcal{C}_{\text{E-E}}^{\text{w/o CSIT}} \triangleq \bigcup_{\alpha(\nu)\in\{0,1\},\forall\nu} \Big\{(R, Q_{\text{avg}}) : R \leq E_\nu[r(\nu)], Q_{\text{avg}} \leq E_\nu\left[Q(\nu)\right]\Big\}, \tag{3.10}$$

while in the case with CSIT, the R-E region is defined as

$$\mathcal{C}_{\text{R-E}}^{\text{with CSIT}} \triangleq \bigcup_{p(\nu)\in\mathcal{P},\alpha(\nu)\in\{0,1\},\forall\nu} \Big\{(R, Q_{\text{avg}}) : R \leq E_\nu[r(\nu)], Q_{\text{avg}} \leq E_\nu\left[Q(\nu)\right]\Big\}. \tag{3.11}$$

Figs. 3.8 (a) and (b) show examples of the O-E region without or with CSIT (see Sections 3.5.1 and 3.5.2 for the details of computing the O-E regions for these two cases) and the R-E region without or with CSIT (see Sections 3.6.1 and 3.6.2 for the corresponding details), respectively. It is assumed that the average transmit power constraint is $P_{\text{avg}} = 0.1$ watt(W) or 20dBm, and the peak power constraint is $P_{\text{peak}} = 0.2$W or 23dBm. The average operating distance between Tx and Rx is assumed to be $d = 5$ meters, which results in a mean value of 40dB of signal power attenuation at a carrier frequency assumed as $f_c = 900$MHz. It is assumed that $h(\nu)$ is an exponentially distributed RV (i.e., Rayleigh fading) with mean -40dB to be consistent with the average pass loss. It is further assumed that $I(\nu)$, which is independent of $h(\nu)$ $\forall\nu$, is an exponentially distributed RV with mean -57dB. The bandwidth of the transmitted signal is assumed to be 10MHz, and the IR noise is assumed to be white Gaussian with power spectral density -120dBm/Hz

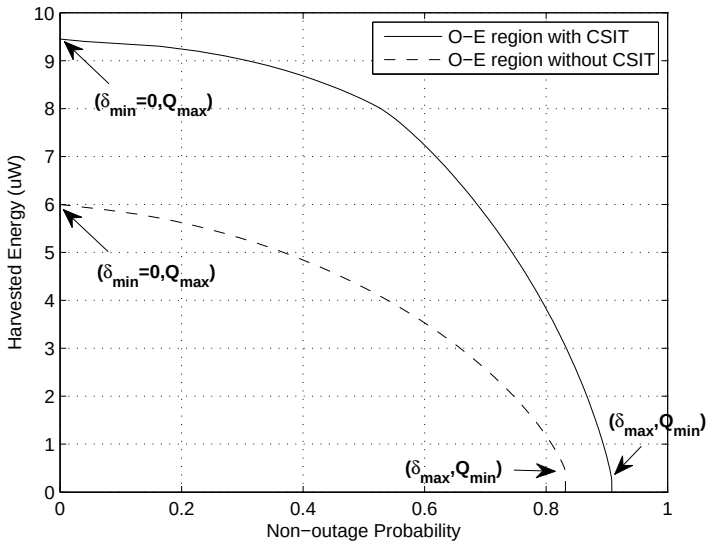

(a) O-E region

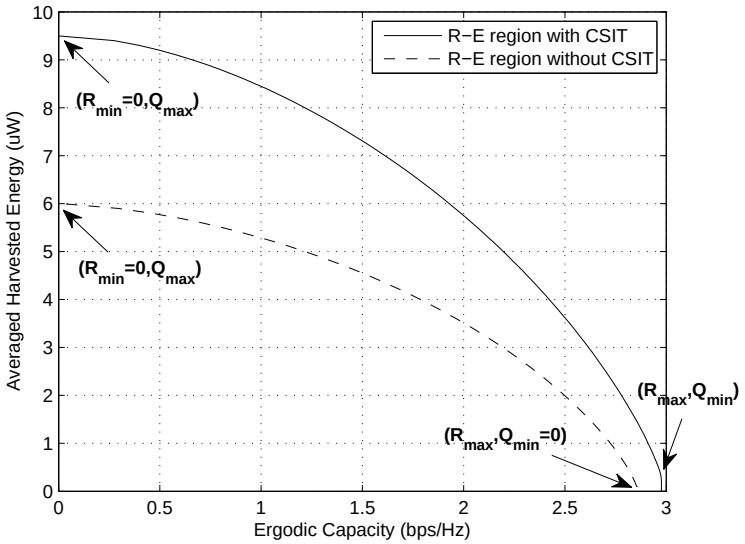

(b) R-E region

Figure 3.8: Examples of O-E region and R-E region with or without CSIT.

or -50dBm over the entire bandwidth of 10MHz. Moreover, the energy conversion efficiency for the energy harvester is assumed to be $\zeta = 0.5$. For the delay-limited information transmission, $r_0 = 1$bps/Hz. It is observed that CSIT helps improve both the achievable outage-energy and rate-energy trade-offs.

It is also observed from Fig. 3.8 that in each region, there are two boundary points that indicate the extreme performance limits, namely, $(\delta_{\max}, Q_{\min})$ and $(\delta_{\min}, Q_{\max})$ for the O-E region, or $(R_{\max}, Q_{\min})$ and $(R_{\min}, Q_{\max})$ for the R-E region. For brevity, characterizations of these vertex points are given in Appendix C.

Since the optimal trade-offs between the non-outage probability/ergodic capacity and the average harvested energy are characterized by the boundary of the corresponding O-E/R-E region, it is important to characterize all the boundary (δ, Q_{avg}) or (R, Q_{avg}) pairs in each case with or without CSIT. From Fig. 3.8, it is easy to observe that if $Q_{\text{avg}} < Q_{\min}$, the non-outage probability $\delta_{\max}$ or ergodic capacity $R_{\max}$ can still be achieved for both cases with and without CSIT. Thus, the remaining boundary of the O-E region yet to be characterized is over the intervals $Q_{\min} \leq Q_{\text{avg}} \leq Q_{\max}$ and $\delta_{\min} \leq \delta \leq \delta_{\max}$, while that of the R-E region is over the intervals $Q_{\min} \leq Q_{\text{avg}} \leq Q_{\max}$ and $R_{\min} \leq R \leq R_{\max}$.

For the O-E region, we introduce the following indicator function for the event of non-outage transmission at fading state ν for the convenience of our subsequent analysis:

$$X(\nu) = \begin{cases} 1, & \text{if } r(\nu) \geq r_0 \\ 0, & \text{otherwise.} \end{cases} \tag{3.12}$$

It thus follows that the non-outage probability δ can be reformulated as

$$\delta = Pr\{r(\nu) \geq r_0\} = E_\nu[X(\nu)]. \tag{3.13}$$

Then, we consider the following two optimization problems.

$$\begin{aligned}(\text{P4}): \ \underset{\{\alpha(\nu)\}}{\texttt{Maximize}} \quad & E_\nu[X(\nu)] \\ \texttt{Subject to} \quad & E_\nu[Q(\nu)] \geq \bar{Q} \\ & \alpha(\nu) \in \{0,1\}, \ \forall \nu\end{aligned}$$

$$\begin{aligned}(\text{P5}): \ \underset{\{p(\nu),\alpha(\nu)\}}{\texttt{Maximize}} \quad & E_\nu[X(\nu)] \\ \texttt{Subject to} \quad & E_\nu[Q(\nu)] \geq \bar{Q} \\ & p(\nu) \in \mathcal{P}, \ \forall \nu \\ & \alpha(\nu) \in \{0,1\}, \ \forall \nu\end{aligned}$$

where $\bar{Q}$ is a target average harvested energy required to maintain the Rx's operation. By solving problem (P4) or (P5) for all $Q_{\min} \leq \bar{Q} \leq Q_{\max}$, we are able to characterize the entire boundary of the O-E region for the case without CSIT (defined in (3.8)) or with CSIT (defined in (3.9)).

Similarly, for the R-E region, we consider the following two optimization problems.

$$\begin{aligned}(\text{P6}): \ \underset{\{\alpha(\nu)\}}{\texttt{Maximize}} \quad & E_\nu[r(\nu)] \\ \texttt{Subject to} \quad & E_\nu[Q(\nu)] \geq \bar{Q} \\ & \alpha(\nu) \in \{0,1\}, \ \forall \nu\end{aligned}$$

$$\begin{aligned}(\text{P7}): \ \underset{\{p(\nu),\alpha(\nu)\}}{\texttt{Maximize}} \quad & E_\nu[r(\nu)] \\ \texttt{Subject to} \quad & E_\nu[Q(\nu)] \geq \bar{Q} \\ & p(\nu) \in \mathcal{P}, \ \forall \nu \\ & \alpha(\nu) \in \{0,1\}, \ \forall \nu.\end{aligned}$$

Then, by solving problem (P6) or (P7) for all $Q_{\min} \leq \bar{Q} \leq Q_{\max}$, we can characterize the boundary of the R-E region for the case without CSIT (defined in (3.10)) or with CSIT (defined in (3.11)).

It is observed that the objective function of problem (P5) is in general not concave in $p(\nu)$ even if $\alpha(\nu)$'s are given. Furthermore, due to the integer constraint $\alpha(\nu) \in \{0, 1\}$, $\forall \nu$, Problems (P4)-(P7) are in general non-convex optimization problems. However, it can be verified that all of them satisfy the "time-sharing" condition given in [6]. To show this for problem (P4), let $\Phi_4(\bar{Q})$ denote the optimal problem value given the harvested energy constraint $\bar{Q}$, and $\{\alpha^a(\nu)\}$ and $\{\alpha^b(\nu)\}$ denote the optimal solutions given the harvested energy constraints $\bar{Q}^a$ and $\bar{Q}^b$, respectively. We need to prove that for any $0 \leq \theta \leq 1$, there always exists at least one solution $\{\alpha^c(\nu)\}$ such that $E_\nu[X^c(\nu)] \geq \theta\Phi_4(\bar{Q}^a) + (1-\theta)\Phi_4(\bar{Q}^b)$ and $E_\nu[Q^c(\nu)] \geq \theta\bar{Q}^a + (1-\theta)\bar{Q}^b$, where $Q^c(\nu) = \big(1-\alpha^c(\nu)\big)\big(h(\nu)P + I(\nu)\big)$ and $X^c(\nu)$ is defined accordingly as in (3.12). Due to the space limitation, the above proof is omitted here. In fact, the "time-sharing" condition implies that $\Phi_4(\bar{Q})$ is concave in $\bar{Q}$, which then guarantees the zero duality gap for Problem (P4) according to the convex analysis in [93]. Similarly, it can be shown that strong duality holds for problems (P5)-(P7). Therefore, in the following two sections, we apply the Lagrange duality method to solve problems (P4)-(P7) to obtain the optimal O-E and R-E trade-offs, respectively.

3.5 Outage-Energy Trade-off

In this section, we study the optimal Rx mode switching without/with transmit power control to achieve different trade-offs between the minimum outage probability and the maximum average harvested energy for both cases without and with CSIT by solving problems (P4) and (P5), respectively.

3.5.1 The Case Without CSIT: Optimal Rx Mode Switching

We first study problem (P4) for the CSIT-unknown case to derive the optimal rule at Rx to switch between EH and ID modes. The Lagrangian of problem (P4) is formulated as

$$L(\alpha(\nu), \lambda) = E_\nu[X(\nu)] + \lambda \left(E_\nu[Q(\nu)] - \bar{Q} \right), \tag{3.14}$$

where $\lambda \geq 0$ is the dual variable associated with the harvested energy constraint $\bar{Q}$. Then, the Lagrange dual function of problem (P4) is expressed as

$$g(\lambda) = \max_{\alpha(\nu)\in\{0,1\},\forall\nu} L(\alpha(\nu), \lambda). \tag{3.15}$$

The maximization problem (3.15) can be decoupled into parallel subproblems all having the same structure and each for one fading state. For a particular fading state ν, the associated subproblem is expressed as

$$\max_{\alpha\in\{0,1\}} \quad L_\nu^{\mathrm{O-E}}(\alpha), \tag{3.16}$$

where $L_\nu^{\mathrm{O-E}}(\alpha) = X + \lambda Q$. Note that we have dropped the index ν for the fading state for brevity.

To solve problem (3.16), we need to compare the values of $L_\nu^{\mathrm{O-E}}(\alpha)$ for $\alpha = 1$ and $\alpha = 0$. It follows from (3.6), (3.12) and (3.14) that when $\alpha = 1$,

$$L_\nu^{\mathrm{O-E}}(\alpha = 1) = \begin{cases} 1, & \text{if } \frac{h}{I+\sigma^2} > \frac{e^{r_0}-1}{P} \\ 0, & \text{otherwise} \end{cases} \tag{3.17}$$

and when $\alpha = 0$,

$$L_\nu^{\mathrm{O-E}}(\alpha = 0) = \lambda h P + \lambda I. \tag{3.18}$$

Thus, the optimal solution to problem (3.16) is obtained as

$$\alpha^* = \begin{cases} 1, & \text{if } \frac{h}{I+\sigma^2} > \frac{e^{r_0}-1}{P} \text{ and } \lambda h P + \lambda I < 1 \\ 0, & \text{otherwise.} \end{cases} \tag{3.19}$$

With a given λ, problem (3.15) can be efficiently solved by solving problem (3.16) for different fading states. Problem (P4) is then solved by iteratively solving problem (3.15) with a fixed λ, and updating λ via a simple bisection method until the harvested energy constraint is met with equality [62].

Next, we examine the optimal solution α^* to problem (P4) to gain more insights to the optimal Rx mode switching in the case without CSIT. With a given harvested energy constraint $\bar{Q}$, we define the region on the (h, I) plane consisting of all the points (h, I) for which the optimal solution to Problem (P4) is $\alpha^* = 1$ (versus $\alpha^* = 0$) as the optimal ID region (versus the optimal EH region). Furthermore, let λ^* denote the optimal dual solution to problem (P4) corresponding to the given $\bar{Q}$. Then, from (3.34) the optimal ID region for problem (P4) is expressed as

$$\mathcal{D}_{\text{ID}}(\lambda^*) \triangleq \left\{ \big(h, I\big) : \frac{h}{I+\sigma^2} > \frac{e^{r_0}-1}{P}, 1 > \lambda^* h P + \lambda^* I, h > 0, I > 0 \right\}. \tag{3.20}$$

The rest of the non-negative (h, I) plane is thus the optimal EH region, i.e.,

$$\mathcal{D}_{\text{EH}}(\lambda^*) \triangleq \mathbb{R}_+^2 \backslash \mathcal{D}_{\text{ID}}(\lambda^*), \tag{3.21}$$

where $\mathbb{R}_+^2$ denotes the two-dimensional nonnegative real domain, and $A \backslash B$ denotes the set $\{x | x \in A \text{ and } x \notin B\}$.

An illustration of $\mathcal{D}_{\text{ID}}(\lambda^*)$ and $\mathcal{D}_{\text{EH}}(\lambda^*)$ is shown in Fig. 3.9 with $\bar{Q} > Q_{\min}$. It is noted that to meet the harvested energy constraint $\bar{Q}$, we need to sacrifice (increase) the outage probability for information transfer by allocating some non-outage fading states in the region $\mathcal{H} = \{(h, I) : \log\big(1 + \frac{hP}{I+\sigma^2}\big) \geq r_0\}$ to EH mode. An interesting question here is to decide which portion of $\mathcal{H}$ should be allocated to EH mode. It is observed from Fig. 3.9 that the optimal way is to allocate all (h, I) pairs

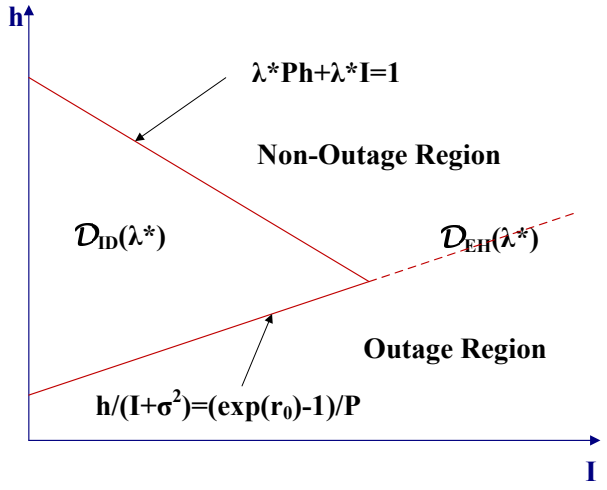

Figure 3.9: Illustration of the optimal ID and EH regions for characterizing O-E trade-offs in the case without CSIT.

satisfying $1 < \lambda^* hP + \lambda^* I$ or $hP + I > \frac{1}{\lambda^*}$ in $\mathcal{H}$ to EH mode, i.e., the fading states with sufficiently large signal plus interference total power values at Rx should be allocated to EH mode. This is reasonable since if we have to allocate a certain number of fading states in $\mathcal{H}$ to EH mode, i.e., increase the transmission outage probability by the same amount, these fading states should be chosen to maximize the harvested energy at Rx.

Furthermore, note that λ^* increases monotonically with $\bar{Q}$. Thus, the boundary line $\lambda^* hP + \lambda^* I = 1$ that separates the optimal ID and EH regions in Fig. 3.9 will be shifted down as λ^* increases, and as a result $\mathcal{D}_{\rm ID}(\lambda^*)$ shrinks. It can be shown that if $\lambda^* \geq \frac{1}{(e^{r_0}-1)\sigma^2}$, then $\mathcal{D}_{\rm ID}(\lambda^*) = \emptyset$, which corresponds to the point $(\delta_{\min} = 0, Q_{\max})$ of the O-E region shown in Fig. 3.8 (a) for the case without CSIT.

It is worth noting that if $I(\nu) = 0$, $\forall \nu$, then the optimal ID region reduces to $\mathcal{D}_{\rm ID}(\lambda^*) = \{h : \frac{(e^{r_0}-1)\sigma^2}{P} \leq h \leq \frac{1}{\lambda^* P}\}$, and the rest of the h-axis is thus the EH region. In this case, the outage fading states $h \in \left(0, \frac{(e^{r_0}-1)\sigma^2}{P}\right)$ are all allocated to EH mode since they cannot be used by ID mode. However, the harvested energy in the outage states only accounts for a small portion of the total harvested energy due to the poor channel gains. Most of the energy is harvested in the interval $h \in \left(\frac{1}{\lambda^* P}, \infty\right)$, i.e.,

when the channel power is above a certain threshold.

3.5.2 The Case With CSIT: Joint Information and Energy Scheduling, Power Control, and Rx Mode Switching

In this subsection, we address the case with CSIT and jointly optimize the energy and information scheduling and power control at Tx, as well as EH/ID mode switching at Rx, as formulated in problem (P5). Let λ and β denote the nonnegative dual variables corresponding to the average harvested energy constraint and average transmit power constraint, respectively. Similarly as for problem (P4), problem (P5) can be decoupled into parallel subproblems each for one particular fading state and expressed as (by ignoring the fading index ν)

$$\max_{0\le p\le P_{\text{peak}},\alpha\in\{0,1\}} \quad L_{\nu}^{\text{O-E}}(p,\alpha), \tag{3.22}$$

where $L_{\nu}^{\text{O-E}}(p,\alpha) = X + \lambda Q - \beta p$. To solve Problem (3.22), we need to compare the optimal values of $L_{\nu}^{\text{O-E}}(p,\alpha)$ for $\alpha = 1$ and $\alpha = 0$, respectively, as shown next.

When $\alpha = 1$, it follows that

$$L_{\nu}^{\text{O-E}}(p,\alpha=1) = \begin{cases} 1-\beta p, & \text{if } p \ge \bar{p} \\ -\beta p, & \text{otherwise} \end{cases} \tag{3.23}$$

where $\bar{p} = \frac{(e^{r_0}-1)(I+\sigma^2)}{h}$. It can be verified that the optimal power allocation for the ID mode to maximize (3.23) subject to $0 \le p \le P_{\text{peak}}$ is the well-known "truncated channel inversion" policy [89] given by

$$p_{\text{ID}} = \begin{cases} \bar{p}, & \text{if } \frac{h}{I+\sigma^2} \ge h_1 \\ 0, & \text{otherwise} \end{cases} \tag{3.24}$$

where $h_1 = \max\{\beta(e^{r_0}-1), \frac{e^{r_0}-1}{P_{\text{peak}}}\}$.

When $\alpha = 0$, it follows that

$$L_\nu^{\mathrm{O-E}}(p, \alpha = 0) = \lambda h p + \lambda I - \beta p. \tag{3.25}$$

Define $h_2 = \frac{\beta}{\lambda}$. Then the optimal power allocation for the EH mode can be expressed as

$$p_{\mathrm{EH}} = \begin{cases} P_{\mathrm{peak}}, & \text{if } h \geq h_2 \\ 0, & \text{otherwise.} \end{cases} \tag{3.26}$$

To summarize, we have

$$L_\nu^{\mathrm{O-E}}(p_{\mathrm{ID}}, \alpha = 1) = \begin{cases} 1 - \beta \bar{p}, & \text{if } \frac{h}{I+\sigma^2} \geq h_1 \\ 0, & \text{otherwise;} \end{cases} \tag{3.27}$$

$$L_\nu^{\mathrm{O-E}}(p_{\mathrm{EH}}, \alpha = 0) = \begin{cases} (\lambda h - \beta) P_{\mathrm{peak}} + \lambda I, & \text{if } h \geq h_2 \\ \lambda I, & \text{otherwise.} \end{cases} \tag{3.28}$$

Then, given any pair of λ and β, the optimal solution to problem (3.22) for fading state ν can be expressed as

$$\alpha^* = \begin{cases} 1, & \text{if } L_\nu^{\mathrm{O-E}}(p_{\mathrm{ID}}, \alpha = 1) > L_\nu^{\mathrm{O-E}}(p_{\mathrm{EH}}, \alpha = 0) \\ 0, & \text{otherwise;} \end{cases} \tag{3.29}$$

$$p^* = \begin{cases} p_{\mathrm{ID}}, & \text{if } \alpha^* = 1 \\ p_{\mathrm{EH}}, & \text{if } \alpha^* = 0. \end{cases} \tag{3.30}$$

Next, to find the optimal dual variables λ^* and β^* for problem (P5), sub-gradient based methods such as the ellipsoid method [62] can be applied. It can be shown that the sub-gradient for updating (λ, β) is $[E_\nu[Q^*(\nu)] - \bar{Q}, P_{\mathrm{avg}} - E_\nu[p^*(\nu)]]$, where $Q^*(\nu)$ and $p^*(\nu)$ denote the harvested energy and transmit power at fading state ν, respectively, after solving problem (3.22) for a given pair of λ and β. Hence, problem (P5) is solved.

Next, we investigate further the optimal information/energy transfer scheduling

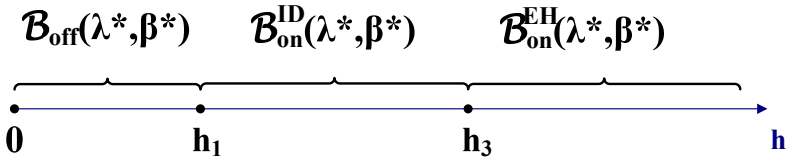

Figure 3.10: Illustration of the optimal Tx and Rx modes for characterizing O-E trade-offs in the case with CSIT. It is assumed that $I(\nu) = 0$, $\forall \nu$, and $h_1 \geq h_2$.

and power control at Tx, as well as the optimal mode switching at Rx. For simplicity, we only study the case of $I(\nu) = 0$, $\forall \nu$. From the above analysis, it follows that there are three possible transmission modes at Tx for the case with CSIT: "information transfer mode" with channel inversion power control, "energy transfer mode" with peak transmit power, and "silent mode" with no transmission, where the first transmission mode corresponds to ID mode at Rx and the second transmission mode corresponds to EH mode at Rx. We thus define $\mathcal{B}_{\text{on}}^{\text{ID}}$, $\mathcal{B}_{\text{on}}^{\text{EH}}$, and $\mathcal{B}_{\text{off}}$ on the non-negative h-axis as the regions corresponding to the above three modes, respectively. Since the explicit expressions for characterizing these regions are complicated and depend on the values of $\bar{Q}$ and P_{avg}, in the following we will study $\mathcal{B}_{\text{on}}^{\text{ID}}$, $\mathcal{B}_{\text{on}}^{\text{EH}}$, and $\mathcal{B}_{\text{off}}$ in the special case of $h_1 \geq h_2$ to shed some light on the optimal design. Let λ^* and β^* denote the optimal dual solutions to problem (P5). With $h_1 \geq h_2$, it can be shown that $\mathcal{B}_{\text{on}}^{\text{ID}} = \{h : h_1 \leq h \leq h_3\}$, $\mathcal{B}_{\text{on}}^{\text{EH}} = \{h : h > h_3\}$ and $\mathcal{B}_{\text{off}} = \{h : h < h_1\}$, where h_3 is the largest root of the equation: $\lambda^* P_{\text{peak}} h^2 - (\beta^* P_{\text{peak}} + 1)h + \beta^*(e^{r_0} - 1)\sigma^2 = 0$. The proof is omitted here due to the space limitation.

An illustration of $\mathcal{B}_{\text{on}}^{\text{ID}}$, $\mathcal{B}_{\text{on}}^{\text{EH}}$, and $\mathcal{B}_{\text{off}}$ for the case of $I(\nu) = 0$, $\forall \nu$, and $h_1 \geq h_2$ is shown in Fig.3.10. Similar to the case without CSIT (cf. Fig. 3.9), the optimal design for the case with CSIT is still to allocate the best channels to the EH mode rather than the ID mode. However, unlike the case without CSIT, when the channel condition is poor, the Tx in the case with CSIT will shut down its transmission to save power.

3.6 Rate-Energy Trade-off

In this section, we investigate the optimal resource allocation schemes to achieve different trade-offs between the maximum ergodic capacity and maximum averaged harvested energy for the two cases without and with CSIT by solving problems (P6) and (P7), respectively.

3.6.1 The Case Without CSIT: Optimal Rx Mode Switching

First, we study problem (P6) for the CSIT-unknown case to derive the optimal switching rule at Rx between EH and ID modes for characterizing different R-E trade-offs. Similarly as in Section 3.5.1, problem (P6) can be decoupled into parallel subproblems each for one particular fading state ν, expressed as

$$\max_{\alpha\in\{0,1\}} \quad L_{\nu}^{\mathrm{R-E}}(\alpha), \tag{3.31}$$

where $L_{\nu}^{\mathrm{R-E}}(\alpha) = r + \lambda Q$ with $\lambda \geq 0$ denoting the dual variable associated with the harvested energy constraint $\bar{Q}$. Note that we have dropped the index ν of the fading state for brevity.

To solve problem (3.31), we need to compare the values of $L_{\nu}^{\mathrm{R-E}}(\alpha)$ for $\alpha = 1$ and $\alpha = 0$. When $\alpha = 1$, it follows that

$$L_{\nu}^{\mathrm{R-E}}(\alpha = 1) = \log\left(1 + \frac{hP}{I + \sigma^2}\right). \tag{3.32}$$

When $\alpha = 0$, it follows that

$$L_{\nu}^{\mathrm{R-E}}(\alpha = 0) = \lambda hP + \lambda I. \tag{3.33}$$

Thus, the optimal solution to problem (3.31) is obtained as

$$\alpha^* = \begin{cases} 1, & \text{if } \log\left(1+\frac{hP}{I+\sigma^2}\right) > \lambda hP + \lambda I \\ 0, & \text{otherwise.} \end{cases} \tag{3.34}$$

To find the optimal dual variable λ^* to problem (P6), a simple bisection method can be applied until the harvested energy constraint is met with equality. Thus, problem (P6) is efficiently solved.

Similar to Section 3.5.1, in the following we characterize the optimal ID region and EH region to get more insights to the optimal Rx mode switching for characterizing different R-E trade-offs. Let λ^* denote the optimal dual variable corresponding to a given energy target $\bar{Q}$. The optimal ID region can then be expressed as

$$\mathcal{D}_{\text{ID}}(\lambda^*) \triangleq \left\{ \left(h, I\right) : \log\left(1+\frac{hP}{I+\sigma^2}\right) > \lambda^* hP + \lambda^* I \right\}. \tag{3.35}$$

The rest of the non-negative (h, I) plane is thus the optimal EH region, i.e.,

$$\mathcal{D}_{\text{EH}}(\lambda^*) \triangleq \mathbb{R}_+^2 \backslash \mathcal{D}_{\text{ID}}(\lambda^*). \tag{3.36}$$

Define $G(h, I) = \log\left(1+\frac{hP}{I+\sigma^2}\right) - (\lambda^* hP + \lambda^* I)$. Fig. 3.11 gives an illustration of the optimal ID region and EH region for a particular value of $\bar{Q} > Q_{\min}$.

Next, we discuss the optimal mode switching rule at Rx for achieving various R-E trade-offs in the case without CSIT. Similar to the case of O-E trade-off, for meeting the harvested energy constraint $\bar{Q}$, we need to sacrifice (decrease) the ergodic capacity for information transfer by allocating some fading states to EH mode. Similar to the discussions in Section 3.5, the optimal rule is to allocate fading states with largest values of h for information transfer to EH mode. The reason is that although fading states with good direct channel gains are most desirable for ID mode, from (3.32) and (3.33) it is observed that the Lagrangian value of ID mode increases logarithmically with h, while that of EH mode increases linearly with h.

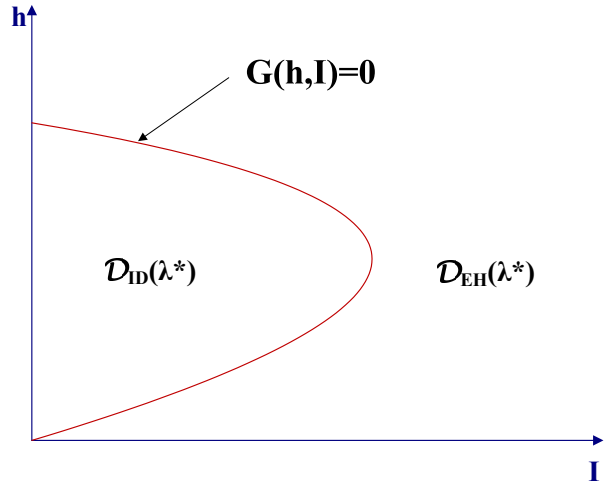

Figure 3.11: Illustration of the optimal ID and EH regions for characterizing R-E trade-offs in the case without CSIT.

As a result, when h is above a certain threshold, the value of $L_\nu^{\mathrm{R-E}}(\alpha = 0)$ will be larger than that of $L_\nu^{\mathrm{R-E}}(\alpha = 1)$. In other words, when h is good enough, we can gain more by switching from ID mode to EH mode.

It is also observed that as the value of λ^* increases, the optimal ID region shrinks. In the following, we derive the value of λ^* corresponding to the point $(R_{\min} = 0, Q_{\max})$ in Fig. 3.8 (b). From Fig. 3.11 it can be observed that $G(h, I)$ has two intersection points with the h-axis, one of which is $(0, 0)$. It can be shown that $G(h, I = 0) = \log\left(1 + \frac{hP}{\sigma^2}\right) - \lambda^* hP$ is a monotonically increasing function of h in the interval $\left(0, \frac{\frac{1}{\lambda^*} - \sigma^2}{P}\right]$, and decreasing function of h in the interval $\left(\frac{\frac{1}{\lambda^*} - \sigma^2}{P}, \infty\right)$. Consequently, if $\frac{\frac{1}{\lambda^*} - \sigma^2}{P} = 0$, i.e., $\lambda^* = \frac{1}{\sigma^2}$, the other intersection point of $G(h, I)$ with the h-axis will coincide with the point $(0, 0)$, and thus $\mathcal{D}_{\mathrm{ID}}(\lambda^*) = \emptyset$ if $\lambda^* \geq \frac{1}{\sigma^2}$.

3.6.2 The Case With CSIT: Joint Information and Energy Scheduling, Power Control, and Rx Mode Switching

In this subsection, we study problem (P7) to achieve different optimal R-E trade-offs for the case of CSIT by jointly optimizing energy and information scheduling and power control at Tx, together with the EH/ID mode switching at Rx.

For problem (P7), let λ and β denote the nonnegative dual variables corresponding to the average harvested energy constraint and average transmit power constraint, respectively. Then, problem (P7) can be decoupled into parallel subproblems each for one particular fading state and expressed as (by ignoring the fading index ν)

$$\max_{0\le p\le P_{\text{peak}},\alpha\in\{0,1\}} \quad L_\nu^{\text{R-E}}(p,\alpha), \tag{3.37}$$

where $L_\nu^{\text{R-E}}(p,\alpha) = r + \lambda Q - \beta p$. To solve Problem (3.37), we need to compare the maximum values of $L_\nu^{\text{R-E}}(p,\alpha)$ for $\alpha = 1$ and $\alpha = 0$, respectively, as shown next.

When $\alpha = 1$, it follows that

$$L_\nu^{\text{R-E}}(p,\alpha=1) = \log\left(1+\frac{hp}{I+\sigma^2}\right) - \beta p. \tag{3.38}$$

It can be shown that the optimal power allocation for this case is the well-known "water-filling" policy [89]. Let $\tilde{p} = \frac{1}{\beta} - \frac{I+\sigma^2}{h}$. The optimal power allocation for information transfer can be expressed as

$$p_{\text{ID}} = [\tilde{p}]_0^{P_{\text{peak}}}, \tag{3.39}$$

where $[x]_a^b \triangleq \max(\min(x,b),a)$.

When $\alpha = 0$, it follows that $L_\nu^{\text{R-E}}(p,\alpha=0)$ has the same expression as that given in (3.25), and consequently, the optimal power allocation for EH mode, p_{EH}, is given by (3.26).

To summarize, for ID mode, if $\frac{1}{\beta} > P_{\text{peak}}$, we have

$$L_\nu^{\text{R-E}}(p_{\text{ID}},\alpha=1) = \begin{cases} \log(1+\frac{hP_{\text{peak}}}{I+\sigma^2}) - \beta P_{\text{peak}}, & \frac{h}{I+\sigma^2} \ge \frac{1}{\frac{1}{\beta}-P_{\text{peak}}} \\ \log\frac{h}{\beta(I+\sigma^2)} - \left(1-\frac{\beta(I+\sigma^2)}{h}\right), & \beta \le \frac{h}{I+\sigma^2} < \frac{1}{\frac{1}{\beta}-P_{\text{peak}}} \\ 0. & \text{otherwise.} \end{cases} \tag{3.40}$$

If $\frac{1}{\beta} \leq P_{\text{peak}}$, we have

$$L_{\nu}^{\text{R-E}}(p_{\text{ID}}, \alpha = 1) = \begin{cases} \log \frac{h}{\beta(I+\sigma^2)} - \left(1 - \frac{\beta(I+\sigma^2)}{h}\right), & \frac{h}{I+\sigma^2} \geq \beta \\ 0, & \text{otherwise} \end{cases} \tag{3.41}$$

For EH mode, the expression of $L_{\nu}^{\text{R-E}}(p_{\text{EH}}, \alpha = 0)$ is the same as that given in (3.28).

Then, given a pair of λ and β, the optimal solution to problem (3.37) for fading state ν can be expressed as

$$\alpha^* = \begin{cases} 1, & \text{if } L_{\nu}^{\text{R-E}}(p_{\text{ID}}, \alpha = 1) > L_{\nu}^{\text{R-E}}(p_{\text{EH}}, \alpha = 0) \\ 0, & \text{otherwise;} \end{cases} \tag{3.42}$$

$$p^* = \begin{cases} p_{\text{ID}}, & \text{if } \alpha^* = 1 \\ p_{\text{EH}}, & \text{if } \alpha^* = 0. \end{cases} \tag{3.43}$$

Next, to find the optimal dual variables λ^* and β^* for problem (P7), similarly as in Section 3.5.2, the ellipsoid method can be applied. Thus, problem (P7) is efficiently solved.

Next, we investigate further the optimal information/energy transfer scheduling and power control at Tx, as well as the optimal mode switching rule at Rx. For simplicity, we only consider the case of $I(\nu) = 0$, $\forall \nu$. Since there is no interference, it can be observed from (3.42) and (3.43) that there are three possible transmission modes at Tx for the case with CSIT: "information transfer mode" with water-filling power control, "energy transfer mode" with peak transmit power, and "silent mode" with no transmission, where the first transmission mode corresponds to ID mode at Rx and the second transmission mode corresponds to EH mode at Rx. Similar to the analysis in Section 3.5.2, we can define $\mathcal{B}_{\text{on}}^{\text{ID}}$, $\mathcal{B}_{\text{on}}^{\text{EH}}$, and $\mathcal{B}_{\text{off}}$ on the non-negative h-axis as the regions corresponding to the above three modes, respectively. Let λ^* and β^* denote the optimal dual solutions to problem (P7). For brevity, in the following we only present the expressions of the above regions in the case of $\frac{1}{\beta^*} \leq P_{\text{peak}}$. It can be shown that in this case, $\mathcal{B}_{\text{on}}^{\text{ID}} = \{h : \beta^*\sigma^2 \leq h \leq h_4\}$, $\mathcal{B}_{\text{on}}^{\text{EH}} = \{h :$

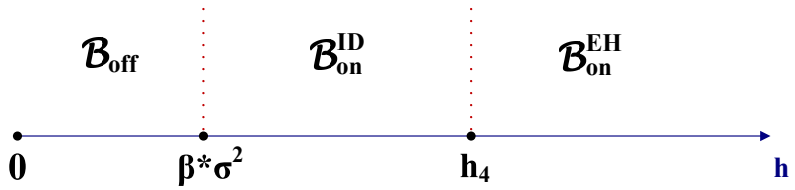

Figure 3.12: Illustration of the optimal Tx and Rx modes for characterizing R-E trade-offs in the case with CSIT. It is assumed that $I(\nu) = 0$, $\forall \nu$, and $\frac{1}{\beta^*} < P_{\text{peak}}$.

$h > h_4\}$ and $\mathcal{B}_{\text{off}} = \{h : h < \beta^*\sigma^2\}$, where h_4 is the largest root of the equation: $\log \frac{h}{\beta^*\sigma^2} - 1 + \frac{\beta^*\sigma^2}{h} - \lambda^* h P_{\text{peak}} + \beta^* P_{\text{peak}} = 0$, which can be obtained by the bisection method over the interval $(\frac{\beta^*}{\lambda^*}, \infty)$. The proof is omitted here due to the space limitation.

An illustration of $\mathcal{B}_{\text{on}}^{\text{ID}}$, $\mathcal{B}_{\text{on}}^{\text{EH}}$, and $\mathcal{B}_{\text{off}}$ in the case without interference and $\beta^* \leq \frac{1}{P_{\text{peak}}}$ is given in Fig. 3.12. Compared with the case without CSIT (cf. Fig. 3.11), it can be similarly observed that the channels with largest power are allocated to EH mode. However, when the channel condition is very poor, the Tx will shut down its transmission to save power in the case with CSIT, instead of transmitting constant power in the case without CSIT.

3.7 Consideration of Rx Energy Consumption

In the above analysis, we have ignored energy consumptions at the Rx for the purpose of exposition. In this section, we extend the result by considering the Rx energy consumption. Firstly, we explain in more details the operations of the Rx in each block and their corresponding energy consumptions as follows. At the beginning of each block, the Rx estimates the channel and interference power gains to determine which of the EH/ID mode it will switch to, where we assume a constant energy Q_0 being consumed. After that, suppose the Rx switches to EH mode. Since practical energy Rxs are mostly passive [2], we assume that the energy consumed by the energy Rx is negligibly small and thus can be ignored. However,

if the Rx switches to ID mode, more substantial energy consumption is required [2]; for simplicity, we assume that a constant power P_I incurs due to the IR when it is switched on. In the following, we will study the effect of the above Rx power consumptions on the optimal operation of the time-switching Rx. Due to the space limitation, we will only study the O-E trade-off in the case without CSIT, while similar results can be obtained for other cases.

Let $Q_I(\nu) = \alpha(\nu)P_I$ denote the Rx power consumption due to ID mode at fading state ν, and $\bar{Q}$ denote the net harvested energy obtained by subtracting Q_0 and $E_\nu[Q_I(\nu)]$ from the harvested energy $E_\nu[Q(\nu)]$. To study the O-E trade-off in the case without CSIT, we modify problem (P4) as

$$\begin{aligned}(\text{P4}'): \ \underset{\{\alpha(\nu)\}}{\texttt{Maximize}} \quad & E_\nu[X(\nu)] \\ \texttt{Subject to} \quad & E_\nu[Q(\nu)] - E_\nu[Q_I(\nu)] - Q_0 \geq \bar{Q} \\ & \alpha(\nu) \in \{0,1\}, \ \forall \nu\end{aligned}$$

Since Q_0 is a constant for all fading states, without loss of generality we absorb this term into $\bar{Q}$ and assume $Q_0 = 0$ in the rest of this chapter for convenience.

Let $\hat{\lambda}^*$ denote the optimal dual variable corresponding to the net harvested energy constraint. We then solve problem (P4') in a similar way as for problem (P4). The optimal solution of problem (P4') can be expressed as

$$\alpha^* = \begin{cases} 1, & \text{if } \frac{h}{I+\sigma^2} > \frac{e^{r_0}-1}{P} \text{ and } \hat{\lambda}^* hP + \hat{\lambda}^* I < 1 - \hat{\lambda}^* P_I \\ 0, & \text{otherwise.} \end{cases} \tag{3.44}$$

As a result, the optima ID region when the Rx energy consumption is considered can be defined as

$$\begin{aligned}\hat{\mathcal{D}}_{\text{ID}}(\hat{\lambda}^*) \triangleq \big\{(h,I): \ & \frac{hP}{I+\sigma^2} \geq e^{r_0} - 1, \\ & 1 - \hat{\lambda}^* P_I \geq \hat{\lambda}^* hP + \hat{\lambda}^* I, \ h \geq 0, \ I \geq 0\big\},\end{aligned} \tag{3.45}$$

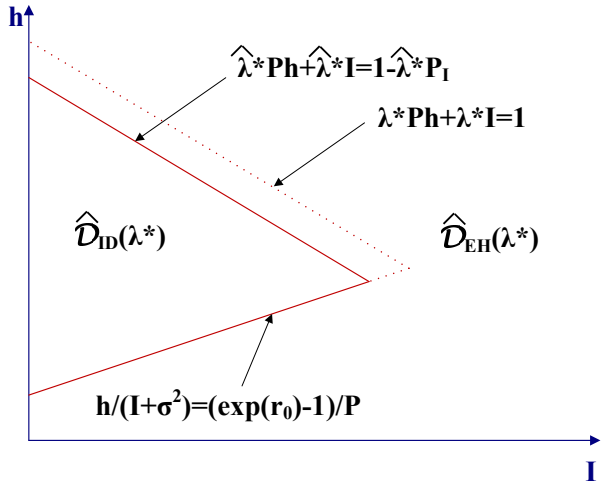

Figure 3.13: Illustration of the optimal ID and EH regions for characterizing O-E trade-offs with versus without Rx energy consumption in the case without CSIT.

and the rest of the plane is the optimal EH region. An illustration of the optimal ID region and EH region is given in Fig. 3.13. By comparing it with Fig. 3.9 for the case without considering the Rx energy consumption, we observe that to harvest the same amount of net energy we need to allocate more fading states in (3.20) to EH mode, i.e., allocating all (h, I) pairs satisfying $\frac{1}{\lambda^*} - P_I \leq hP + I \leq \frac{1}{\lambda^*}$ to EH mode with $P_I > 0$.

Fig. 3.14 shows an example of the O-E region without CSIT but considering the Rx power consumption. The setup is the same as that for Fig. 3.8. It is observed that the Rx power consumption degrades the O-E trade-off. However, $Q_{\max}$ does not change the value because it is achieved when all the fading states are allocated to EH mode and thus P_I has no effects. Moreover, it is observed that when $P_I = 0.5$uW, the same maximum non-outage probability $\delta_{\max}$ as that of the case without Rx energy consumption (i.e., $P_I = 0$) is achieved, while when $P_I = 2$uW, a smaller $\delta_{\max}$ is achieved. The reason is as follows. If P_I is not large enough, the energy harvested in the outage fading states can offset the Rx power consumption in the non-outage fading states. As a result, all the non-outage fading states can still be allocated to ID mode. Otherwise, if P_I is too large, then we have to sacrifice some non-outage

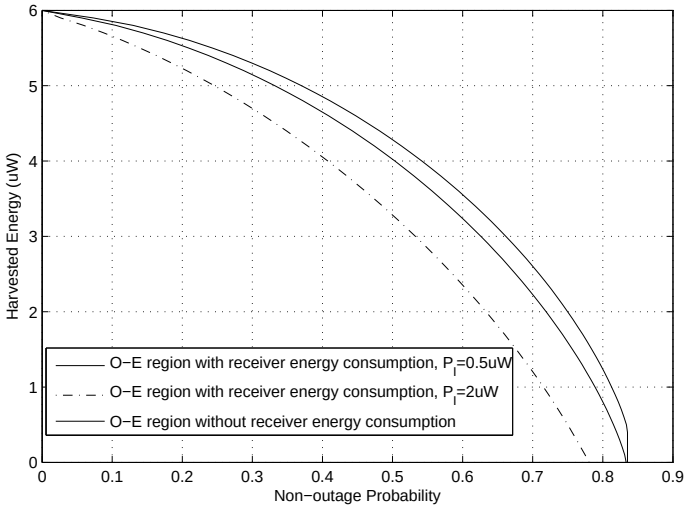

Figure 3.14: O-E region with versus without Rx energy consumption in the case without CSIT.

fading states to EH mode to harvest more energy for ID mode, and thus the value of $\delta_{\max}$ is reduced.

3.8 Performance Evaluation

In this section, we evaluate the performance of the proposed optimal schemes as compared to three suboptimal schemes (to be given later) that are designed to reduce the complexity at Rx and thus yields suboptimal O-E or R-E trade-offs. We assume that Rx needs to have an average harvested energy $\bar{Q}$ to maintain its normal operation. Thus, with a given $\bar{Q}$, we will compute and then compare the minimum outage probability or the maximum ergodic capacity achievable by the optimal and suboptimal schemes.

First, we introduce three suboptimal Rx mode switching rules, namely, *Periodic Switching*, *Interference-Based Switching*, and *SINR-Based Switching* as follows.

- **Periodic Switching**: In this scheme, Rx switches between ID mode and EH mode periodically regardless of the CSI. For convenience, let θ with $0 \leq \theta \leq 1$

denote the portion of time switched to EH mode; then $1-\theta$ denotes the portion of time for ID mode. The value of θ is determined such that the given energy constraint $\bar{Q}$ is satisfied. For example, for the O-E trade-off without CSIT, the maximum harvested energy $Q_{\max}$ is given in (C.1). Thus, θ can be obtained as $\theta = \frac{\bar{Q}}{Q_{\max}}$. For other trade-off cases, θ can be obtained similarly.

- **Interference-Based Switching**: In this scheme, we assume that Rx's mode switching is determined solely by the interference power $I(\nu)$. When $I(\nu) > I_{\text{thr}}$ where I_{thr} denotes a preassigned threshold, Rx switches to EH mode; otherwise, it switches to ID mode. The value of I_{thr} is determined so as to meet the given energy constraint $\bar{Q}$, and the derivation of I_{thr}'s for different trade-off cases are omitted for brevity.

- **SINR-Based Switching**: In this scheme, the mode switching is based on the Rx's SINR $\frac{h(\nu)}{I(\nu)+\sigma^2}$. If $\frac{h(\nu)}{I(\nu)+\sigma^2} > \Gamma_{\text{thr}}$ where Γ_{thr} denotes a predesigned SINR threshold, Rx switches to ID mode; otherwise, it switches to EH mode. The value of Γ_{thr} is determined so as to meet the given energy constraint $\bar{Q}$, while the derivation of Γ_{thr}'s for different trade-off cases are omitted due to the space limitation.

Moreover, if CSIT is available, Tx can implement the optimal power control to minimize the outage probability or maximize the ergodic capacity for information transfer, according to each of the above three suboptimal Rx's mode switching rules.

Next, we show the performance comparison of the three suboptimal schemes with the optimal scheme given in Section 3.5.1 for delay-limited transmission without CSIT and that given in Section 3.6.2 for no-delay-limited transmission with CSIT in Figs. 3.15 and 3.16, respectively. The setup is as follows. The PPC is $P_{\text{peak}} = 20$, the noise power is $\sigma^2 = 0.5$, and for the O-E case, the constant rate requirement is $r_0 = 0.2$ nats/sec/Hz. We further assume that $h(\nu)$ and $I(\nu)$ are independent exponentially distributed RVs with mean 1 and 3, respectively. In addition, the energy target at Rx is set to be $\bar{Q} = 2$.

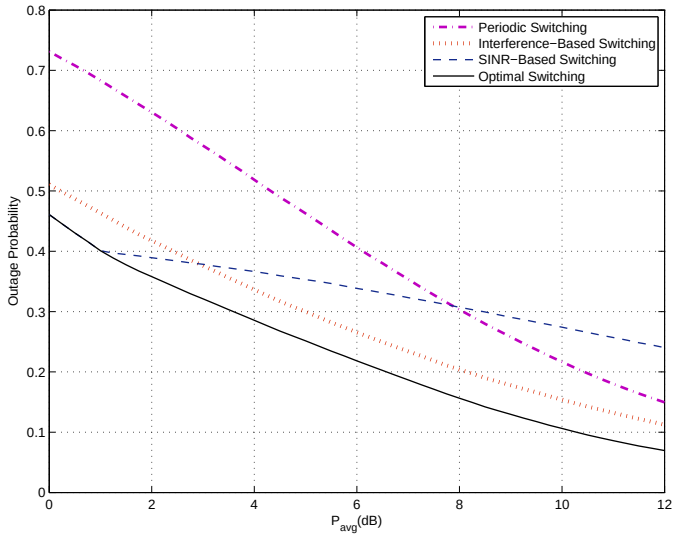

Figure 3.15: Outage probability comparison for delay-limited information transfer in the case without CSIT and $\bar{Q} = 2$.

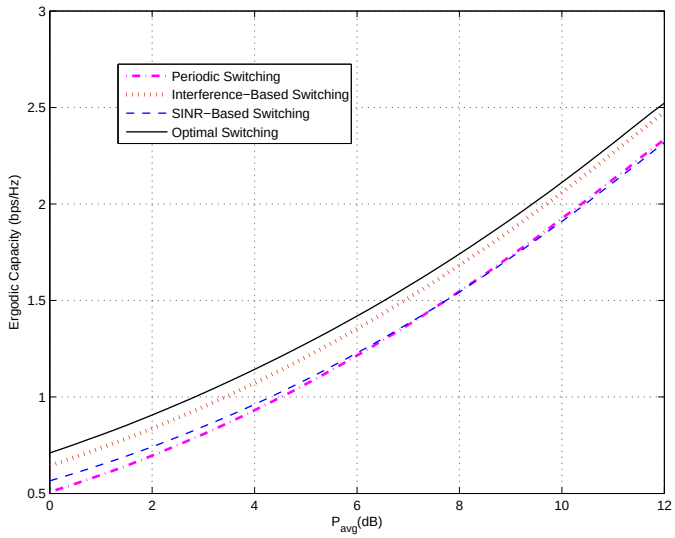

Figure 3.16: Ergodic capacity comparison for no-delay-limited information transfer in the case with CSIT and $\bar{Q} = 2$.

Fig. 3.15 shows the achievable minimum outage probability of different schemes with given $\bar{Q} = 2$ for the delay-limited information transmission without CSIT. It is observed that in general the interference-based switching works pretty well since its performance is similar to that of the optimal switching derived in Section 3.5.1 for all values of P_{avg} with only a small gap. On the contrary, the periodic switching rule does not perform well with an outage probability loss of about $10\% - 20\%$ as compared to the optimal switching.

Another interesting observation is on the performance of the SINR-based switching. It is observed from Fig. 3.15 that when $P_{\text{avg}} \leq 1$dB, the performance of SINR-based switching is the same as that of the optimal switching. However, as P_{avg} increases, its performance degrades. When $P_{\text{avg}} > 8$dB, its achievable outage probability is even higher than that of periodic switching. The above observations can be explained as follows. It can be seen from (C.2) in Appendix that if we view $Q_{\min}$ as a function of P, the following trade-off arises: if the value of P is larger, less number of fading states are allocated to EH mode, but more energy are harvested in each fading state allocated to EH mode. To analyze the behavior of $Q_{\min}$ over P, for the case with $h(\nu) \sim \exp(\lambda_1)$ and $I(\nu) \sim \exp(\lambda_2)$, we can derive an explicit expression of $Q_{\min}$ as follows:

$$Q_{\min} \triangleq f(P) = -\frac{\lambda_2 e^{-\frac{\lambda_1(e^{r_0}-1)\sigma^2}{P}} P}{\lambda_2 P + \lambda_1(e^{r_0}-1)}\Big(\frac{e^{r_0} P}{\lambda_2 P + \lambda_1(e^{r_0}-1)} + \frac{P}{\lambda_1} + (e^{r_0}-1)\sigma^2\Big) + \frac{1}{\lambda_2} + \frac{P}{\lambda_1}. \tag{3.46}$$

It can be shown that in our setup ($\lambda_1 = 1$, $\lambda_2 = \frac{1}{3}$, $r_0 = 0.2$ and $\sigma^2 = 0.5$), $f(P)$ is a monotonically decreasing function with respect to P when $0\text{dB} \leq P \leq 12\text{dB}$. Moreover, when $P = 1$dB, $f(P) = 1.9998$. Thus, if $P \leq 1$dB, it follows that $Q_{\min} \geq \bar{Q} = 2$. In other words, if $P \leq 1$dB, the minimum outage probability with harvested energy constraint $\bar{Q} = 2$ is achieved when Rx switches to ID mode in the fading states $\mathcal{H} = \{(h, I) | \log\big(1 + \frac{hP}{I+\sigma^2}\big) \geq r_0\}$ and switches to EH mode in any subset of $\bar{\mathcal{H}} = \mathbb{R}_+^2 \backslash \mathcal{H}$ to meet the energy constraint. Consequently, the SINR-based

switching is optimal when P is small. When $P >$ 1dB, the minimum harvested energy $Q_{\min}$ cannot meet the energy constraint, and as shown in Section 3.5.1, the optimal switching is to allocate some fading states with the largest value of $hP + I$ in $\mathcal{H}$ to EH mode. However, the SINR-based switching does the opposite way: it tends to allocate the fading states with small value of h to EH mode. Thus, when P is large and a certain number of fading states are allocated to EH mode, the incremental harvested energy by the SINR-based switching is far from that by the optimal switching. To recover this energy loss, more fading states need to be allocated to EH mode. This is why the SINR-based switching results in very high outage probability when P becomes large.

Fig. 3.16 shows the achievable maximum rate of different schemes with given $\bar{Q} = 2$ for the no-delay-limited information transmission with CSIT. Similar to Fig. 3.15, it is observed from Fig. 3.16 that the performance of the interference-based switching is very close to that of the optimal switching derived in Section 3.6.2, while the performances of the other two suboptimal switching rules are notably worse. Under certain conditions (e.g., when SNR$>$ 8dB in Fig. 3.16), the performance of the SINR-based switching can be even worse than that of the periodic switching. This is as expected since although high SINR is preferred by ID, the optimal mode switching rule derived in Section 3.6.2 is determined by both the values of h and I, but has no direct relationship to the ratio of them, i.e., the SINR value. Thus, the performance of the SINR-based switching cannot be guaranteed.

3.9 PS-based SWIPT in SISO Fading Channel

As shown in Fig. 3.4, there are two practical schemes at the Rx side to implement SWIPT: TS and PS. In Sections 3.3-3.7, we have investigated the TS scheme in details. For the completeness, we briefly introduce the PS-based SWIPT in a SISO fading channel in this section.

As shown in Fig. 3.17, we consider a wireless SISO link consisting of one pair of single-antenna Tx and Rx over the flat-fading channel. Note that compared to

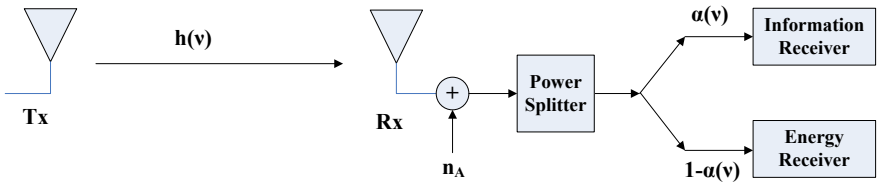

Figure 3.17: SISO system model.

the TS scheme shown in Fig. 3.6, we omit the aggregate interference here for the purpose of exposition. In the following, we introduce how PS works in details. As shown in Fig. 3.17, at Rx, the RF-band signal is received with an additive noise n_A introduced by the Rx antenna, which is assumed to be a CSCG RV with zero mean and variance σ_A^2, denoted by $n_A \sim \mathcal{CN}(0, \sigma_A^2)$, in its baseband equivalent. The RF-band signal is then fed into a power splitter [86] where the signal plus the antenna noise is split to the IR and ER [75] separately. For each fading state ν, the portion of signal power split to ID is denoted by $\alpha(\nu)$ with $0 \leq \alpha(\nu) \leq 1$, and that to EH as $1 - \alpha(\nu)$, where in general $\alpha(\nu)$ can be adjusted over different fading states. Note that this is different from (3.1) for TS with only a binary power allocation between ID and EH. The ID circuit introduces an additional baseband noise n_{ID} to the signal split to the IR, which is assumed to be a CSCG RV with zero mean and variance σ^2, and independent of the antenna noise n_A. As a result, the equivalent noise power for ID is $\alpha(\nu)\sigma_A^2 + \sigma^2$ at fading state ν. On the other hand, in addition to the split signal energy, the ER can harvest $(1 - \alpha(\nu))\sigma_A^2$ amount of energy (normalized by the slot duration) due to the antenna noise n_A. However, in practice, n_A has a negligible influence on both the ID and EH since σ_A^2 is usually much smaller than the noise power introduced by the IR, σ^2, and thus even lower than the average power of the received signal. Thus, in the rest of this chapter, we assume $\sigma_A^2 = 0$ for simplicity.

Fig. 3.18 illustrates the coding and decoding scheme for PS for both the cases without and with CSIT, which is very similar to that for TS shown in Fig. 3.7. For simplicity, in the following we only study the R-E trade-offs for PS. Note that with

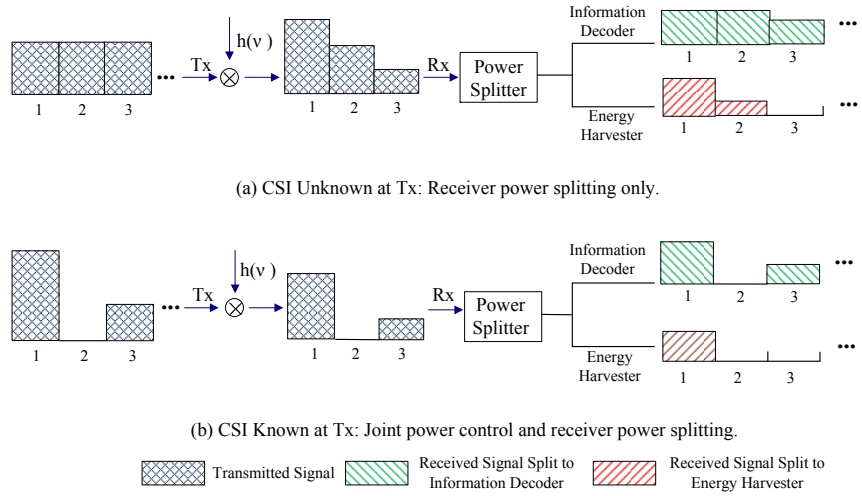

Figure 3.18: Encoding and decoding strategies for wireless information transfer with opportunistic EH (via dynamic PS). The height of block shown in the figure denotes the signal power.

PS, the achievable rate for the Tx-Rx link and the harvested energy at Rx at fading state ν are still expressed as (3.3) and (3.6), respectively, but with $I(\nu) = 0, \forall \nu$. As a result, in the case without CSIT, the R-E region for PS is defined as

$$\mathcal{C}_{\text{R-E}}^{\text{w/o CSIT}} \triangleq \bigcup_{p(\nu)=P, 0\leq\alpha(\nu)\leq 1, \forall\nu} \Big\{ (R, Q_{\text{avg}}) : R \leq E_\nu[r(\nu)], Q_{\text{avg}} \leq E_\nu\left[Q(\nu)\right] \Big\}, \tag{3.47}$$

while in the case with CSIT, the R-E region is defined as

$$\mathcal{C}_{\text{R-E}}^{\text{with CSIT}} \triangleq \bigcup_{p(\nu)\in\mathcal{P}, 0\leq\alpha(\nu)\leq 1, \forall\nu} \Big\{ (R, Q_{\text{avg}}) : R \leq E_\nu[r(\nu)], Q_{\text{avg}} \leq E_\nu\left[Q(\nu)\right] \Big\}. \tag{3.48}$$

Compared with the R-E regions for TS given in (3.10) and (3.11), the only difference lies in that $\alpha(\nu)$ can now be an arbitrary value between 0 and 1 in the case of PS. As a result, similar to the case of TS, the Pareto boundary of the R-E regions for

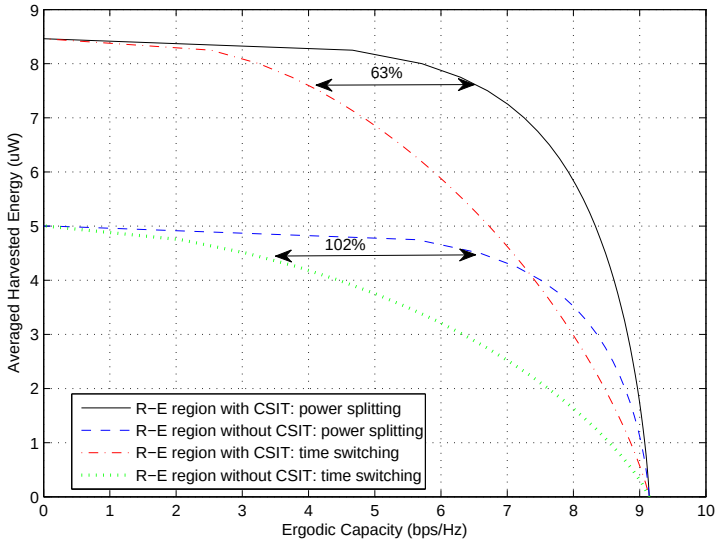

Figure 3.19: Examples of R-E region with versus without CSIT.

the PS case without CSIT (defined in (3.47)) and with CSIT (defined in (3.48)) can be characterized by solving (P6) and (P7) for different $\bar{Q}$'s, respectively, but with $0 \leq \alpha(\nu) \leq 1, \forall \nu$. For more details of computing these regions, please refer to [94].

Fig. 3.19 shows an example of the R-E region without versus with CSIT by the PS scheme. The setup is the same as that for Fig. 3.8 in Section 3.4. For comparison, we also show the R-E regions by TS under the above setup with or without CSIT. It is observed that the CSIT helps improve the rate-energy trade-off at the Rx for both PS and TS schemes, while PS achieves significantly improved R-E trade-offs than TS for both the cases with or without CSIT. For example, when 90% of the maximum harvested energy is achieved, the ergodic capacity is increased by 63% for the case with CSIT and 102% for the case without CSIT. Moreover, it is observed from Fig. 3.19 that when the average harvested energy is smaller than 4.1uW, PS for the case without CSIT even outperforms TS for the case with CSIT. It is worth noting that with CSIT, the ergodic capacity can be increased by the water-filling based power allocation. However, with high SNR, the rate gain by Tx power control is negligibly small. As a result, in Fig. 3.19 the maximum ergodic

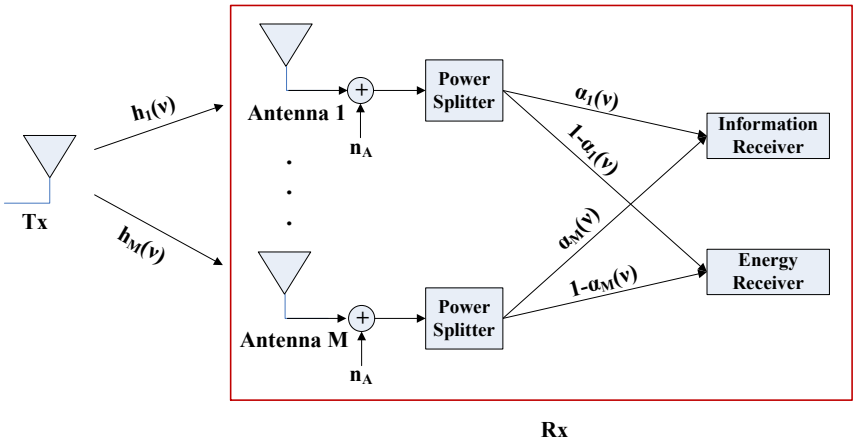

Figure 3.20: PS for the SIMO system.

capacity (achieved by setting $\alpha(\nu) = 1, \forall \nu$) in the case without CSIT is very close to that in the case with CSIT.

3.10 PS and TS for SIMO Fading Channel

In this section, we extend the results for PS and TS in the SISO fading channel to the SIMO fading channel, i.e., when the Rx is equipped with multiple antennas.

3.10.1 PS for SIMO Fading Channel

First, we study the PS scheme for the SIMO system, as shown in Fig. 3.20. Assuming that the Rx is equipped with $M > 1$ antennas, then at any fading state ν, the complex channel and the channel power gain from Tx to the mth antenna of Rx are denoted by $g_m(\nu)$ and $h_m(\nu) = |g_m(\nu)|^2$, $1 \leq m \leq M$, respectively. Without loss of generality, similar to the SISO case, at fading state ν, each receiving antenna m can split $0 \leq \alpha_m(\nu) \leq 1$ portion of the received signal power to the IR, and the remaining $1 - \alpha_m(\nu)$ portion of power to the ER.

For the IR, it is assumed that the maximal ratio combining (MRC) is applied over the signals split from the M receiving antennas. Therefore, at fading state ν,

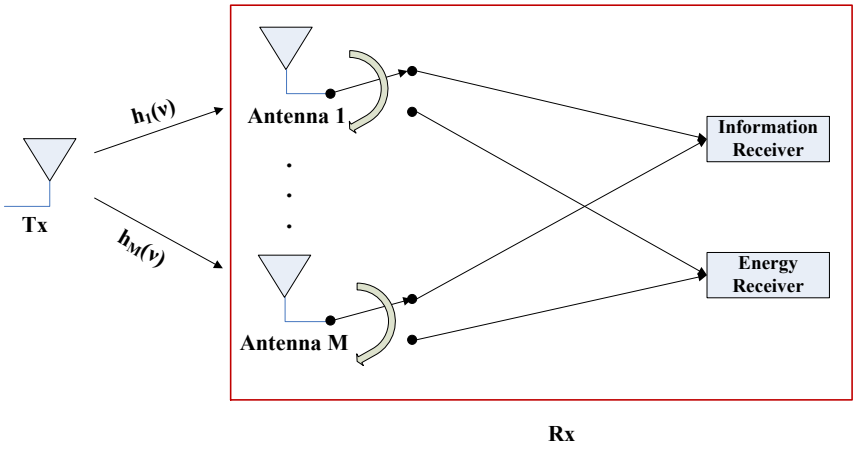

Figure 3.21: Antenna switching for the SIMO system.

the achievable rate can be expressed as

$$r(\nu) = \log\left(1 + \sum_{m=1}^{M} \frac{\alpha_m(\nu) h_m(\nu) p(\nu)}{\sigma^2}\right). \tag{3.49}$$

Moreover, the total harvested energy from the signals split from the M receiving antennas at the ER can be expressed as

$$Q(\nu) = \sum_{m=1}^{M} (1 - \alpha_m(\nu)) h_m(\nu) p(\nu). \tag{3.50}$$

Then, with $r(\nu)$ and $Q(\nu)$ given by (3.49) and (3.50), we can define the achievable R-E regions for the SIMO system in both the cases without and with CSIT as $\mathcal{C}_{\text{R-E}}^{\text{w/o CSIT (SIMO)}}$ and $\mathcal{C}_{\text{R-E}}^{\text{CSIT (SIMO)}}$, respectively, similarly to (3.47) and (3.48) in the SISO case, and characterize their boundaries by solving problems similarly to (P6) and (P7). For more details of how to characterize the Parato boundary of $\mathcal{C}_{\text{R-E}}^{\text{w/o CSIT (SIMO)}}$ and $\mathcal{C}_{\text{R-E}}^{\text{CSIT (SIMO)}}$, please refer to [94].

3.10.2 TS for SIMO Fading Channel

Note that PS for the SIMO system requires multiple power splitters each equipped at one receiving antenna to adjust the PS ratio at each fading state. Practically, this could be very costly to implement. Therefore, we further consider a low-complexity implementation for PS in the SIMO system with multiple receiving antennas, namely antenna switching [2]. As shown in Fig. 3.21, at each fading state, instead of splitting the power at each receiving antenna, the antenna switching scheme simply connects one subset of the receiving antennas (denoted by $\Phi_{\mathrm{ID}}(\nu)$) to IR, with the remaining subset of antennas (denoted by $\Phi_{\mathrm{EH}}(\nu)$) to ER, i.e.,

$$\alpha_m(\nu) = \begin{cases} 1, & \text{if } m \in \Phi_{\mathrm{ID}}, \\ 0, & \text{if } m \in \Phi_{\mathrm{EH}}, \end{cases} \quad 1 \leq m \leq M. \tag{3.51}$$

It is worth noting that antenna switching can be shown equivalent to PS with $\alpha_m(\nu) = \frac{\sum_{m \in \Phi_{\mathrm{ID}}} h_m(\nu) p(\nu)}{\sum_{m=1}^{M} h_m(\nu) p(\nu)}$ for $\forall m, \nu$. However, since antenna switching only requires a switcher at each receiving antenna instead of the more costly power splitter in PS, it is more practically favorable. Note that the Parato boundary of the R-E regions with antenna switching in both the cases without and with CSIT can be obtained by solving (P6) and (P7) with $\alpha_m(\nu)$'s given in (3.51), the details of which can be found in [94].

3.10.3 Performance Comparison between TS and PS in SIMO Fading Channel

In the following, we provide numerical results to compare the performance of PS and TS for the SIMO system. The SIMO channel setup is similar to that in the SISO case for Figs. 3.8 and 3.19 with independent and identically distributed (i.i.d.) exponentially distributed h_m's for each of the receiving antennas.

Figs. 3.22 and 3.23 compare the achievable R-E regions by the PS and TS/antenna switching in the SIMO system without versus with CSIT. It is observed

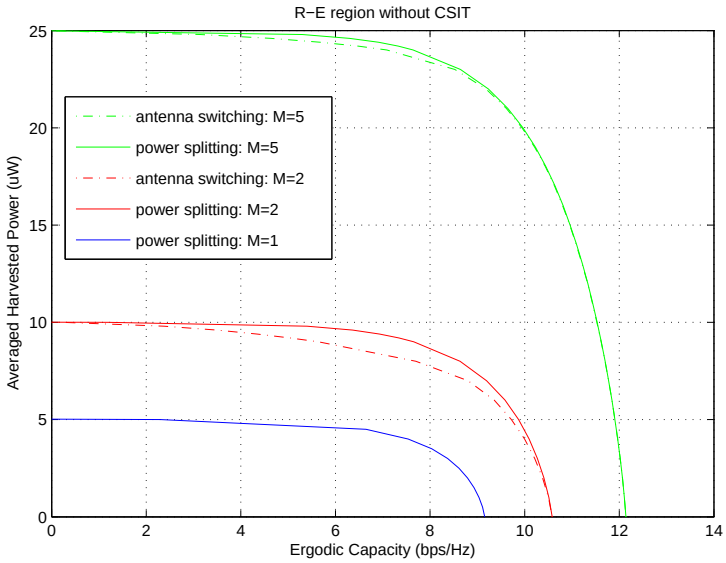

Figure 3.22: R-E regions of PS versus antenna switching for the SIMO system without CSIT.

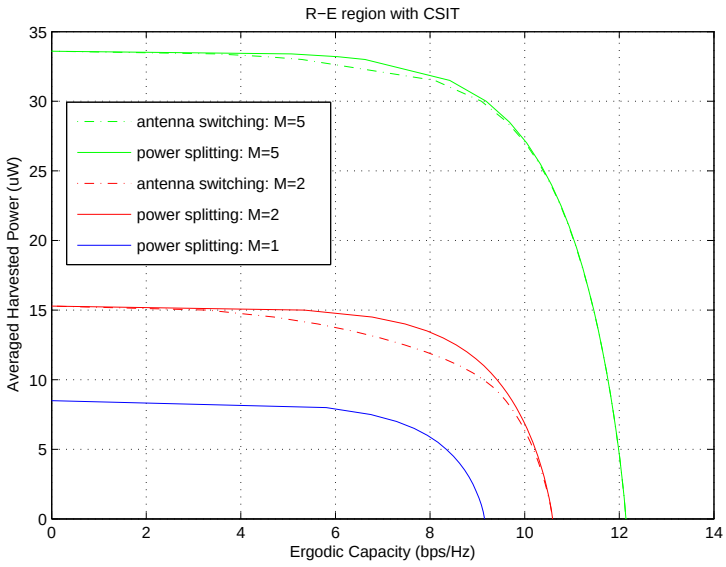

Figure 3.23: R-E regions of PS versus antenna switching for the SIMO system with CSIT.

that as compared to the case of SISO system with $M = 1$, a significantly enlarged R-E region is achieved by using two receiving antennas ($M = 2$). It is also observed that as M increases, the performance of the antenna switching approaches to that of the PS. Since antenna switching is a generalization of TS for the SISO system to the SIMO system, this observation is in sharp contrast to that in Fig. 3.19 where there exists a significant R-E performance loss by TS as compared to PS for the SISO system. This suggests that antenna switching for the SIMO system with a sufficiently large M can be an appealing low-complexity implementation of PS in practice.

3.11 Chapter Summary

In this chapter, we focused our study on the information and energy joint scheduling problem in SWIPT systems with TS Rx, where the interference can be utilized as a source of wireless power. Under a point-to-point flat-fading channel setup with time-varying interference, we derived the optimal ID/EH mode switching rules at the Rx to optimize the outage probability/ergodic capacity versus harvested energy trade-offs. When the CSI is known at the Tx, joint optimization of Tx information/energy scheduling and power control with the Rx ID/EH mode switching was also investigated. Interestingly, we showed that for WIT with opportunistic EH, the best strategy to achieve the optimal O-E and R-E trade-offs is to allocate the fading states with the best direct channel gains to power transfer rather than information transfer. Then, we briefly introduced the PS scheme in the SISO fading channel. Last, we extended the results in SISO system to the SIMO system with multiple receiving antennas, and showed that the practical antenna switching scheme can perform very closely to the optimal PS scheme as the number of receiving antennas increases. Our results provide useful insights to optimally design the SWIPT system over practical wireless channels with fundamental impairments of fading and co-channel interference.

Chapter 4

Physical-Layer Security in SWIPT with MISO Beamforming

4.1 Introduction

In Chapter 3, a point-to-point SWIPT system was investigated. In this chapter, we extend our study to the multiuser SWIPT system. To meet the practical requirement that the ER in general operates with much higher received power as compared to the IR, ERs usually need to be deployed in more proximity to the Tx than IRs in the multiuser SWIPT system. However, due to the broadcast nature of wireless channels, one critical issue arises that the messages sent to IRs can be eavesdropped by ERs, which possess better channels from the Tx. In this chapter, we study this new physical-layer security problem in a multiuser MISO SWIPT system where one multi-antenna Tx sends information and energy simultaneously to an IR and multiple ERs, each with one single antenna. Two problems are investigated with different practical aims: the first problem maximizes the secrecy rate for the IR subject to individual harvested energy constraints of ERs, while the second problem maximizes the weighted sum-energy transferred to ERs subject to a secrecy rate constraint for IR. We solve these two non-convex problems optimally by a general two-stage procedure. First, by fixing the SINR target for ERs (in the first problem) or IR (in the second problem), we obtain the optimal transmit beamforming and power allocation solution by applying the technique of SDR. Then, each of the two problems is solved by a one-dimension search over the optimal SINR target for ERs or IR. Furthermore, for each problem, suboptimal solutions of lower complexity

are proposed in which information and energy beamforming vectors are separately designed from their power allocation. It is worth noting that besides the role as an energy source for WPT as in Chapter 3, in this chapter the interference to the ERs is intentionally generated to play the additional role of AN to facilitate the secrecy information transmission to the IR.

4.2 Literature Review

4.2.1 Energy Beamforming and Near-Far based Scheduling in Multiuser SWIPT Systems

In Chapter 3, two practical receiver schemes for SWIPT, namely TS and PS [2], were introduced. Motivated by such practical designs, substantial researches have been done to advance SWIPT to various multiuser setups, including the BC, e.g., [95–97], the GIC, e.g., [98–100], the relay channel, e.g., [101–106], and the OFDMA systems, e.g., [107, 108]. Furthermore, [109, 110] propose new coding schemes for SWIPT.

Besides the practical circuit limitation that the Rx cannot decode information and harvest energy from the same signal, there are two new challenges in the implementation of SWIPT in a multiuser wireless system. The first challenge is how to enhance the efficiency for WPT, especially for the users at the edge of the coverage area of the Tx. One appealing solution to compensate the pass loss in SWIPT is by employing multiple antennas at the Tx. If the Tx is equipped with multiple-antenna, efficient beamforming techniques can be applied to more effectively focus the signal sent to desired receivers for ID and/or EH. The idea of applying beamforming in SWIPT is first proposed in [2] under the MIMO BC setup with one IR and one ER. Interestingly, it is shown in [2] that one energy beam is optimal at the transmitter to maximize the energy harvested by the ER, which is in sharp contrast to the celebrated spatial multiplexing technique used in the point-to-point MIMO communication system in which multiple information

beams are generally needed to maximize the transmission rate [111]. Inspired by [2], SWIPT with multi-antenna is also studied in [95–101,112,113] under different setups. For example, [112] extends [2] to the general case with arbitrary numbers of IRs and ERs in TS-based SWIPT, where the weighted sum-energy harvested by the ERs is maximized subject to IRs' individual SINR constraints. Specifically, two types of IRs (referred to as Type I and Type II, respectively) are considered in [112], at which the interference caused by the pseudo-random energy signals cannot and can be cancelled, respectively. It is shown that for Type I IRs, no dedicated energy beam is needed in the optimal solution, while for Type II IRs, one energy beam is in general needed. Furthermore, a similar problem is studied in [97] for the case of co-located IRs and ERs in PS-based SWIPT, where transmit beamforming vectors and receive PS ratios are jointly optimized to minimize the transmit power of the AP subject to Rxs' SINR and harvested energy constraints.

Another challenge in implementing multi-user SWIPT is the sensitivity issue for IRs and ERs. In practice, IRs and ERs typically operate with very different power sensitivity, e.g., -60dBm for the IR versus -10dBm for the ER. To meet this practical requirement, a "near-far" or Rx-location based scheme for SWIPT is proposed in [2]. As shown in Fig. 4.1, with the near-far based scheme, ERs are deployed in more proximity to the Tx than IRs for receiving higher signal power for more effective energy reception.

4.2.2 Physical-Layer Security

The Rx-location based transmission scheme for SWIPT gives rise to a new information security issue since ERs, which are closer to the Tx and thus have better channels than IRs, can more easily eavesdrop the information sent to IRs. It is thus important to address this challenging security problem in SWIPT. Traditionally, cryptography technique has been widely used in the higher layers of communication protocols to achieve information secrecy. Recently, an alternative approach, namely "physical-layer security", has attracted significant attentions. In the following, we

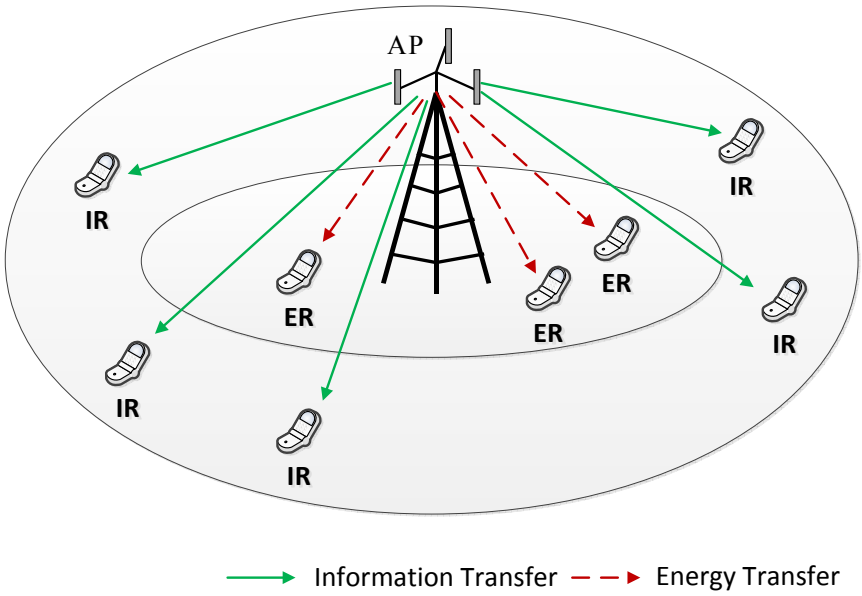

Figure 4.1: A SWIPT system with "near" ERs and "far" IRs.

provide a brief literature review on the physical-layer security research from both the information-theoretic and signal-processing perspectives.

The information-theoretic study of the physical-layer security can be traced back to Wyner's seminal work [114]. Under the assumption that the channel of the eavesdropper is a degraded version of that of the legitimate Rx, [114] shows that the secrecy capacity for the discrete memoryless channel is the difference between the respective mutual informations of the two users. This result is later generalized to the non-degraded case in [115] and the SISO Gaussian wiretap channel in [116]. Motivated by these prior works, substantial information-theoretic studies have been pursued on physical-layer security. For example, the secrecy capacity for the MISO Gaussian wiretap channel is characterized in [117], and that for the MIMO Gaussian wiretap channel is derived in [118–121] via different techniques. Furthermore, the secrecy capacity for the fading wiretap channel is investigated in [122, 123]. For more information about this area of research, please refer to [124] and the reference therein.

Besides information-theoretic approaches, physical-layer security has also been

extensively studied from the signal-processing perspective. For the MISO Gaussian wiretap channel with one legitimate Rx and one eavesdropper, [125] shows that beamforming is optimal to achieve the secrecy capacity, where the optimal beamforming solution is also obtained. Furthermore, an alternating optimization approach is applied in [126] to obtain the suboptimal transmit covariance solution for the MIMO case. For the MISO Gaussian wiretap channel with multiple eavesdroppers, [127] shows that there is an interesting equivalence between the secrecy rate maximization problem and the spectrum sharing capacity maximization problem in a cognitive radio network with the so-called interference temperature constraints for the primary users [128]. Based on the results in [128], beamforming is shown to be optimal for the secrecy rate maximization problem and the optimal beamforming solution is efficiently obtained in [127]. Moreover, [129] extends [127] to the case when the eavesdroppers are equipped with multiple antennas based on the technique of semidefinite program (SDP). The secrecy rate maximization problem in fading channel is also studied in [130–132]. It is worth noting that the above works are under the assumption that the Tx has perfect knowledge of the eavesdroppers' channels, which may not be valid in practical systems since in general the eavesdroppers are passive devices. As a result, various robust schemes are investigated in [133–138] with only imperfect CSI of the eavesdroppers.

Furthermore, a novel approach, namely "AN-assisted secrecy information transmission", is proposed in [3]. In this approach, a fraction of the transmit power is allocated to send artificially generated noise signals to reduce the amount of information that can be decoded by the eavesdroppers. Since in practice eavesdroppers' channels are in general unknown at the Tx, an isotropic transmission scheme is proposed in [3] where the power of AN is uniformly distributed in the null space of the legitimate Rx's channel, and the performance of this practical approach is shown to be nearly optimal at the high SNR regime [139]. With imperfect knowledge of eavesdroppers' channels at the Tx, various AN-aided secrecy transmission schemes are proposed for different channel setups [140–143]. Finally,

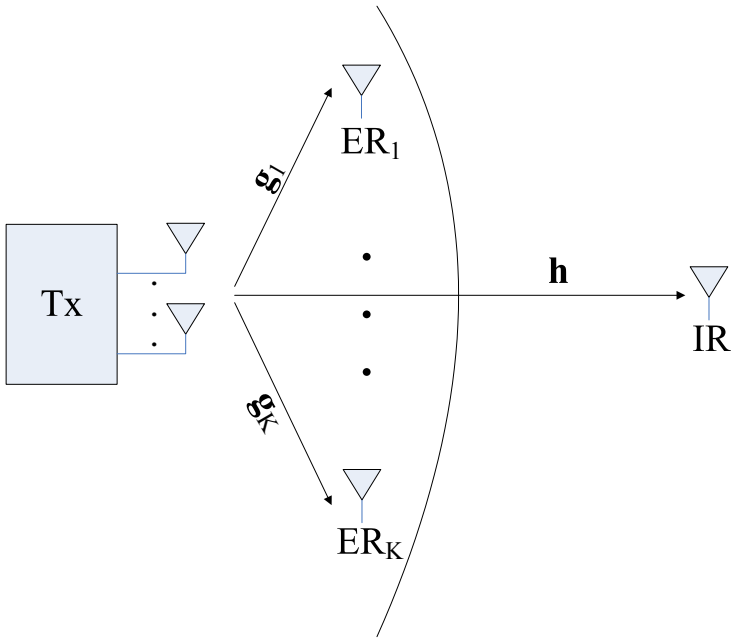

Figure 4.2: A MISO SWIPT system with K "near" ERs and one "far" IR.

the MISO beamforming design problem for the AN-aided secrecy transmission under the assumption that eavesdroppers' channels are perfectly known at the Tx is studied in e.g., [144–146].

4.3 System Model

In this chapter, we consider a multiuser MISO downlink system for SWIPT over a given frequency band as shown in Fig. 4.2. It is assumed that there is one single IR, and K ERs denoted by the set $\mathcal{K}_{\rm EH} = \{{\rm ER}_1, \cdots, {\rm ER}_K\}$, where the IR is assumed to be more distant away from the Tx than all ERs to meet their different received power requirements. Suppose that Tx is equipped with $M > 1$ antennas, while each IR/ER is equipped with one single antenna. We assume linear transmit beamforming at Tx, where the IR is assigned with one dedicated information beam, while the K ERs are in total assigned with $d \leq M$ energy beams without loss of generality. Therefore, the complex baseband transmitted signal of Tx can be

expressed as

$$\boldsymbol{x} = \boldsymbol{v}_0 s_0 + \sum_{i=1}^{d} \boldsymbol{w}_i s_i, \tag{4.1}$$

where $\boldsymbol{v}_0 \in \mathbb{C}^{M\times 1}$ and $\boldsymbol{w}_i \in \mathbb{C}^{M\times 1}$ denote the information beamforming vector and the ith energy beamforming vector, $1 \leq i \leq d$, respectively; s_0 denotes the transmitted signal for the IR, while s_i's, $i = 1, \cdots, d$, denote the energy-carrying signals for energy beams. It is assumed that s_0 is a CSCG random variable with zero mean and unit variance, denoted by $s_0 \sim \mathcal{CN}(0, 1)$. Furthermore, s_i's, $1 \leq i \leq d$, in general can be arbitrary independent random signals each with unit average power. Since in this chapter we consider secret information transmission to the IR, the energy signals s_i, $1 \leq i \leq d$, also play the role of AN to reduce the information rate eavesdropped by ERs [3]. As a result, similarly as [3], we assume that s_i's are i.i.d. CSCG random variables denoted by $s_i \sim \mathcal{CN}(0, 1)$, $\forall i$, since the worst-case noise distribution for the eavesdropping ERs is known to be Gaussian. Suppose that Tx has a transmit sum-power constraint $\bar{P}$; from (4.1), we thus have $E[\boldsymbol{x}^H \boldsymbol{x}] = \|\boldsymbol{v}_0\|^2 + \sum_{i=1}^{d} \|\boldsymbol{w}_i\|^2 \leq \bar{P}$.

In this chapter, we assume a quasi-static fading environment and for convenience denote $\boldsymbol{h} \in \mathbb{C}^{M\times 1}$ and $\boldsymbol{g}_k \in \mathbb{C}^{M\times 1}$ as the conjugated complex channel vectors from Tx to IR and ER_k, $k = 1, \cdots, K$, respectively, where $\boldsymbol{h}$ and $\boldsymbol{g}_k$'s are assumed to be linearly independent. Note that in the case of $K > M$, linear independence in this chapter implies that for any $M \times M$ matrix $\tilde{\boldsymbol{H}}$, in which the M row vectors constitute any subset of channel vectors from $\boldsymbol{h}^H$ and $\boldsymbol{g}_k^H$'s, we have $\text{rank}(\tilde{\boldsymbol{H}}) = M$. Furthermore, let $\rho_h^2 = \|\boldsymbol{h}\|^2/M$ and $\rho_{g_k}^2 = \|\boldsymbol{g}_k\|^2/M$ denote the average per-antenna power of the IR's and ER_k's channels, respectively; then it is assumed that $\rho_{g_k}^2 > \rho_h^2$, $\forall k$, to be consistent with the Rx-location based transmission scheduling (cf. Fig. 4.2). It is worth noting that in the SWIPT system of our interest, since ERs need to assist the Tx in obtaining their channel knowledge to design transmit beamforming to satisfy their individual energy requirements, it is

further assumed that $\boldsymbol{h}$ and $\boldsymbol{g}_k$'s are perfectly known at Tx. [1] The signal received at IR is then expressed as

$$y_0 = \boldsymbol{h}^H \boldsymbol{x} + z_0, \tag{4.2}$$

where $z_0 \sim \mathcal{CN}(0, \sigma_0^2)$ denotes the additive noise at IR. Furthermore, the signal received at ER_k can be expressed as

$$y_k = \boldsymbol{g}_k^H \boldsymbol{x} + z_k, \quad k = 1, \cdots, K, \tag{4.3}$$

where $z_k \sim \mathcal{CN}(0, \sigma_k^2)$ denotes the additive noise at ER_k. It is assumed that z_k's are independent over k.

According to (4.2), the SINR at IR can be expressed as

$$\mathrm{SINR}_0 = \frac{|\boldsymbol{v}_0^H \boldsymbol{h}|^2}{\sum\limits_{i=1}^{d} |\boldsymbol{w}_i^H \boldsymbol{h}|^2 + \sigma_0^2}. \tag{4.4}$$

From (4.3), the SINR at ER_k (suppose that it is an eavesdropper to decode the message for the IR instead of harvesting energy) can be expressed as

$$\mathrm{SINR}_k = \frac{|\boldsymbol{v}_0^H \boldsymbol{g}_k|^2}{\sum\limits_{i=1}^{d} |\boldsymbol{w}_i^H \boldsymbol{g}_k|^2 + \sigma_k^2}, \quad k = 1, \cdots, K. \tag{4.5}$$

The achievable secrecy rate at IR is thus given by [147]:

$$r_0 = \min_{1 \le k \le K} \quad \log_2 (1 + \mathrm{SINR}_0) - \log_2 (1 + \mathrm{SINR}_k). \tag{4.6}$$

Notice that the above achievable rate may be a conservative one in practical SWIPT systems since it is unlikely that all ERs will not harvest energy but instead eavesdrop information for the IR.

[1] This is different from transitional secrecy system where the CSI of the eavesdroppers is imperfect at the Tx since they are passive devices.

On the other hand, for wireless power transfer, due to the broadcast nature of wireless channels, the energy carried by all information and energy beams, i.e., $\boldsymbol{v}_0$ and $\boldsymbol{w}_i$'s ($1 \leq i \leq d$), can all be harvested at each ER. Hence, assuming unit slot duration, the harvested energy of ER_k in each slot is given by [2]:

$$E_k = \zeta \left(|\boldsymbol{v}_0^H \boldsymbol{g}_k|^2 + \sum_{i=1}^{d} |\boldsymbol{w}_i^H \boldsymbol{g}_k|^2 \right), \quad 1 \leq k \leq K, \tag{4.7}$$

where $0 < \zeta \leq 1$ denotes the EH efficiency.

4.4 Problem Formulation

In this chapter, two secrecy beamforming design problems are considered as follows. First, we aim to maximize the secrecy rate of the IR subject to individual harvested energy constraints for all ERs. The first design problem is thus given by

$$\begin{aligned} (\text{P8}): \ \underset{\boldsymbol{v}_0, \{\boldsymbol{w}_i\}}{\texttt{Maximize}} \quad & r_0 \\ \texttt{Subject to} \quad & \zeta \left(|\boldsymbol{v}_0^H \boldsymbol{g}_k|^2 + \sum_{i=1}^{d} |\boldsymbol{w}_i^H \boldsymbol{g}_k|^2 \right) \geq \bar{E}_k, \quad \forall k, \\ & \|\boldsymbol{v}_0\|^2 + \sum_{i=1}^{d} \|\boldsymbol{w}_i\|^2 \leq \bar{P}, \end{aligned}$$

where $\bar{E}_k$ denotes the harvested energy constraint for ER_k. Note that (P8) is applicable for the scenario when ERs have strict EH requirements while the IR only requires an opportunistic information transmission.

Also we are interested in maximizing the weighted sum-energy transferred to ERs subject to a given secrecy rate constraint for IR. Therefore, the problem is

formulated as

$$\begin{aligned}(\text{P9}): \ \underset{\boldsymbol{v}_0,\{\boldsymbol{w}_i\}}{\texttt{Maximize}} \quad & \sum_{k=1}^{K}\mu_k\zeta\left(|\boldsymbol{v}_0^H\boldsymbol{g}_k|^2+\sum_{i=1}^{d}|\boldsymbol{w}_i^H\boldsymbol{g}_k|^2\right)\\ \texttt{Subject to} \quad & r_0\geq\bar{r}_0,\\ & \|\boldsymbol{v}_0\|^2+\sum_{i=1}^{d}\|\boldsymbol{w}_i\|^2\leq\bar{P},\end{aligned}$$

where $\mu_k \geq 0$ denotes the energy weight for ER_k, and $\bar{r}_0$ is the target secrecy rate for IR. (P9) applies for the scenario when the IR has a stringent rate requirement (e.g. delay-limited transmission) but ERs require opportunistic EH (with different priorities).

Notice that there are two conflicting goals in designing the information beamforming vector $\boldsymbol{v}_0$ for both problems (P8) and (P9). On one hand, to maximize the harvested energy at each ER, the power of the received signal at ER_k due to the information beam, i.e., $|\boldsymbol{v}_0^H\boldsymbol{g}_k|^2$, is desired to be as large as possible. However, on the other hand, from the viewpoint of secrecy rate maximization according to (4.4)-(4.6), it follows that $|\boldsymbol{v}_0^H\boldsymbol{g}_k|^2$ should be minimized at each ER_k to avoid any "leakage" information. To resolve the above conflict, we need to properly design the energy beamforming vectors $\boldsymbol{w}_i$, $i = 1, \cdots, d$, since they not only provide direct wireless energy transfer to ERs, but also play the important role of AN to reduce the ERs' SINR in (4.5) for decoding the IR's message.

Since both the secrecy rate r_0 for IR given in (4.6) and the harvested energy E_k of ER_k given in (4.7) are non-concave functions with respect to $\boldsymbol{v}_0$ and $\boldsymbol{w}_i$'s, problems (P8) and (P9) are both non-convex in general, and thus the strong duality does not apply for them [62]. As a result, (P8) and (P9) do not have equivalent solutions under Lagrangian duality. In the following two sections, we address the solutions to these two problems, respectively.

4.5 Proposed Solutions to Secrecy Rate Maximization

In this section, we present both optimal and suboptimal solutions to (P8). First, we study the feasibility of this problem by setting $r_0 = 0$ to (P8) with $\boldsymbol{v}_0 = \mathbf{0}$ for given $\bar{E}_k$'s and $\bar{P}$, i.e,

$$\begin{aligned}(\text{P8}-\text{NoIT}): \ \underset{\{\boldsymbol{w}_i\}}{\texttt{Maximize}} \quad & 0 \\ \texttt{Subject to} \quad & \zeta\left(\sum_{i=1}^{d}|\boldsymbol{w}_i^H\boldsymbol{g}_k|^2\right) \geq \bar{E}_k, \quad 1 \leq k \leq K, \\ & \sum_{i=1}^{d}\|\boldsymbol{w}_i\|^2 \leq \bar{P}.\end{aligned}$$

Note that this problem corresponds to the case when there is no information transmission to IR, and thus $\boldsymbol{w}_i$'s play the only role of energy beams. Define $\boldsymbol{Q} = \sum_{i=1}^{d}\boldsymbol{w}_i\boldsymbol{w}_i^H$. Then we can reformulate (P8-NoIT) as a SDP given by

$$\begin{aligned}(\text{P8}-\text{NoIT}-\text{SDP}): \ \underset{\boldsymbol{Q}}{\texttt{Maximize}} \quad & 0 \\ \texttt{Subject to} \quad & \zeta\text{Tr}(\boldsymbol{G}_k\boldsymbol{Q}) \geq \bar{E}_k, \quad 1 \leq k \leq K, \\ & \text{Tr}(\boldsymbol{Q}) \leq \bar{P}, \\ & \boldsymbol{Q} \succeq \mathbf{0},\end{aligned}$$

where $\boldsymbol{G}_k = \boldsymbol{g}_k\boldsymbol{g}_k^H$. Note that if there exists a feasible solution $\boldsymbol{Q}^*$ to (P8-NoIT-SDP), then with $d = \text{rank}(\boldsymbol{Q}^*)$, the energy beams $\boldsymbol{w}_i^*$, $i = 1, \cdots, d$, obtained by the eigenvalue decomposition (EVD) of $\boldsymbol{Q}^*$, are also feasible to (P8-NoIT). Thereby, the feasibility of (P8) can be checked by solving (P8-NoIT-SDP) via existing software, e.g., CVX [69]. Without loss of generality, in the rest of this chapter, we assume that (P8) is feasible.

Next, we consider the other special case of (P8) when there is no energy transfer

requirement, i.e., $\bar{E}_k = 0$, $\forall k$. In this case, (P8) reduces to

$$(\text{P8}-\text{NoET}): \quad \underset{\boldsymbol{v}_0,\{\boldsymbol{w}_i\}}{\texttt{Maximize}} \quad r_0$$
$$\texttt{Subject to} \quad \|\boldsymbol{v}_0\|^2 + \sum_{i=1}^{d} \|\boldsymbol{w}_i\|^2 \leq \bar{P}.$$

Note that this problem is the conventional secrecy rate maximization under a MISO BC setup and has been solved in [144], for which the details are omitted for brevity. We will discuss the main difference of the optimal solution to (P8) from that of (P8-NoET) in [144] due to the additional harvested energy constraints for ERs in Section 4.5.1 (see Remark 4.5.2).

4.5.1 Optimal Solution

In this subsection, we propose a SDR-based algorithm to solve problem (P8) optimally by reformulating it into two sub-problems. First, similar to [127], we have the following lemma.

Lemma 4.5.1. *There exists a SINR constraint $\gamma_e > 0$ at all ERs such that the following problem*

$$(\text{P8.1}): \quad \underset{\boldsymbol{v}_0,\{\boldsymbol{w}_i\}}{\texttt{Maximize}} \quad \frac{|\boldsymbol{v}_0^H \boldsymbol{h}|^2}{\sum_{i=1}^{d} |\boldsymbol{w}_i^H \boldsymbol{h}|^2 + \sigma_0^2}$$
$$\texttt{Subject to} \quad \frac{|\boldsymbol{v}_0^H \boldsymbol{g}_k|^2}{\sum_{i=1}^{d} |\boldsymbol{w}_i^H \boldsymbol{g}_k|^2 + \sigma_k^2} \leq \gamma_e, \quad 1 \leq k \leq K,$$
$$\zeta \left(|\boldsymbol{v}_0^H \boldsymbol{g}_k|^2 + \sum_{i=1}^{d} |\boldsymbol{w}_i^H \boldsymbol{g}_k|^2 \right) \geq \bar{E}_k, \quad 1 \leq k \leq K,$$
$$\|\boldsymbol{v}_0\|^2 + \sum_{i=1}^{d} \|\boldsymbol{w}_i\|^2 \leq \bar{P},$$

has the same optimal solution to (P8).

Proof. The proof follows directly by showing that for any given optimal solution

of (P8), denoted by $\boldsymbol{v}_0^*$ and $\{\boldsymbol{w}_i^*\}$, it is also optimal for (P8.1) with $\gamma_e = \max\limits_{1\le k\le K} |\boldsymbol{g}_k^H \boldsymbol{v}_0^*|^2 / \left(\sum_{i=1}^d |\boldsymbol{g}_k^H \boldsymbol{w}_i^*|^2 + \sigma_k^2\right)$. □

Let $g_1(\gamma_e)$ denote the optimal value of problem (P8.1) with a given $\gamma_e > 0$. Then, we have the following lemma.

Lemma 4.5.2. *The optimal value of (P8) is the same as that of the following problem.*

$$(\text{P8.2}): \quad \underset{\gamma_e>0}{\texttt{Maximize}} \quad \log_2\left(\frac{1+g_1(\gamma_e)}{1+\gamma_e}\right).$$

Proof. Please refer to Appendix D. □

Let γ_e^* denote the optimal solution to problem (P8.2). Lemmas 4.5.1 and 4.5.2 then imply that with $\gamma_e = \gamma_e^*$, (P8) and (P8.1) have the same optimal solution. Therefore, (P8) can be solved in the following two steps: First, given any $\gamma_e > 0$, we solve (P8.1) to find $g_1(\gamma_e)$; then, we solve (P8.2) to find the optimal γ_e^*, which can be done by a simple one-dimension search over $\gamma_e > 0$. Hence, in the rest of this subsection, we focus on solving (P8.1).

Note that (P8.1) is still non-convex. Define $\boldsymbol{S} = \boldsymbol{v}_0\boldsymbol{v}_0^H$ and $\boldsymbol{Q} = \sum_{i=1}^d \boldsymbol{w}_i\boldsymbol{w}_i^H$. Then it follows that $\text{rank}(\boldsymbol{S}) \le 1$ and $\text{rank}(\boldsymbol{Q}) \le d$. By ignoring the rank-one constraint on $\boldsymbol{S}$, the SDR of problem (P8.1) can be expressed as

$$\begin{aligned}
(\text{P8.1}-\text{SDR}): \quad \underset{\boldsymbol{S},\boldsymbol{Q}}{\texttt{Maximize}} \quad & \frac{\text{Tr}(\boldsymbol{H}\boldsymbol{S})}{\text{Tr}(\boldsymbol{H}\boldsymbol{Q})+\sigma_0^2} \\
\texttt{Subject to} \quad & \text{Tr}(\boldsymbol{G}_k\boldsymbol{S}) \le \gamma_e(\text{Tr}(\boldsymbol{G}_k\boldsymbol{Q})+\sigma_k^2), \quad \forall k, && (4.8)\\
& \zeta(\text{Tr}(\boldsymbol{G}_k\boldsymbol{S})+\text{Tr}(\boldsymbol{G}_k\boldsymbol{Q})) \ge \bar{E}_k, \quad \forall k, && (4.9)\\
& \text{Tr}(\boldsymbol{S})+\text{Tr}(\boldsymbol{Q}) \le \bar{P}, && (4.10)\\
& \boldsymbol{S} \succeq \boldsymbol{0}, \quad \boldsymbol{Q} \succeq \boldsymbol{0}, && (4.11)
\end{aligned}$$

where $\boldsymbol{H} = \boldsymbol{h}\boldsymbol{h}^H$ and $\boldsymbol{G}_k = \boldsymbol{g}_k\boldsymbol{g}_k^H$. If the optimal solution to problem (P8.1-SDR), denoted by $\boldsymbol{S}^*$ and $\boldsymbol{Q}^*$, satisfies $\text{rank}(\boldsymbol{S}^*) = 1$, then the optimal information beam $\boldsymbol{v}_0^*$

and the optimal $d = \text{rank}(\boldsymbol{Q}^*)$ number of energy beams $\boldsymbol{w}_i^*$, $i = 1, \cdots, d$, for problem (P8.1) can be obtained from the EVDs of $\boldsymbol{S}^*$ and $\boldsymbol{Q}^*$, respectively; otherwise, if $\text{rank}(\boldsymbol{S}^*) > 1$, then the optimal value of problem (P8.1-SDR) only serves as an upper bound on that of problem (P8.1). In the following, we check whether $\text{rank}(\boldsymbol{S}^*) = 1$ always holds or not for (P8.1-SDR).

(P8.1-SDR) is non-convex since its objective function is non-concave over $\boldsymbol{S}$ and $\boldsymbol{Q}$. However, we can apply the Charnes-Cooper transformation [148, 149] to reformulate (P8.1-SDR) as an equivalent convex problem.

Lemma 4.5.3. *Problem (P8.1-SDR) is equivalent to the following problem.*

$$
\begin{aligned}
(\text{P8.1}-\text{SDR}-\text{Eqv}): \quad \underset{\boldsymbol{S},\boldsymbol{Q},t}{\texttt{Maximize}} \quad & \text{Tr}(\boldsymbol{H}\boldsymbol{S}) \\
\texttt{Subject to} \quad & \text{Tr}(\boldsymbol{H}\boldsymbol{Q}) + t\sigma_0^2 = 1, && (4.12)\\
& \text{Tr}(\boldsymbol{G}_k\boldsymbol{S}) \le \gamma_e(\text{Tr}(\boldsymbol{G}_k\boldsymbol{Q}) + t\sigma_k^2), \quad \forall k, && (4.13)\\
& \zeta(\text{Tr}(\boldsymbol{G}_k\boldsymbol{S}) + \text{Tr}(\boldsymbol{G}_k\boldsymbol{Q})) \ge t\bar{E}_k, \quad \forall k, && (4.14)\\
& \text{Tr}(\boldsymbol{S}) + \text{Tr}(\boldsymbol{Q}) \le t\bar{P}, && (4.15)\\
& \boldsymbol{S} \succeq \boldsymbol{0}, \quad \boldsymbol{Q} \succeq \boldsymbol{0}, \quad t > 0. && (4.16)
\end{aligned}
$$

Proof. First, given any feasible solution $(\boldsymbol{S}, \boldsymbol{Q})$ to problem (P8.1-SDR), it can be shown that with the solution $(\boldsymbol{S}/(\text{Tr}(\boldsymbol{H}\boldsymbol{Q}) + \sigma_0^2), \boldsymbol{Q}/(\text{Tr}(\boldsymbol{H}\boldsymbol{Q}) + \sigma_0^2), 1/(\text{Tr}(\boldsymbol{H}\boldsymbol{Q}) + \sigma_0^2))$, (P8.1-SDR-Eqv) achieves the same objective value as that of (P8.1-SDR). Second, given any feasible solution $(\boldsymbol{S}, \boldsymbol{Q}, t)$ to (P8.1-SDR-Eqv), it can be similarly shown that with the solution $(\boldsymbol{S}/t, \boldsymbol{Q}/t)$, (P8.1-SDR) achieves the same objective value as that of (P8.1-SDR-Eqv). Therefore, (P8.1-SDR) and (P8.1-SDR-Eqv) have the same optimal value. Lemma 4.5.3 is thus proved. □

According to Lemma 4.5.3, we can obtain the optimal solution to (P8.1-SDR) by solving (P8.1-SDR-Eqv).

Remark 4.5.1. *It is worth noting that in the literature, problem (P8.1-SDR-Eqv) belongs to the so-called "separable SDP" [150] since there are more than one design*

variables, i.e., $\boldsymbol{S}$ *and* $\boldsymbol{Q}$*. According to [150, Theorem 3.2], there exists an optimal solution* $(\boldsymbol{S}^*, \boldsymbol{Q}^*)$ *to (P8.1-SDR-Eqv) such that* $\text{rank}^2(\boldsymbol{S}^*) + \text{rank}^2(\boldsymbol{Q}^*) \leq 2K + 2$*, where* $2K + 2$ *denotes the number of linear constraints given in (4.12)-(4.15). However, this is not sufficient to show* $\text{rank}(\boldsymbol{S}^*) = 1$ *because* K *in our problem can be arbitrarily large. As a result, the well-known result in [150] for separable SDPs cannot be applied in our case to show the tightness of SDR in (P8.1-SDR-Eqv). It is also worth noting that for the special case of one design variable, the tightness condition of SDR has been widely studied in the literature [151]- [152], and the best result known so far is for the tightness of SDR with up to four linear constraints [152]. However, since in (P8.1-SDR-Eqv) there are two variables and* $2K + 2 > 4$ *constraints since* $K > 1$ *in general, the results in [151]- [152] also cannot be applied to our problem. For more information about the tightness condition of SDR, the readers can refer to [7].*

Since (P8.1-SDR-Eqv) is convex and satisfies the Slater's condition, its duality gap is zero [62]. Let λ, $\{\beta_k\}$, $\{\alpha_k\}$, and θ denote the dual variables of (P8.1-SDR-Eqv) associated with the equality constraint in (4.12), the SINR constraints of ERs in (4.13), the harvested energy constraints of ERs in (4.14), and the sum-power constraint in (4.15), respectively. Then the Lagrangian of problem (P8.1-SDR-Eqv) is expressed as

$$L_1(\boldsymbol{S}, \boldsymbol{Q}, \lambda, \{\beta_k\}, \{\alpha_k\}, \theta) = \text{Tr}(\boldsymbol{A}_1\boldsymbol{S}) + \text{Tr}(\boldsymbol{B}_1\boldsymbol{Q}) + \xi_1 t + \lambda, \tag{4.17}$$

where

$$\boldsymbol{A}_1 = \boldsymbol{H} - \sum_{k=1}^{K} \beta_k \boldsymbol{G}_k + \sum_{k=1}^{K} \alpha_k \zeta \boldsymbol{G}_k - \theta \boldsymbol{I}, \tag{4.18}$$

$$\boldsymbol{B}_1 = -\lambda \boldsymbol{H} + \sum_{k=1}^{K} \beta_k \gamma_e \boldsymbol{G}_k + \sum_{k=1}^{K} \alpha_k \zeta \boldsymbol{G}_k - \theta \boldsymbol{I}, \tag{4.19}$$

$$\xi_1 = -\lambda \sigma_0^2 + \sum_{k=1}^{K} \beta_k \gamma_e \sigma_k^2 - \sum_{k=1}^{K} \alpha_k \bar{E}_k + \theta \bar{P}. \tag{4.20}$$

Let λ^*, $\{\beta_k^* \geq 0\}$, $\{\alpha_k^* \geq 0\}$, and $\theta^* \geq 0$ denote the optimal dual solutions to problem (P8.1-SDR-Eqv). Then, we have the following lemma.

Lemma 4.5.4. *The optimal dual solution to problem (P8.1-SDR-Eqv) satisfies that* $\lambda^* > 0$ *and* $\theta^* > 0$ *when* $\gamma_e > 0$.

Proof. Please refer to Appendix E. □

With $\theta^* > 0$, it follows that in the optimal solution of problem (P8.1-SDR-Eqv), the sum-power constraint (4.15) must be satisfied with equality due to the complementary slackness [62]. Define

$$\boldsymbol{D}_1^* = -\lambda^* \boldsymbol{H} - \sum_{k=1}^{K} \beta_k^* \boldsymbol{G}_k + \sum_{k=1}^{K} \alpha_k^* \zeta \boldsymbol{G}_k - \theta^* \boldsymbol{I}, \tag{4.21}$$

and $l_1 = \text{rank}(\boldsymbol{D}_1^*)$. Furthermore, let $\boldsymbol{\Pi}_1 \in \mathbb{C}^{M \times (M-l_1)}$ denote the orthogonal basis of the null space of $\boldsymbol{D}_1^*$, where $\boldsymbol{\Pi}_1 = \boldsymbol{0}$ if $l_1 = M$, and $\boldsymbol{\pi}_{1,n}$ denote the nth column of $\boldsymbol{\Pi}_1$. Then based on Lemma 4.5.4, we have the following proposition.

Proposition 4.5.1. *The optimal solution* $(\boldsymbol{S}^*, \boldsymbol{Q}^*, t^*)$ *to problem (P8.1-SDR-Eqv) satisfies the following conditions:*

1. $\text{rank}(\boldsymbol{Q}^*) \leq \min(K, M)$;

2. $\boldsymbol{S}^*$ *can be expressed as*

$$\boldsymbol{S}^* = \sum_{n=1}^{M-l_1} a_n \boldsymbol{\pi}_{1,n} \boldsymbol{\pi}_{1,n}^H + b \boldsymbol{\tau}_1 \boldsymbol{\tau}_1^H, \tag{4.22}$$

   where $a_n \geq 0$, $\forall n$, $b > 0$, *and* $\boldsymbol{\tau}_1 \in \mathbb{C}^{M \times 1}$ *has unit-norm and satisfies* $\boldsymbol{\tau}_1^H \boldsymbol{\Pi}_1 = \boldsymbol{0}$.

3. *If* $\boldsymbol{S}^*$ *given in (4.22) has the rank larger than one, i.e., there exists at least an*

n such that $a_n > 0$, then the following solution

$$\bar{\boldsymbol{S}}^* = b\boldsymbol{\tau}_1\boldsymbol{\tau}_1^H, \tag{4.23}$$

$$\bar{\boldsymbol{Q}}^* = \boldsymbol{Q}^* + \sum_{n=1}^{M-l_1} a_n \boldsymbol{\pi}_{1,n}\boldsymbol{\pi}_{1,n}^H, \tag{4.24}$$

$$\bar{t}^* = t^*, \tag{4.25}$$

with $\mathrm{rank}(\bar{\boldsymbol{S}}^*) = 1$ *is also optimal to problem (P8.1-SDR-Eqv).*

Proof. Please refer to Appendix F. □

With Proposition 4.5.1, we are ready to find the optimal solution to problem (P8.1-SDR) with a rank-one covariance matrix for $\boldsymbol{S}$ as follows. First, we solve (P8.1-SDR-Eqv) via CVX. If the obtained solution $(\boldsymbol{S}^*, \boldsymbol{Q}^*, t^*)$ satisfies that $\mathrm{rank}(\boldsymbol{S}^*) = 1$, then $(\boldsymbol{S}^*/t^*, \boldsymbol{Q}^*/t^*)$ will be the optimal solution to (P8.1-SDR) according to Lemma 4.5.3. Otherwise, if $\mathrm{rank}(\boldsymbol{S}^*) > 1$, we can construct a new solution $(\bar{\boldsymbol{S}}^*, \bar{\boldsymbol{Q}}^*, \bar{t}^*)$ with $\mathrm{rank}(\bar{\boldsymbol{S}}^*) = 1$ according to (4.22)-(4.25). Then, $(\bar{\boldsymbol{S}}^*/\bar{t}^*, \bar{\boldsymbol{Q}}^*/\bar{t}^*)$ will be the optimal solution to (P8.1-SDR). Therefore, the rank-one relaxation on $\boldsymbol{S}$ in (P8.1-SDR) results in no loss of optimality to (P8.1), and given any $\gamma_e > 0$, the value of $g_1(\gamma_e)$ can be obtained by solving (P8.1-SDR-Eqv). Furthermore, since $\mathrm{rank}(\boldsymbol{Q}^*) \leq \min(K, M)$ in Proposition 4.5.1, it implies that in the case of $K < M$, at most K energy beams are needed in the optimal solution of (P8), i.e., $d \leq K$.

It is worth noting that in general, Proposition 4.5.1 only guarantees the existence of a rank-one optimal covariance solution $\boldsymbol{S}^*$ to (P8.1-SDR-Eqv) and thus (P8.1). One interesting question is thus under what conditions the rank-one solution $\boldsymbol{S}^*$ to (P8.1-SDR-Eqv) is unique. To answer this question, we define the following two sets as

$$\Psi = \{k | \beta_k^* = 0,\ k = 1, \cdots, K\}, \tag{4.26}$$

$$\bar{\Psi} = \{k | \beta_k^* > 0,\ k = 1, \cdots, K\}. \tag{4.27}$$

Moreover, define $\bar{\boldsymbol{G}}_1 = [\boldsymbol{h}, \{\boldsymbol{g}_k\}]^H$, $\forall k \in \bar{\Psi}$, in which the row vectors consist of the channels of IR, i.e., $\boldsymbol{h}^H$, and a subset of ERs, i.e., $\boldsymbol{g}_k^H$'s, whose SINR constraints are tight in the optimal solution to (P8.1-SDR-Evq) with $\beta_k^* > 0$ due to the complimentary slackness. Then we have the following proposition.

Proposition 4.5.2. *The optimal solution* $(\boldsymbol{S}^*, \boldsymbol{Q}^*, t^*)$ *to (P8.1-SDR-Eqv) always satisfies that* $\text{rank}(\boldsymbol{S}^*) = 1$ *if there is no non-trivial (non-zero) solution* $\boldsymbol{x} \in \mathbb{C}^{M\times 1}$ *to the following equations:*

$$\begin{cases} \boldsymbol{x}^H \left(\sum\limits_{k\in\Psi} \alpha_k^* \zeta \boldsymbol{G}_k - \theta^* \boldsymbol{I} \right) \boldsymbol{x} = 0, \\ \bar{\boldsymbol{G}}_1 \boldsymbol{x} = \boldsymbol{0}. \end{cases} \tag{4.28}$$

Proof. Please refer to Appendix G. □

Let $|\bar{\Psi}|$ denote the cardinality of the set $\bar{\Psi}$. Based on Proposition 4.5.2, we then have the following two corollaries.

Corollary 4.5.1. *In the case of* $K < M-1$*, if* $|\bar{\Psi}| = K$*, i.e., the SINR constraint (4.13) is tight for all ERs, then the optimal solution* $(\boldsymbol{S}^*, \boldsymbol{Q}^*, t^*)$ *to (P8.1-SDR-Eqv) always satisfies that* $\text{rank}(\boldsymbol{S}^*) = 1$.

Proof. If $|\bar{\Psi}| = K$, i.e., $\Psi = \emptyset$, then we have $\sum_{k\in\Psi} \alpha_k^* \zeta \boldsymbol{G}_k - \theta^* \boldsymbol{I} = -\theta^* \boldsymbol{I}$. Since $\theta^* > 0$ according to Lemma 4.5.4, there is no non-zero solution to the equation $-\theta^* \boldsymbol{x}^H \boldsymbol{x} = 0$. According to Proposition 4.5.2, Corollary 4.5.1 is thus proved. □

Corollary 4.5.2. *In the case of* $K \geq M-1$*, if* $|\bar{\Psi}| \geq M-1$*, then the optimal solution* $(\boldsymbol{S}^*, \boldsymbol{Q}^*, t^*)$ *to (P8.1-SDR-Eqv) always satisfies that* $\text{rank}(\boldsymbol{S}^*) = 1$.

Proof. Since all the channels are assumed to be linearly independent, if $|\bar{\Psi}| \geq M-1$, then we have $\text{rank}(\bar{\boldsymbol{G}}_1) = M$, and thus there is no non-zero solution to the equation $\bar{\boldsymbol{G}}_1 \boldsymbol{x} = \boldsymbol{0}$. According to Proposition 4.5.2, Corollary 4.5.2 is thus proved. □

According to the complementary slackness, if $\beta_k^* > 0$, then the SINR constraint for ER_k must be tight in problem (P8.1-SDR-Eqv). In other words, $|\bar{\Psi}|$ denotes

the number of ERs whose SINR constraints are active in the optimal solution to (P8.1-SDR-Eqv). Therefore, Corollaries 4.5.1 and 4.5.2 imply that if $|\bar{\Psi}| \geq \min(M-1, K)$, i.e., the SINR constraint in (4.13) is tight for at least $\min(M-1, K)$ ERs, $\text{rank}(\boldsymbol{S}^*) = 1$ must hold for (P8.1-SDR-Eqv). Note that in our assumed system setup, all ERs are closer to the Tx than the IR and as a result, they all have better channels for eavesdropping the IR's message. It is thus expected that the SINR constraint in (4.13) should be active for all ERs with a very high probability. Therefore, the condition given in Corollaries 4.5.1 and 4.5.2, i.e., $|\bar{\Psi}| \geq \min(M-1, K)$, can be considered to be practically satisfied, under which the uniqueness of the rank-one optimal covariance solution $\boldsymbol{S}^*$ to (P8.1-SDR-Eqv) also holds.

Remark 4.5.2. *It is worth pointing out two main differences in the optimal beamforming solution to (P8) with versus without the EH constraints. First, consider the case of one single ER, i.e., $K = 1$, in (P8). In this case, without the EH constraint, it has been shown in [119, 121] that the secrecy capacity for the IR is given by*

$$C_{\text{s}} = \max_{\|\boldsymbol{v}_0\|^2 \leq \bar{P}} \quad \log_2\left(1 + \frac{|\boldsymbol{v}_0^H \boldsymbol{h}|^2}{\sigma_0^2}\right) - \log_2\left(1 + \frac{|\boldsymbol{v}_0^H \boldsymbol{g}_1|^2}{\sigma_1^2}\right). \tag{4.29}$$

Notice that AN is not needed in achieving C_{s}, which is also the optimal value of (P8-NoET) in the case of $K = 1$, and the optimal beamforming solution for the IR to achieve C_{s} has been obtained in [125, 127]. In contrast, with the EH constraint added to (P8), in order to deliver the required wireless energy to the ER and at the same time achieve the maximum secrecy rate for the IR, AN is in general needed according to Proposition 4.5.1, since it follows that $\text{rank}(\boldsymbol{Q}^*) \leq 1$ *in the case of $K = 1$, i.e., one energy beam is in general needed to power the ER and in the meanwhile carry the AN to interfere with it from eavesdropping the IR's message. Second, consider the more general case with multiple ERs, i.e., $K > 1$. In this case, without considering EH constraints at ERs, (P8) reduces to (P8-NoET), which has been solved in [144]. It was shown in [144], [145] that if all the channels are linearly independent, SDR can always obtain the unique optimal rank-one covariance (beamforming) solution*

for the IR. However, with the additional EH constraints added for ERs, it is in general not always true that SDR yields a rank-one covariance solution for IR, as shown in Proposition 4.5.1. However, we are able to show in Proposition 4.5.1 that the optimal rank-one covariance solution for IR always exists and can be obtained by a simple reconstruction of the optimal solution.

Remark 4.5.3. *It is also worth noting that the optimal solution obtained for (P8) is applicable for the special case of maximizing the IR's rate but without considering the secret transmission as given by the following problem.*

$$
\begin{aligned}
(\mathrm{P8-NoSC}): \quad & \underset{\boldsymbol{v}_0,\{\boldsymbol{w}_i\}}{\texttt{Maximize}} \quad \log_2\left(1+\frac{|\boldsymbol{v}_0^H\boldsymbol{h}|^2}{\sum\limits_{i=1}^{d}|\boldsymbol{w}_i^H\boldsymbol{h}|^2+\sigma_0^2}\right) \\
& \texttt{Subject to} \quad \zeta\left(|\boldsymbol{v}_0^H\boldsymbol{g}_k|^2+\sum_{i=1}^{d}|\boldsymbol{w}_i^H\boldsymbol{g}_k|^2\right)\geq \bar{E}_k, \quad \forall k, \\
& \qquad\qquad \|\boldsymbol{v}_0\|^2+\sum_{i=1}^{d}\|\boldsymbol{w}_i\|^2\leq \bar{P}.
\end{aligned}
$$

It is observed that (P8-NoSC) is equivalent to (P8.1) by setting $\gamma_e=\infty$ in the first constraint. Therefore, similar to problem (P8.1), SDR can be applied to obtain the optimal beamforming solution to (P8-NoSC).

4.5.2 Suboptimal Solutions

The optimal solution to (P8) proposed in Section 4.5.1 requires a joint optimization of the information/energy beamforming vectors and their power allocation. In this subsection, we propose two suboptimal solutions for (P8) which can be designed with lower complexity than the optimal solution. Similar to [3], in our proposed suboptimal solutions, the energy beams $\boldsymbol{w}_i$, $i=1,\cdots,d$, are all restricted to lie in the null space of the IR's channel $\boldsymbol{h}$ such that they cause no interference to IR. However, the information beam $\boldsymbol{v}_0$ is aligned to the null space of the ERs' channels $\boldsymbol{G}=[\boldsymbol{g}_1,\cdots,\boldsymbol{g}_K]^H$ in the first suboptimal solution in order

to eliminate the information leaked to all ERs, but to the same direction as $\boldsymbol{h}$ in the second suboptimal solution to maximize the IR's SINR. Note that the first suboptimal solution is only applicable when $K < M$ since otherwise the null space of $\boldsymbol{G}$ is empty. In the following, we present the two proposed suboptimal solutions in more details.

Suboptimal Solution I

Supposing that $K < M$, then the first suboptimal solution aims to solve problem (P8) with the additional constraints: $\boldsymbol{v}_0^H \boldsymbol{g}_k = 0$, $\forall k$, and $\boldsymbol{w}_i^H \boldsymbol{h} = 0$, $\forall i$. Consider first the information beam $\boldsymbol{v}_0$. Let the singular value decomposition (SVD) of $\boldsymbol{G}$ be denoted as

$$\boldsymbol{G} = \boldsymbol{U}\boldsymbol{\Lambda}\boldsymbol{V}^H = \boldsymbol{U}\boldsymbol{\Lambda}[\bar{\boldsymbol{V}}\ \tilde{\boldsymbol{V}}]^H, \tag{4.30}$$

where $\boldsymbol{U} \in \mathbb{C}^{K\times K}$ and $\boldsymbol{V} \in \mathbb{C}^{M\times M}$ are unitary matrices, i.e., $\boldsymbol{U}\boldsymbol{U}^H = \boldsymbol{U}^H\boldsymbol{U} = \boldsymbol{I}$, $\boldsymbol{V}\boldsymbol{V}^H = \boldsymbol{V}^H\boldsymbol{V} = \boldsymbol{I}$, and $\boldsymbol{\Lambda}$ is a $K \times M$ rectangular diagonal matrix. Furthermore, $\bar{\boldsymbol{V}} \in \mathbb{C}^{M\times K}$ and $\tilde{\boldsymbol{V}} \in \mathbb{C}^{M\times(M-K)}$ consist of the first K and the last $M-K$ right singular vectors of $\boldsymbol{G}$, respectively. It can be shown that $\tilde{\boldsymbol{V}}$ with $\tilde{\boldsymbol{V}}^H\tilde{\boldsymbol{V}} = \boldsymbol{I}$ forms an orthogonal basis for the null space of $\boldsymbol{G}$. Thus, to guarantee that $\boldsymbol{G}\boldsymbol{v}_0 = \boldsymbol{0}$, $\boldsymbol{v}_0$ must be in the following form:

$$\boldsymbol{v}_0 = \sqrt{\tilde{P}_0}\tilde{\boldsymbol{V}}\tilde{\boldsymbol{v}}_0, \tag{4.31}$$

where $\tilde{P}_0 = \|\boldsymbol{v}_0\|^2$ denotes the transmit power of the information beam, and $\tilde{\boldsymbol{v}}_0$ is an arbitrary $(M-K)\times 1$ complex vector of unit norm. It can be shown that to maximize the IR's received power, $\tilde{\boldsymbol{v}}_0$ should be aligned to the same direction as the equivalent channel $\tilde{\boldsymbol{V}}^H\boldsymbol{h}$, i.e., $\tilde{\boldsymbol{v}}_0^* = \tilde{\boldsymbol{V}}^H\boldsymbol{h}/\|\tilde{\boldsymbol{V}}^H\boldsymbol{h}\|$. Given that all the energy beams

are aligned to the null space of $\boldsymbol{h}$, the achievable secrecy rate of IR is expressed as

$$r_0^{(\mathrm{I})} = \log_2\left(1 + \frac{\tilde{P}_0 \|\tilde{\boldsymbol{V}}^H \boldsymbol{h}\|^2}{\sigma_0^2}\right). \tag{4.32}$$

Next, consider the energy beam $\boldsymbol{w}_i$'s. Define the projection matrix as $\boldsymbol{T} = \boldsymbol{I} - \boldsymbol{h}\boldsymbol{h}^H/\|\boldsymbol{h}\|^2$. Without loss of generality, we can express $\boldsymbol{T} = \tilde{\boldsymbol{X}}\tilde{\boldsymbol{X}}^H$, where $\tilde{\boldsymbol{X}} \in \mathbb{C}^{M\times(M-1)}$ satisfies $\tilde{\boldsymbol{X}}^H\tilde{\boldsymbol{X}} = \boldsymbol{I}$. It can be shown that $\tilde{\boldsymbol{X}}$ forms an orthogonal basis for the null space of $\boldsymbol{h}^H$. Thus, to guarantee that $\boldsymbol{h}^H\boldsymbol{w}_i = 0$, $\forall i$, $\boldsymbol{w}_i$ must be in the following form:

$$\boldsymbol{w}_i = \tilde{\boldsymbol{X}}\tilde{\boldsymbol{w}}_i, \quad i = 1, \cdots, d, \tag{4.33}$$

where $\tilde{\boldsymbol{w}}_i$ is an arbitrary $(M-1)\times 1$ complex vector. In this case, the energy harvested at ER_k is thus given by

$$E_k^{(\mathrm{I})} = \zeta \sum_{i=1}^{d} |\boldsymbol{w}_i^H \boldsymbol{g}_k|^2 = \zeta\left(\sum_{i=1}^{d} \tilde{\boldsymbol{w}}_i^H \tilde{\boldsymbol{G}}_k \tilde{\boldsymbol{w}}_i\right), \quad 1 \le k \le K, \tag{4.34}$$

where $\tilde{\boldsymbol{G}}_k = \tilde{\boldsymbol{X}}^H \boldsymbol{G}_k \tilde{\boldsymbol{X}}$.

It can be observed from (4.32) that to maximize the secrecy rate $r_0^{(\mathrm{I})}$, $\tilde{P}_0$ should be as large as possible. Therefore, the optimal energy beams can be obtained by solving the following problem.

$$\begin{aligned}(\mathrm{P8-Sub1}): \ \underset{\{\tilde{\boldsymbol{w}}_i\}}{\texttt{Minimize}} \quad & \sum_{i=1}^{d} \|\tilde{\boldsymbol{w}}_i\|^2 \\ \texttt{Subject to} \quad & \zeta\left(\sum_{i=1}^{d} \tilde{\boldsymbol{w}}_i^H \tilde{\boldsymbol{G}}_k \tilde{\boldsymbol{w}}_i\right) \ge \bar{E}_k, \quad 1 \le k \le K.\end{aligned}$$

Define $\tilde{\boldsymbol{Q}} = \sum_{i=1}^{d} \tilde{\boldsymbol{w}}_i \tilde{\boldsymbol{w}}_i^H$. Then the SDP reformulation of (P8-Sub1) can be

expressed as

$$(\text{P8}-\text{Sub1}-\text{SDP}): \quad \underset{\tilde{\boldsymbol{Q}}}{\texttt{Minimize}} \quad \text{Tr}(\tilde{\boldsymbol{Q}})$$
$$\texttt{Subject to} \quad \zeta \text{Tr}(\tilde{\boldsymbol{G}}_k \tilde{\boldsymbol{Q}}) \geq \bar{E}_k, \quad 1 \leq k \leq K.$$

Assuming that (P8-Sub1-SDP) is feasible, then it can be solved via CVX. Denote the optimal solution for this problem as $\tilde{\boldsymbol{Q}}^*$. Then the optimal solution to (P8-Sub1), denoted by $\tilde{\boldsymbol{w}}_i^*$'s, can be obtained by the EVD of $\tilde{\boldsymbol{Q}}^*$, and the corresponding optimal energy beams can be obtained as

$$\boldsymbol{w}_i^* = \tilde{\boldsymbol{X}} \tilde{\boldsymbol{w}}_i^*, \quad 1 \leq i \leq d, \tag{4.35}$$

where $d = \text{rank}(\tilde{\boldsymbol{Q}}^*)$. Furthermore, the optimal power allocation for the information beam is given by $\tilde{P}_0^* = \bar{P} - \sum_{i=1}^d \|\boldsymbol{w}_i^*\|^2$; by assuming $\tilde{P}^* > 0$, the optimal information beam is thus obtained as

$$\boldsymbol{v}_0^* = \sqrt{\tilde{P}_0^*} \tilde{\boldsymbol{V}} \tilde{\boldsymbol{v}}_0^* = \frac{\sqrt{\bar{P} - \sum_{i=1}^d \|\boldsymbol{w}_i^*\|^2} \tilde{\boldsymbol{V}} \tilde{\boldsymbol{V}}^H \boldsymbol{h}}{\|\tilde{\boldsymbol{V}}^H \boldsymbol{h}\|}. \tag{4.36}$$

Suboptimal Solution II

The second suboptimal solution aims to solve problem (P8) with the additional constraints: $\boldsymbol{v}_0 = \sqrt{\hat{P}_0} \boldsymbol{h}/\|\boldsymbol{h}\|$ and $\boldsymbol{w}_i^H \boldsymbol{h} = 0$, $\forall i$, where $\hat{P}_0 = \|\boldsymbol{v}_0\|^2$ denotes the transmit power allocated to the information beam. To reduce the design complexity in this case, we further assume that the energy beams are in the form of $\boldsymbol{w}_i = \sqrt{\bar{P} - \hat{P}_0} \boldsymbol{w}_i^* / \sqrt{\sum_{i=1}^d \|\boldsymbol{w}_i^*\|^2}$, $1 \leq i \leq d$, where $\boldsymbol{w}_i^*$'s are the energy beams obtained by Suboptimal Solution I in (4.35). Therefore, the secrecy rate of the IR is expressed

as

$$r_0^{(\mathrm{II})} = \min_{1\le k\le K} \quad \log_2\left(1+\frac{\hat{P}_0\|\boldsymbol{h}\|^2}{\sigma_0^2}\right) - \log_2\left(1+\frac{\hat{P}_0|\boldsymbol{h}^H\boldsymbol{g}_k|^2}{\|\boldsymbol{h}\|^2\left(\sum_{i=1}^{d}((\bar{P}-\hat{P}_0)|\boldsymbol{g}_k^H\boldsymbol{w}_i^*|^2/\sum_{j=1}^{d}\|\boldsymbol{w}_j^*\|^2)+\sigma_k^2\right)}\right). \tag{4.37}$$

Furthermore, the harvested energy by ER_k is expressed as

$$E_k^{(\mathrm{II})} = \zeta\left(\frac{\hat{P}_0|\boldsymbol{h}^H\boldsymbol{g}_k|^2}{\|\boldsymbol{h}\|^2}+\sum_{i=1}^{d}\frac{(\bar{P}_0-\hat{P}_0)|\boldsymbol{g}_k^H\boldsymbol{w}_i^*|^2}{\sum_{j=1}^{d}\|\boldsymbol{w}_j^*\|^2}\right), \quad \forall k. \tag{4.38}$$

Define the set of feasible power allocation for the information beam as $\hat{\mathcal{P}}_0 = \{\hat{P}_0|E_k^{(\mathrm{II})} \ge \bar{E}_k,\ 1\le k\le K,\ 0<\hat{P}_0\le\bar{P}\}$, which is assumed to be non-empty. To maximize the secrecy rate of the IR subject to individual harvested energy constraints of ERs, we need to solve the following problem.

$$(\mathrm{P8-Sub2}): \ \underset{\hat{P}_0}{\texttt{Maximize}} \quad r_0^{(\mathrm{II})}$$
$$\texttt{Subject to} \quad \hat{P}_0\in\hat{\mathcal{P}}_0.$$

The optimal solution to (P8-Sub2), denoted by $\hat{P}_0^*$, can be obtained by a one-dimension search over the set $\hat{\mathcal{P}}_0$.

4.6 Proposed Solutions to Weighted Sum-Energy Maximization

In this section, we present the optimal solution as well as two suboptimal solutions to (P9). Similar to (P8), we first study the feasibility of (P9) for a given pair of $\bar{r}_0$ and $\bar{P}$ in the following problem.

$$\begin{aligned}(\text{P9}-\text{NoET}): \ \underset{\boldsymbol{v}_0,\{\boldsymbol{w}_i\}}{\texttt{Maximize}} \quad & 0 \\ \texttt{Subject to} \quad & r_0 \geq \bar{r}_0 \\ & \|\boldsymbol{v}_0\|^2 + \sum_{i=1}^{d} \|\boldsymbol{w}_i\|^2 \leq \bar{P}.\end{aligned}$$

Note that this problem corresponds to the case where no energy transfer is required, and thus $\boldsymbol{w}_i$'s play the only role of AN. The feasibility problem (P9-NoET) can be easily solved by checking whether $\bar{r}_0$ is no larger than the optimal value of (P8-NoET) in Section 4.5.1. Without loss of generality, in the rest of this chapter, we assume that (P9) is feasible.

Next, we consider another special case of (P9) where no information transmission is required to the IR, i.e., $\bar{r}_0 = 0$. In this case, $\boldsymbol{v}_0 = \boldsymbol{0}$ and thus (P9) reduces to

$$\begin{aligned}(\text{P9}-\text{NoIT}): \ \underset{\{\boldsymbol{w}_i\}}{\texttt{Maximize}} \quad & \sum_{k=1}^{K} \mu_k \zeta \left(\sum_{i=1}^{d} |\boldsymbol{w}_i^H \boldsymbol{g}_k|^2 \right) \\ \texttt{Subject to} \quad & \sum_{i=1}^{d} \|\boldsymbol{w}_i\|^2 \leq \bar{P}.\end{aligned}$$

Let ψ and $\boldsymbol{\eta}$ denote the maximum eigenvalue and its corresponding unit-norm eigenvector of the matrix $\sum_{k=1}^{K} \mu_k \zeta \boldsymbol{g}_k \boldsymbol{g}_k^H$, respectively. From [2], the optimal value of problem (P9-NoIT) is known to be

$$E_{\max} = \psi \bar{P}, \tag{4.39}$$

which is achieved by $\boldsymbol{w}_i^* = \sqrt{p_i}\boldsymbol{\eta}$, $1 \le i \le d$, for any set of p_i's satisfying $p_i \ge 0$, $\forall i$, and $\sum_{i=1}^d p_i = \bar{P}$. In other words, the optimal solution to problem (P9-NoIT) is to align all the energy beams to the same direction as $\boldsymbol{\eta}$, a technique known as "energy beamforming" [2].

4.6.1 Optimal Solution

In this subsection, we propose the optimal solution to (P9). Similar to (P8), (P9) can be reformulated into two sub-problems shown in the sequel. First, we have the following lemma (the proof of which is similar to that of Lemma 4.5.1 and is thus omitted).

Lemma 4.6.1. *There exists a SINR constraint $\gamma_0 > 0$ at IR such that the following problem*

$$
\begin{aligned}
(\text{P9.1}): \quad \underset{\boldsymbol{v}_0,\{\boldsymbol{w}_i\}}{\texttt{Maximize}} \quad & \sum_{k=1}^K \mu_k \zeta \left(|\boldsymbol{v}_0^H \boldsymbol{g}_k|^2 + \sum_{i=1}^d |\boldsymbol{w}_i^H \boldsymbol{g}_k|^2 \right) \\
\texttt{Subject to} \quad & \frac{|\boldsymbol{v}_0^H \boldsymbol{h}|^2}{\sum_{i=1}^d |\boldsymbol{w}_i^H \boldsymbol{h}|^2 + \sigma_0^2} \ge \gamma_0, \\
& \frac{|\boldsymbol{v}_0^H \boldsymbol{g}_k|^2}{\sum_{i=1}^d |\boldsymbol{w}_i^H \boldsymbol{g}_k|^2 + \sigma_k^2} \le \frac{1+\gamma_0}{2^{\bar{r}_0}} - 1, \ \forall k, \\
& \|\boldsymbol{v}_0\|^2 + \sum_{i=1}^d \|\boldsymbol{w}_i\|^2 \le \bar{P},
\end{aligned}
$$

has the same optimal solution to (P9).

Let $g_2(\gamma_0)$ denote the optimal value of problem (P9.1) with a given $\gamma_0 > 0$. Then, we have the following lemma.

Lemma 4.6.2. *The optimal value of problem (P9) is the same as that of the following problem*

$$
(\text{P9.2}): \quad \underset{\gamma_0 > 0}{\texttt{Maximize}} \quad g_2(\gamma_0).
$$

The proof of Lemma 4.6.2 is similar to that of Lemma 4.5.2 and is thus omitted for brevity. Let γ_0^* denote the optimal solution to problem (P9.2). Lemmas 4.6.1 and 4.6.2 then imply that with $\gamma_0 = \gamma_0^*$, problems (P9) and (P9.1) have the same optimal solution. Therefore, similar to (P8), problem (P9) can be solved in the following two steps: First, given any $\gamma_0 > 0$, we solve problem (P9.1) to find $g_2(\gamma_0)$; then, we solve problem (P9.2) to obtain the optimal γ_0^* by a one-dimension search over $\gamma_0 > 0$. In the rest of this subsection, we focus on solving (P9.1), which is non-convex.

Define $\boldsymbol{S} = \boldsymbol{v}_0\boldsymbol{v}_0^H$ and $\boldsymbol{Q} = \sum_{i=1}^{d} \boldsymbol{w}_i\boldsymbol{w}_i^H$. Then the SDR of (P9.1) can be expressed as

$$
\begin{aligned}
(\text{P9.1}-\text{SDR}): \quad \underset{\boldsymbol{S},\boldsymbol{Q}}{\texttt{Maximize}} \quad & \sum_{k=1}^{K} \mu_k \zeta \left(\text{Tr}(\boldsymbol{G}_k\boldsymbol{S}) + \text{Tr}(\boldsymbol{G}_k\boldsymbol{Q})\right) \\
\texttt{Subject to} \quad & \text{Tr}(\boldsymbol{H}\boldsymbol{S}) \geq \gamma_0 \left(\text{Tr}(\boldsymbol{H}\boldsymbol{Q}) + \sigma_0^2\right), && (4.40)\\
& \frac{\text{Tr}(\boldsymbol{G}_k\boldsymbol{S})}{\gamma_e} \leq \text{Tr}(\boldsymbol{G}_k\boldsymbol{Q}) + \sigma_k^2, \ \forall k, && (4.41)\\
& \text{Tr}(\boldsymbol{S}) + \text{Tr}(\boldsymbol{Q}) \leq \bar{P}, && (4.42)\\
& \boldsymbol{S} \succeq \boldsymbol{0}, \quad \boldsymbol{Q} \succeq \boldsymbol{0}, && (4.43)
\end{aligned}
$$

where $\boldsymbol{H} = \boldsymbol{h}\boldsymbol{h}^H$, $\boldsymbol{G}_k = \boldsymbol{g}_k\boldsymbol{g}_k^H$, and $\gamma_e = (1+\gamma_0)/2^{\bar{r}_0} - 1$. Similar to (P8.1), if the optimal solution to problem (P9.1-SDR), denoted by $\boldsymbol{S}^*$ and $\boldsymbol{Q}^*$, satisfies $\text{rank}(\boldsymbol{S}^*) = 1$, then the optimal information beam $\boldsymbol{v}_0^*$ and energy beam $\boldsymbol{w}_i^*$'s, $i = 1, \cdots, d$ ($d = \text{rank}(\boldsymbol{Q}^*)$), for problem (P9.1) can be obtained from the EVDs of $\boldsymbol{S}^*$ and $\boldsymbol{Q}^*$, respectively; otherwise if $\text{rank}(\boldsymbol{S}^*) > 1$, the optimal value of problem (P9.1-SDR) only serves as an upper bound on that of problem (P9.1). In the following, we show that there always exists an optimal solution with $\text{rank}(\boldsymbol{S}^*) = 1$ for (P9.1-SDR).

Since (P9.1-SDR) is convex, it can be solved by CVX. Suppose that the resulting optimal solution $(\boldsymbol{S}^*, \boldsymbol{Q}^*)$ satisfies $\text{rank}(\boldsymbol{S}^*) > 1$. Let E^* denote the optimal value

of (P9.1-SDR) achieved by $(\boldsymbol{S}^*, \boldsymbol{Q}^*)$. Then consider the following problem.

$$(\text{P9.1}-\text{SDR}-\text{New}): \quad \underset{\boldsymbol{S},\boldsymbol{Q}}{\texttt{Maximize}} \quad \frac{\text{Tr}(\boldsymbol{H}\boldsymbol{S})}{\text{Tr}(\boldsymbol{H}\boldsymbol{Q})+\sigma_0^2}$$

$$\texttt{Subject to} \quad (4.41),\ (4.42),\ (4.43), \tag{4.44}$$

$$\sum_{k=1}^{K} \mu_k \zeta(\text{Tr}(\boldsymbol{G}_k\boldsymbol{S}) + \text{Tr}(\boldsymbol{G}_k\boldsymbol{Q})) \geq E^*. \tag{4.45}$$

It can be shown that with $(\boldsymbol{S}^*, \boldsymbol{Q}^*)$, the resulting value of (P9.1-SDR-New) is γ_0. Let $(\bar{\boldsymbol{S}}^*, \bar{\boldsymbol{Q}}^*)$ denote the optimal solution to (P9.1-SDR-New), and $\bar{\gamma}_0$ be the optimal value. Then we have $\bar{\gamma}_0 \geq \gamma_0$. As a result, with the new solution $(\bar{\boldsymbol{S}}^*, \bar{\boldsymbol{Q}}^*)$, all the constraints in (P9.1-SDR), i.e, (4.40)-(4.43), are satisfied, and the optimal value E^* is still achieved. Therefore, the optimal solution to (P9.1-SDR-New) is also optimal to (P9.1-SDR). Furthermore, similar to (P8.1-SDR) (see Proposition 4.5.1), it can be shown that there always exists a rank-one optimal covariance solution for $\boldsymbol{S}$ to (P9.1-SDR-New). Therefore, we can conclude that there always exists an optimal solution $(\boldsymbol{S}^*, \boldsymbol{Q}^*)$ to (P9.1-SDR) with $\text{rank}(\boldsymbol{S}^*) = 1$, and there is no loss of optimality for (P9.1) due to the rank relaxation on $\boldsymbol{S}$ in (P9.1-SDR).

At last, similar to Proposition 4.5.2 and Corollaries 4.5.1 and 4.5.2 in Section 4.5.1, it can be shown that if $|\bar{\Psi}| \geq \min(M-1, K)$, where $\bar{\Psi}$ is still given in (4.27) but with β_k^*'s denoting the optimal dual solution to (P9.1-SDR) corresponding to (4.41), $\text{rank}(\boldsymbol{S}^*) = 1$ is always true for (P9.1-SDR).

Remark 4.6.1. *It is worth noting that in [112], a similar problem to (P9) has been studied without considering the secret information transmission to IRs, which in the case of one single IR under the same setup of this chapter is equivalent to the*

following simplified problem of (P9).

$$(\text{P9}-\text{NoSC}): \quad \underset{\boldsymbol{v}_0,\{\boldsymbol{w}_i\}}{\texttt{Maximize}} \quad \sum_{k=1}^{K}\mu_k\zeta\left(|\boldsymbol{v}_0^H\boldsymbol{g}_k|^2+\sum_{i=1}^{d}|\boldsymbol{w}_i^H\boldsymbol{g}_k|^2\right)$$

$$\texttt{Subject to} \quad \log_2\left(1+\frac{|\boldsymbol{v}_0^H\boldsymbol{h}|^2}{\sum_{i=1}^{d}|\boldsymbol{w}_i^H\boldsymbol{h}|^2+\sigma_0^2}\right)\geq\tilde{r}_0,$$

$$\|\boldsymbol{v}_0\|^2+\sum_{i=1}^{d}\|\boldsymbol{w}_i\|^2\leq\bar{P},$$

where $\tilde{r}_0$ denotes the given rate constraint for IR (without secrecy consideration). Note that an important result shown in [112, Proposition 3.1] is that the optimal solution to problem (P9-NoSC) should satisfy that $\boldsymbol{w}_i^*=\boldsymbol{0}$, $\forall\ 1\leq i\leq d$, i.e., no energy beam is needed, while only the information beam $\boldsymbol{v}_0$ is adjusted for achieving the information rate target for IR and yet maximizing the weighted sum-energy transferred to ERs. However, with the newly introduced secrecy rate constraint in (P9), energy beams are in general needed in the optimal solution, since they help generate AN to reduce the information rate eavesdropped by ERs, especially when ERs have better channels than IR from the Tx.

4.6.2 Suboptimal Solutions

Similarly as for (P8), in this subsection, we propose two suboptimal solutions for (P9), which can be designed with lower complexity. Similar to the two suboptimal solutions proposed in Section 4.5.2 for (P8), in the following we assume that the energy beams $\boldsymbol{w}_i$ $(i=1,\cdots,d)$ in (P9) are all in the null space of the IR's channel $\boldsymbol{h}$. Furthermore, the information beam $\boldsymbol{v}_0$ is aligned to the null space of the ERs' channels $\boldsymbol{G}=[\boldsymbol{g}_1,\cdots,\boldsymbol{g}_K]^H$ in the first suboptimal solution, while it is in the same direction as $\boldsymbol{h}$ for the second suboptimal solution. Again, the first suboptimal solution is only applicable when $K<M$. In the following, we present the two suboptimal solutions in more details.

Suboptimal Solution I

Supposing that $K < M$, then the first suboptimal solution aims to solve problem (P9) with the additional constraints: $\boldsymbol{v}_0^H \boldsymbol{g}_k = 0$, $\forall k$, and $\boldsymbol{w}_i^H \boldsymbol{h} = 0$, $\forall i$. To satisfy the above constraints, $\boldsymbol{v}_0$ and $\boldsymbol{w}_i$'s should be in the form of (4.31) and (4.33), respectively. Furthermore, with $\tilde{\boldsymbol{v}}_0^* = \tilde{\boldsymbol{V}}^H \boldsymbol{h} / \|\tilde{\boldsymbol{V}}^H \boldsymbol{h}\|$, the secrecy rate of the IR under this scheme is given in (4.32). Since all ERs cannot harvest energy from the information beam, to maximize the weighted sum-energy transferred to ERs, $\tilde{P}_0$ should be set to the smallest power to make $r_0^{(\mathrm{I})} = \bar{r}_0$. It thus follows

$$\tilde{P}_0^* = \frac{(2^{\bar{r}_0} - 1)\sigma_0^2}{\|\tilde{\boldsymbol{V}}^H \boldsymbol{h}\|^2}. \tag{4.46}$$

To summarize, in this suboptimal solution, we have

$$\boldsymbol{v}_0^* = \sqrt{\tilde{P}_0^*}\tilde{\boldsymbol{V}}\tilde{\boldsymbol{v}}_0^* = \frac{\sqrt{(2^{\bar{r}_0} - 1)\sigma_0^2}\tilde{\boldsymbol{V}}\tilde{\boldsymbol{V}}^H \boldsymbol{h}}{\|\tilde{\boldsymbol{V}}^H \boldsymbol{h}\|^2}. \tag{4.47}$$

Notice that the harvested energy of ER_k under this suboptimal solution is in the form of (4.34). Thus, to find the optimal $\tilde{\boldsymbol{w}}_i^*$'s, we need to solve the following problem.

$$\begin{aligned} (\mathrm{P9-Sub1}): \quad \underset{\{\tilde{\boldsymbol{w}}_i\}}{\texttt{Maximize}} \quad & \sum_{k=1}^{K} \mu_k \zeta \left(\sum_{i=1}^{d} \tilde{\boldsymbol{w}}_i^H \tilde{\boldsymbol{G}}_k \tilde{\boldsymbol{w}}_i \right) \\ \texttt{Subject to} \quad & \sum_{i=1}^{d} \|\tilde{\boldsymbol{w}}_i\|^2 \le \bar{P} - \tilde{P}_0^*. \end{aligned}$$

Note that in the above, we have assumed $\bar{P} \ge \tilde{P}_0^*$. Let $\tilde{\psi}$ and $\tilde{\boldsymbol{\eta}}$ denote the maximum eigenvalue and its corresponding unit-norm eigenvector of the matrix $\sum_{k=1}^{K} \mu_k \zeta \tilde{\boldsymbol{G}}_k$, respectively. Similar to problem (P9-NoIT), it can be shown that the optimal value of problem (P9-Sub1) is $\tilde{E}_{\max} = \tilde{\psi}(\bar{P} - \tilde{P}_0^*)$, which is achieved by $\tilde{\boldsymbol{w}}_i^* = \sqrt{\tilde{p}_i}\tilde{\boldsymbol{\eta}}$, $1 \le i \le d$, for any set of $\tilde{p}_i$'s satisfying $\sum_{i=1}^{d} \tilde{p}_i = \bar{P} - \tilde{P}_0^*$. In practice, it is preferable to send only one energy beam to minimize the complexity of beamforming

implementation at the Tx; thus, we have

$$\boldsymbol{w}_i^* = \begin{cases} \sqrt{\bar{P} - \tilde{P}_0^*}\tilde{\boldsymbol{X}}\tilde{\boldsymbol{\eta}}, & \text{if } i = 1, \\ 0, & \text{otherwise.} \end{cases} \tag{4.48}$$

Note that unlike Suboptimal Solution I for (P8) shown in (4.35), one single energy beam is sufficient in this case.

Suboptimal Solution II

The second suboptimal solution aims to solve problem (P9) with the additional constraints: $\boldsymbol{v}_0 = \sqrt{\hat{P}_0}\boldsymbol{h}/\|\boldsymbol{h}\|$ and $\boldsymbol{w}_i^H\boldsymbol{h} = 0$, $\forall i$, where $\hat{P}_0 = \|\boldsymbol{v}_0\|^2$ denotes the transmit power of the information beam. Similar to (4.48), it can be shown that the optimal energy beams should be in the following form:

$$\boldsymbol{w}_i = \begin{cases} \sqrt{\bar{P} - \hat{P}_0}\tilde{\boldsymbol{X}}\tilde{\boldsymbol{\eta}}, & \text{if } i = 1, \\ 0, & \text{otherwise.} \end{cases} \tag{4.49}$$

Next, we derive the optimal power allocation for $\hat{P}_0$, denoted by $\hat{P}_0^*$. It can be shown that the secrecy rate of IR in this scheme is given by

$$r_0^{(\mathrm{II})} = \min_{1\le k\le K} \log_2\left(1 + \frac{\hat{P}_0\|\boldsymbol{h}\|^2}{\sigma_0^2}\right) - \log_2\left(1 + \frac{\hat{P}_0|\boldsymbol{h}^H\boldsymbol{g}_k|^2}{\|\boldsymbol{h}\|^2((\bar{P}-\hat{P}_0)|\tilde{\boldsymbol{\eta}}^H\tilde{\boldsymbol{X}}^H\boldsymbol{g}_k|^2 + \sigma_k^2)}\right). \tag{4.50}$$

Define the set of feasible power allocation as $\hat{\mathcal{P}}_0 = \{\hat{P}_0 | r_0^{(\mathrm{II})} \ge \bar{r}_0, 0 < \hat{P}_0 \le \bar{P}\}$, which is assumed to be non-empty. To maximize the weighted sum-energy transferred to ERs subject to the secrecy rate constraint of the IR, we need to solve the following

power allocation problem.

$$(\text{P9}-\text{Sub2}): \quad \underset{\hat{P}_0}{\texttt{Maximize}} \quad \frac{\sum_{k=1}^{K}\mu_k\zeta\hat{P}_0|\boldsymbol{h}^H\boldsymbol{g}_k|^2}{\|\boldsymbol{h}\|^2}+\sum_{k=1}^{K}\mu_k\zeta(\bar{P}-\hat{P}_0)|\tilde{\boldsymbol{\eta}}^H\tilde{\boldsymbol{X}}^H\boldsymbol{g}_k|^2$$
$$\texttt{Subject to} \quad \hat{P}_0\in\hat{\mathcal{P}}_0.$$

Let $\hat{P}_0^{\min}$ and $\hat{P}_0^{\max}$ denote the minimal and maximal elements in the set $\hat{\mathcal{P}}_0$, respectively. Then it can be shown that the optimal power allocation to (P9-Sub2) is given by

$$\hat{P}_0^*=\begin{cases}\hat{P}_0^{\max}, & \text{if } \frac{\sum_{k=1}^{K}\mu_k|\boldsymbol{h}^H\boldsymbol{g}_k|^2}{\|\boldsymbol{h}\|^2}\geq\sum_{k=1}^{K}\mu_k|\tilde{\boldsymbol{\eta}}^H\tilde{\boldsymbol{X}}^H\boldsymbol{g}_k|^2,\\ \hat{P}_0^{\min}, & \text{otherwise.}\end{cases} \tag{4.51}$$

4.7 Numerical Example

In this section, we provide numerical examples to validate our results. In the first numerical example, we consider a MISO SWIPT system in which Tx is equipped with $M=4$ antennas, and there are $K=3$ ERs.[2] We assume that the signal attenuation from Tx to all ERs is 30dB corresponding to an equal distance of 1 meter, i.e., $\rho_{g_k}^2=-30$dB, $1\leq k\leq K$, and that from Tx to the IR is 70dB corresponding to a distance of 20 meters, i.e., $\rho_h^2=-70$dB. The channel vectors $\boldsymbol{g}_k$'s and $\boldsymbol{h}$ are randomly generated from i.i.d. Rayleigh fading with the respective average power values specified as above. We set $\bar{P}=1$Watt (W) or 30dBm, $\zeta=50\%$, and $\sigma_k^2=-50$dBm, $0\leq k\leq K$. We also set $\mu_k=1$, $1\leq k\leq K$ in (P9); thus, the sum-energy harvested by all ERs is considered.

First, we illustrate the two-stage optimization approach to solve (P8) and (P9), as proposed in Section 4.5.1 and Section 4.6.1, respectively. Figs. 4.3(a) and 4.3(b) show the plot of $\log_2\left(\frac{1+g_1(\gamma_e)}{1+\gamma_e}\right)$ over $\gamma_e>0$ in (P8) with the individual harvested energy constraints $\bar{E}_k$'s of ERs set as 1mW, $\forall k$, and the plot of $g_2(\gamma_0)$ over $\gamma_0>0$

[2]Note that $K<M$ in this example; thus, Suboptimal Solution I for (P8) or (P9) is feasible.

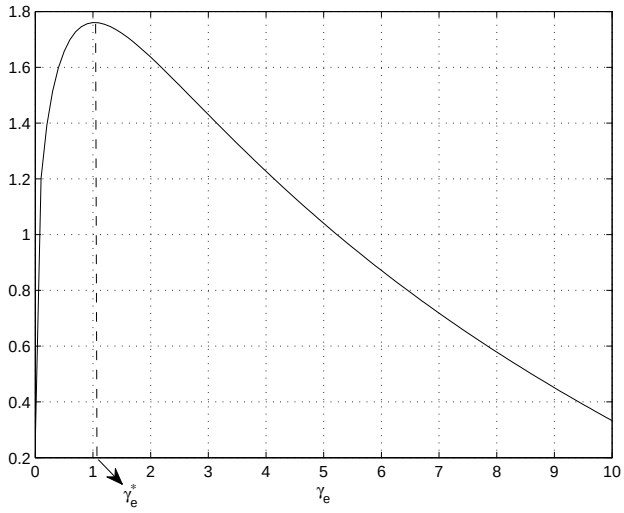

(a) $\log_2\left(\frac{1+g_1(\gamma_e)}{1+\gamma_e}\right)$ versus γ_e.

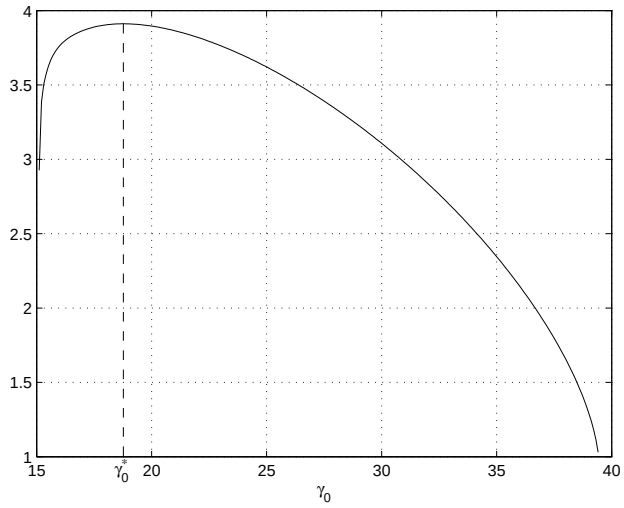

(b) $g_2(\gamma_0)$ versus γ_0.

Figure 4.3: Uniqueness of γ_e^* in (P8.2) and γ_0^* in (P9.2).

in (P9) with the secrecy rate constraint of IR $\bar{r}_0$ set as 4bps/Hz, respectively. It is observed that in this particular setup (and many others used in our simulations for which the results are not shown here due to the space limitation) there is only one single maximum point in each of the two plotted functions; however, we are unable yet to verify analytically the concavity or even the quasi-concavity of these two functions.

Next, similar to Chapter 3, we adopt the R-E region, which consists of all the achievable (secrecy) rate and harvested energy pairs for a given sum-power constraint $\bar{P}$, to compare the performances of the optimal and suboptimal solutions for (P8) proposed in Section 4.5. Note that in general the R-E region in our setup is a $(K+1)$-dimension region given one IR and K ERs. For simplicity, in the following we assume that all ERs have identical energy constraints, denoted by $E \geq 0$; thus, the R-E region reduces to a two-dimension region, which is given by

$$\mathcal{C}_{\text{R-E (P8)}} \triangleq \bigcup_{\|\boldsymbol{v}_0\|^2+\sum_{i=1}^{d}\|\boldsymbol{w}_i\|^2\leq\bar{P}} \Big\{(R,E): R \leq r_0, E \leq E_k, \forall k\Big\}, \tag{4.52}$$

where r_0 and E_k are given in (4.6) and (4.7), respectively. Note that by solving (P8) with $\bar{E}_k = \bar{E}$, $\forall k$, and by changing the values of $\bar{E}$, we can characterize the boundary of the resulting R-E region defined in (4.52).

Fig. 4.4 compares the R-E regions achieved by different information and energy beamforming solutions for (P8). It is observed that the optimal solution achieves the best R-E trade-offs. Moreover, Suboptimal Solution II is observed to perform better than Suboptimal Solution I, especially when the achievable secrecy rate for the IR is large. However, it is worth noting that Suboptimal Solution I has the lowest complexity among the three proposed solutions. Notice that for this suboptimal solution, closed-form expressions of the optimal information/energy beamforming vectors and their power allocation are given in (4.36) and (4.35), respectively. Furthermore, with no information leakage to ERs with the designed information beamforming, i.e., $\boldsymbol{v}_0^H \boldsymbol{g}_k = 0$, $\forall k$, there is no need to design a special codebook for

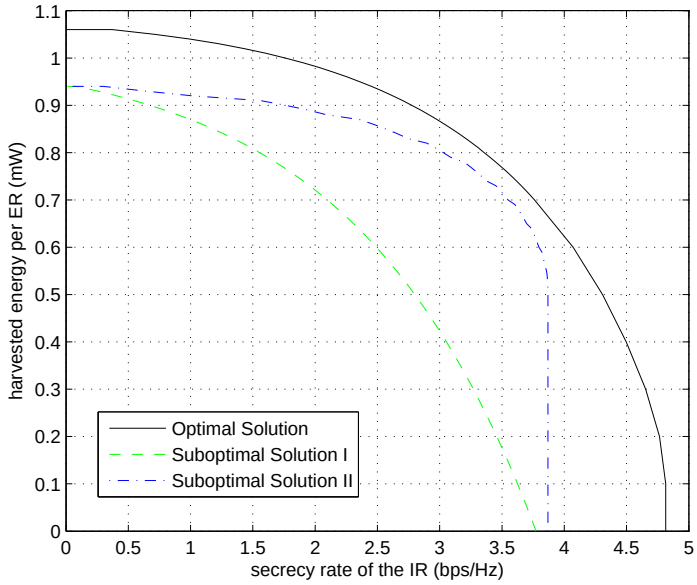

Figure 4.4: Achievable R-E region by the proposed solutions for (P8).

the secrecy information signal at the Tx [119, 121].

Next, we compare the performances of the optimal and suboptimal solutions proposed for (P9) in Section 4.6. In this case, the R-E region in general consists of all pairs of the achievable (secrecy) rate for IR and the harvested sum-energy for ERs for a given sum-power constraint $\bar{P}$. Specifically, the R-E region is defined as

$$\mathcal{C}_{\text{R-E (P9)}} \triangleq \bigcup_{\|\boldsymbol{v}_0\|^2+\sum_{i=1}^{d}\|\boldsymbol{w}_i\|^2\leq\bar{P}} \left\{(R,E): R\leq r_0, E\leq \sum_{k=1}^{K} E_k\right\}. \tag{4.53}$$

Note that by solving problem (P9) with different values of $\bar{r}_0$, we can characterize the boundary of the resulting R-E region defined in (4.53).

Fig. 4.5 shows three R-E regions achieved by different information and energy beamforming schemes for (P9). It is observed that similar to Fig. 4.5, the optimal solution achieves the best R-E trade-offs, while Suboptimal Solution II works better than Suboptimal Solution I. From the results in both Figs. 4.4 and 4.5, it is inferred

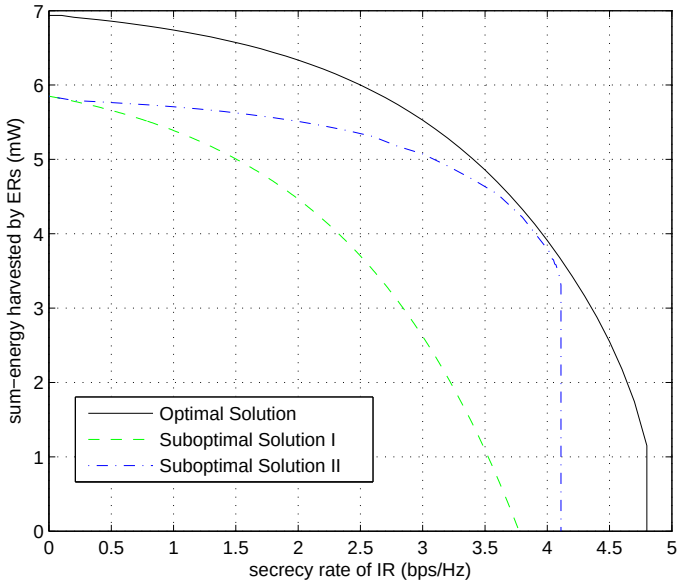

Figure 4.5: Achievable R-E region by the proposed solutions for (P9).

that in general it is more beneficial to align the information beam $\boldsymbol{v}_0$ to the same direction as the IR's channel $\boldsymbol{h}$ rather than to the null space of ERs' channels in both (P8) and (P9).

In the second numerical example, we consider a MISO SWIPT system as shown in Fig. 4.6, where there are $K = 7$ ERs and the IR is equipped with $M = 9$ antennas. In this example, we use the far-field uniform linear antenna array [153] to model the channels. Specifically,

$$\boldsymbol{h} = \rho_h \times [1, e^{j\theta_0}, \cdots, e^{j(M-1)\theta_0}]^T, \tag{4.54}$$

$$\boldsymbol{g}_k = \rho_{g_k} \times [1, e^{j\theta_k}, \cdots, e^{j(M-1)\theta_k}]^T, \quad k = 1, \cdots, K, \tag{4.55}$$

where $\rho_h^2 = -70$dB, $\rho_{g_k}^2 = -30$dB, $1 \leq k \leq K$, and $\theta_n = -\frac{2\pi d \sin(\phi_n)}{\lambda}$, $n = 0, 1, \cdots, K$, with d denoting the spacing between successive antenna elements at the Tx, λ denoting the carrier wavelength, and ϕ_0 denoting the direction of the IR to Tx, and ϕ_n for that of ER_n to Tx, $1 \leq n \leq K$. We set $d = \frac{\lambda}{2}$, and

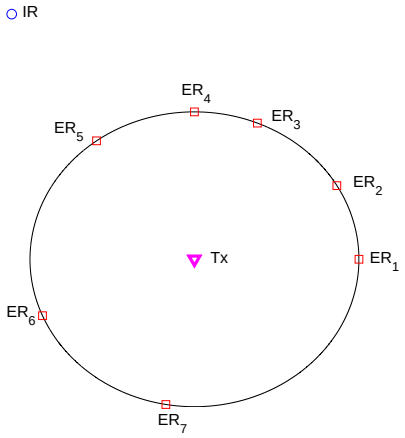

Figure 4.6: Locations of the IR and ERs.

$\{\phi_0, \phi_1, \cdots, \phi_7\} = \{\frac{11\pi}{16}, 0, \frac{\pi}{6}, \frac{3\pi}{8}, \frac{\pi}{2}, \frac{45\pi}{64}, \frac{9\pi}{8}, \frac{13\pi}{9}\}$. The other parameters are set the same as those in the first numerical example.

In this example, we activate one more ER at each time (from ER_1 to ER_7). Fig. 4.7 shows the secrecy rate achieved by our proposed optimal and suboptimal algorithms for (P8) against the number of active ERs in the system with $\bar{E}_k = 0.8\text{mW}$, $\forall k$. It is observed that with more ERs (or eavesdroppers) activated, the achievable secrecy rate for the IR is reduced for all proposed algorithms. It is also observed that when ER_5 is activated, there is a drastic decrease in the secrecy rate achieved for the IR. This is because as shown in Fig. 4.6, ER_5 is aligned in a direction very close to that of the IR ($\phi_5 \approx \phi_0$) but with higher channel power due to shorter distance from the Tx. Furthermore, it is observed that after ER_5 is activated, both Suboptimal Solutions I and II achieve zero secrecy rate. The reason is as follows. Note that for both of these two suboptimal solutions, the energy beams $\boldsymbol{w}_i$'s are aligned into the null space of $\boldsymbol{h}$, i.e., $\boldsymbol{w}_i^H \boldsymbol{h} = 0$, $\forall i$. However, in this example the direction of $\boldsymbol{g}_5$ is very close to that of $\boldsymbol{h}$. It thus follows that $\boldsymbol{w}_i^H \boldsymbol{g}_5 \approx 0$, $\forall i$. In other words, the energy beams cannot play the role of AN to reduce ER_5's SINR in this case. Moreover, since ER_5 has better channel than the IR, the achievable secrecy

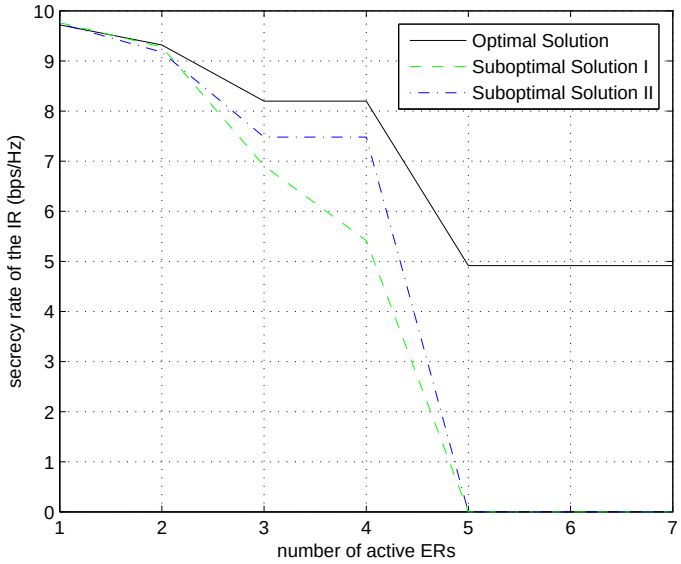

Figure 4.7: The secrecy rate of the IR over the number of active ERs with given per-ER energy constraint, $\bar{E}_k = 0.8$mW.

rate becomes close to zero.

Fig. 4.8 shows the sum-energy harvested by all ERs by the proposed optimal and suboptimal algorithms for (P9) against the number of active ERs with $\bar{r}_0 =$ 4bps/Hz. It is observed that with more ERs, the sum-energy harvested is increased in all cases. Furthermore, it is observed that when $K \leq 4$, the performance of both Suboptimal Solutions I and II is very close to that of the optimal solution. However, after ER_5 is activated, both of the suboptimal solutions achieve zero sum-energy because the secrecy rate constraint cannot be satisfied in (P9) due to the same reason as given for Fig. 4.7. From the results in Figs. 4.7 and 4.8, it is inferred that even in the challenging scenario where one ER is aligned in a direction very close to (but not the same as) the IR, our proposed optimal algorithm still achieves good performance thanks to the jointly optimized beamforming and power allocation design. However, in this case both the two suboptimal solutions cannot perform well.

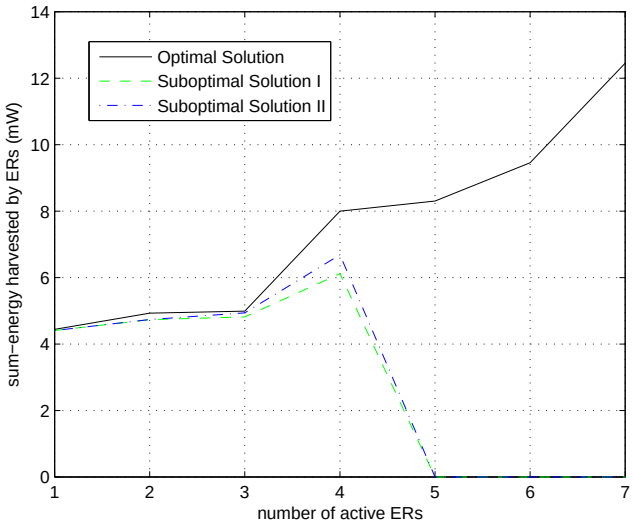

Figure 4.8: The sum-energy harvested by ERs over the number of active ERs with given secrecy rate constraint for the IR, $\bar{r}_0 = 4$bps/Hz.

4.8 Chapter Summary

In this chapter, we addressed the important problem of physical-layer security in a multiuser downlink SWIPT system. Under the MISO setup with one single IR and multiple ERs, the joint information and energy beamforming design was investigated to maximize the secret information transmission rate to the IR and yet guarantee the target amount of energy transferred to ERs, or vice verse. We proposed efficient algorithms to optimally solve the formulated non-convex design problems by applying the technique of SDR, and furthermore showed that SDR has no loss of optimality by exploiting the particular structures of the studied problems. Two suboptimal beamforming designs with lower complexity were also presented, and their performances were compared against that of the optimal solution in terms of achievable (secrecy) rate-energy trade-off. Our results revealed important new insights on how to optimally manage the interference in a multiuser SWIPT system since it plays both the roles of an energy-carrying signal for wireless energy transfer as well as an AN to enable the secrecy information transmission.

Chapter 5

Conclusion and Future Work

5.1 Conclusion

This thesis has made a comprehensive and in-depth investigation of the optimal resource allocation strategies in wireless communication and SWIPT systems by applying assorted optimization techniques. We summarize the main contributions of this thesis as follows.

- In Chapter 2, we proposed a novel approach to solve the challenging WSR maximization problem in the GIC with information transmission only. By maximizing the WSR in the achievable rate region of the GIC directly, our proposed algorithms achieved the global optimality of the non-convex WSR maximization problems in SISO-IC, SIMO-IC and MISO-IC, respectively, via combining the techniques of monotonic optimization and rate profile. The proposed methodologies are also useful for solving other performance optimization problems in general multiuser communication systems with non-convex performance trade-off region among the users.

- In Chapter 3, we proposed a novel idea to opportunistically utilize the wireless interference to harvest energy in SWIPT systems. We obtained the optimal mode switching rule between ID and EH at the receiver for a point-to-point SWIPT system over a narrowband flat-fading channel subject to time-varying co-channel interference. Moreover, in the case with CIST,

we also obtained the optimal transmit power allocation jointly with the optimal information and energy transmission scheduling. Our results provide fundamental design principles for SWIPT subject to time-varying channel and co-channel interference.

- In Chapter 4, we investigated a new security problem in multiuser SWIPT systems from a physical-layer signal processing perspective. Building upon the celebrated AN approach, we proposed a new transmission scheme by utilizing the AN signal also for WPT. Under this new scheme, the optimal design of joint information and energy beamforming at the transmitter was obtained based on the technique of SDR. Our studies provide promising new principles for designing SWIPT systems with secrecy communications.

5.2 Future Work

We highlight several future work directions in the following which we deem important and worthy of further investigations by extending the results presented in this thesis.

For WSR maximization in the GIC, it will be interesting to improve the convergence speed of the algorithms proposed in Chapter 2, especially when the number of users is large. Furthermore, the WSR maximization in MIMO-IC is not yet addressed in Chapter 2. Future work is needed to solve this more general problem by properly extending the solutions for the SINR feasibility problems when both the transmitters and receivers are equipped with multiple antennas. Last but not least, as shown in Fig. 2.7, in general there is a significant performance gap between the existing suboptimal algorithms and the proposed optimal algorithm for the case of MISO-IC. Therefore, how to reduce this gap with more efficient suboptimal algorithms is another direction for future work.

For the joint information and energy scheduling for SWIPT in the point-to-point fading channel studied in Chapter 3, the signal and interference are both assumed

to be within the same narrow band. It is thus interesting to investigate how to manage the interference in a SWIPT system operating over a broadband, which may in general span over multiple narrow bands each with or without the co-channel interference. Furthermore, it is also promising to extend our results in Chapter 3 for the single-user setup to the more general multi-user setups.

For the security problem in SWIPT, for the purpose of exposition only one single IR is assumed in Chapter 4. How to extend the results to the more general case with multiple IRs is thus worth pursuing in future work. Furthermore, only physical layer security techniques are applied in Chapter 4. How to combine this approach with cryptography techniques in the higher communication protocol layers to further improve the secrecy communication performance in SWIPT systems is thus another interesting problem to investigate in the future.

Last but not least, as an initial attempt on studying the SWIPT systems, this thesis is mainly aimed to address fundamental issues in SWIPT such as interference management strategies. To focus our study, we make some ideal assumptions such as perfect channel knowledge in the thesis. It is thus interesting to study the effects of imperfect channel estimation on practical SWIPT systems in future.

Appendix A

Proof of Lemma 2.6.1

Note that under the sum power constraint, a similar result to this lemma has been shown in [154]. However, the proof in [154] is not directly applicable in our case since in (2.36), there is an individual power constraint rather than the sum power constraint. Thus, we need to provide a new proof for this lemma shown as follows.

Suppose that there are two solutions to (2.36), denoted by $(\bar{\boldsymbol{p}}, C(\bar{\boldsymbol{W}}))$ and $(\bar{\boldsymbol{p}}', C'(\bar{\boldsymbol{W}}))$. Define a sequence of θ_k's as $\theta_k = \frac{\bar{p}'_k}{\bar{p}_k}$, $\forall k$. We can re-arrange θ_k's in a decreasing order by

$$\theta_{t1} \geq \theta_{t2} \geq \cdots \geq \theta_{tK}. \tag{A.1}$$

Since according to (2.32) we have $\bar{p}_i = \bar{p}'_i = P_i^{\max}$, it follows that $\theta_i = 1$ must hold. Hence, $\theta_{t1} \geq \theta_i = 1$. Moreover, in (A.1), at least one strict inequality must hold because otherwise $\theta_k = 1$, $\forall k$, which then implies that only one unique solution to (2.36) exists.

Next, we derive the SINR balancing value of user $t1$ as follows:

$$\begin{aligned} C'_{t1}(\bar{\boldsymbol{W}}) &= \frac{\bar{p}'_{t1}\|\bar{\boldsymbol{w}}_{t1}^H \boldsymbol{h}_{t1,t1}\|^2}{\bar{\boldsymbol{w}}_{t1}^H(\sum\limits_{j\neq t1}\bar{p}'_j \boldsymbol{h}_{t1,j}\boldsymbol{h}_{t1,j}^H + \sigma_{t1}^2\boldsymbol{I})\bar{\boldsymbol{w}}_{t1}\bar{\gamma}_{t1}} \\ &= \frac{\bar{p}_{t1}\|\bar{\boldsymbol{w}}_{t1}^H \boldsymbol{h}_{t1,t1}\|^2}{\bar{\boldsymbol{w}}_{t1}^H(\sum\limits_{j\neq t1}\bar{p}_j \boldsymbol{h}_{t1,j}\boldsymbol{h}_{t1,j}^H\frac{\theta_j}{\theta_{t1}} + \sigma_{t1}^2\boldsymbol{I}\frac{1}{\theta_{t1}})\bar{\boldsymbol{w}}_{t1}\bar{\gamma}_{t1}} \\ &> \frac{\bar{p}_{t1}\|\bar{\boldsymbol{w}}_{t1}^H \boldsymbol{h}_{t1,t1}\|^2}{\bar{\boldsymbol{w}}_{t1}^H(\sum\limits_{j\neq t1}\bar{p}_j \boldsymbol{h}_{t1,j}\boldsymbol{h}_{t1,j}^H + \sigma_{t1}^2\boldsymbol{I})\bar{\boldsymbol{w}}_{t1}\bar{\gamma}_{t1}} \\ &= C_{t1}(\bar{\boldsymbol{W}}). \end{aligned} \tag{A.2}$$

Based on (2.31), we have

$$C'(\bar{\boldsymbol{W}}) = C'_{t1}(\bar{\boldsymbol{W}}) > C_{t1}(\bar{\boldsymbol{W}}) = C(\bar{\boldsymbol{W}}). \tag{A.3}$$

Similarly, we can show that $C'_{tK}(\bar{\boldsymbol{W}}) < C_{tK}(\bar{\boldsymbol{W}})$, which yields

$$C'(\bar{\boldsymbol{W}}) = C'_{tK}(\bar{\boldsymbol{W}}) < C_{tK}(\bar{\boldsymbol{W}}) = C(\bar{\boldsymbol{W}}). \tag{A.4}$$

Since (A.3) and (A.4) contradict to each other, there must be one unique solution to (2.36). Lemma 2.6.1 is thus proven.

Appendix B

Price-Based Algorithm for SIMO-IC and MISO-IC

In this part, we provide the details of the suboptimal price-based algorithms for Problems (P1.2) in SIMO-IC and (P1.3) in MISO-IC, which can be viewed as extensions of the ADP algorithm proposed in [28] for SISO-IC. In ADP, each user announces a price that reflects its sensitivity to the interference from all other users, and then updates its transmit power by maximizing its own utility offset by the sum interference price received from all the other users. It was shown in [28] that ADP can converge to the solution that has the same Karush-Kuhn-Tucker (KKT) conditions as that of the WSR maximization problem, and is thus guaranteed to achieve at least a locally optimal solution. In the following, we extend the ADP algorithm in [28] to SIMO-IC and MISO-IC, but without the proof of convergence.

Price-Based Algorithm for SIMO-IC

In this part, we extend the ADP or price-based algorithm to SIMO-IC. First, without loss of generality, we substitute the optimal MMSE-based receive beamforming vectors for $\boldsymbol{w}_k$'s into the SINR expression given in (2.4). Then, given any transmit power vector $\boldsymbol{p}$, the achievable rate for user k can be expressed as

$$\begin{aligned} R_k(\boldsymbol{p}) &= \log_2(1+\gamma_k^{\text{SIMO}-\text{IC}}) \\ &= \log_2\left(1+p_k\boldsymbol{h}_{k,k}^H(\sum_{j\neq k}p_j\boldsymbol{h}_{k,j}\boldsymbol{h}_{k,j}^H+\sigma_k^2\boldsymbol{I})^{-1}\boldsymbol{h}_{k,k}\right). \end{aligned} \tag{B.1}$$

Thus in Problem (P1.2), we only need to find the optimal transmit power solution, without the need to consider the receive beamforming optimization.

Next, we present the KKT optimality conditions of Problem (P1.2) with the

objective function specified in (B.1). For any locally optimal power solution $\boldsymbol{p}^*$, there exist unique Lagrangian multipliers $\boldsymbol{\lambda} = (\lambda_1, \cdots, \lambda_K)$ such that for any $k = 1, \cdots, K$,

$$\mu_k \frac{\partial R_k(\boldsymbol{p}^*)}{\partial p_k} + \sum_{j \neq k} \mu_j \frac{\partial R_j(\boldsymbol{p}^*)}{\partial p_k} = \lambda_k, \tag{B.2}$$

$$\lambda_k (P_k^{\max} - p_k) = 0, \tag{B.3}$$

$$\lambda_k \geq 0. \tag{B.4}$$

Now, for the price-based algorithm, define the price charged by receiver j to transmitter k, which indicates the sensitivity of the achievable rate of receiver j subject to the power change of transmitter k, as

$$\pi_{j,k} = -\frac{\partial R_j(\boldsymbol{p})}{\partial p_k} = \frac{p_j \| \boldsymbol{h}_{j,j}^H (\sum_{i \neq j} p_i \boldsymbol{h}_{j,i} \boldsymbol{h}_{j,i}^H + \sigma_j^2 \boldsymbol{I})^{-1} \boldsymbol{h}_{j,k} \|^2}{\ln 2 \left(1 + p_j \boldsymbol{h}_{j,j}^H (\sum_{i \neq j} p_i \boldsymbol{h}_{j,i} \boldsymbol{h}_{j,i}^H + \sigma_j^2 \boldsymbol{I})^{-1} \boldsymbol{h}_{j,j} \right)}. \tag{B.5}$$

Consequently, we see that the KKT conditions in (B.2), (B.3) and (B.4) are both necessary and sufficient for the optimal solution to the following problem for user k, $k = 1, \cdots, K$:

$$\begin{aligned} \underset{p_k}{\texttt{Maximize}} \quad & \mu_k \log_2 \left(1 + p_k \boldsymbol{h}_{k,k}^H (\sum_{j \neq k} p_j \boldsymbol{h}_{k,j} \boldsymbol{h}_{k,j}^H + \sigma_k^2 \boldsymbol{I})^{-1} \boldsymbol{h}_{k,k} \right) - p_k \sum_{j \neq k} \mu_j \pi_{j,k} \\ \texttt{Subject to} \quad & p_k \leq P_k^{\max}, \end{aligned} \tag{B.6}$$

where p_j and $\pi_{j,k}$ are fixed, $\forall j \neq k$.

Similar to the ADP algorithm in [28], we propose the following algorithm to update the price and transmit power iteratively for all users in SIMO-IC. Specifically, at each iteration the algorithm does the following:

1. Each user announces its price obtained using (B.5) to all the other users;

2. Each user updates its transmit power by solving Problem (B.6), i.e.,

$$p_k = \left[\frac{\mu_k}{\ln 2 \sum_{j \neq k} \mu_j \pi_{j,k}} - \frac{1}{\boldsymbol{h}_{k,k}^H (\sum_{j \neq k} p_j \boldsymbol{h}_{k,j} \boldsymbol{h}_{k,j}^H + \sigma_k^2 \boldsymbol{I})^{-1} \boldsymbol{h}_{k,k}} \right]_0^{P_k^{\max}}, \quad \forall k, \tag{B.7}$$

where $[x]_a^b = \max(\min(x, b), a)$.

Because Problems (P1.2) and (B.6) possess the same KKT optimality conditions, when the above algorithm converges to a set of optimal solutions to problems in (B.6) for all k's, this set of solutions will be at least a locally optimal solution to Problem (P1.2).

Price-Based Algorithm for MISO-IC

Next, we extend the ADP algorithm to MISO-IC. For any given transmit beamforming vectors $\boldsymbol{V}$, we first define the price for user k as

$$\pi_k = -\frac{\partial R_k}{\partial \Gamma_k} = \frac{\|\boldsymbol{h}_{k,k}^H \boldsymbol{v}_k\|^2}{\ln 2 (\|\boldsymbol{h}_{k,k}^H \boldsymbol{v}_k\|^2 + \Gamma_k + \sigma_k^2)(\Gamma_k + \sigma_k^2)}, \tag{B.8}$$

where $\Gamma_k = \sum_{j \neq k} \|\boldsymbol{h}_{k,j}^H \boldsymbol{v}_j\|^2$ is the total interference power at the kth receiver. Let $\boldsymbol{S}_k = \boldsymbol{v}_k \boldsymbol{v}_k^H$, $\forall k$. Given fixed interference prices and beamforming vectors of all other users, the following problem is to be solved by any user k for its own transmit beamforming update:

$$\begin{aligned} \underset{\boldsymbol{S}_k}{\texttt{Maximize}} \quad & \mu_k \log_2 (1 + \frac{\boldsymbol{h}_{k,k}^H \boldsymbol{S}_k \boldsymbol{h}_{k,k}}{\Gamma_k + \sigma_k^2}) - \sum_{j \neq k} \mu_j \pi_j \boldsymbol{h}_{k,j}^H \boldsymbol{S}_k \boldsymbol{h}_{j,k} \\ \texttt{Subject to} \quad & \mathrm{Tr}(\boldsymbol{S}_k) \leq P_k^{\max} \\ & \boldsymbol{S}_k \succeq 0, \end{aligned} \tag{B.9}$$

where $\boldsymbol{S}_k \succeq 0$ means that $\boldsymbol{S}_k$ is a positive semi-definite matrix. Similar to the previous case of SIMO-IC, we can show that the KKT conditions of Problem (B.9) with $k = 1, \cdots, K$ are also those of Problem (P1.3) by replacing $\boldsymbol{v}_k \boldsymbol{v}_k^H$ with $\boldsymbol{S}_k$, $\forall k$.

However, Problem (P1.3) requires that the optimal solution $\boldsymbol{S}_k^*$ in Problem (B.9) to be rank-one, which is not guaranteed a priori. Thus, Problem (B.9) is a relaxation of the original WSR maximization problem (P1.3) without considering the rank-one constraint.

Interestingly, it was recently shown in [34] that the optimal solution to Problem (B.9) is always of rank-one, i.e., $\boldsymbol{S}_k^* = \boldsymbol{v}_k \boldsymbol{v}_k^H$. Hence, we propose a price-based algorithm for MISO-IC in a similar way to that for SIMO-IC. When this algorithm converges to a set of optimal solutions to problems in (B.9) with $k = 1, \cdots, K$, this set of solutions are all rank-one and thus corresponds to at least a locally optimal solution to Problem (P1.3).

For this price-based algorithm for MISO-IC, the interference price can be iteratively updated according to (B.8). As for the update of beamforming vectors, we need to solve Problem (B.9) for each user k. It can be verified that Problem (B.9) is convex with strictly feasible points, and thus it can be solved by the standard Lagrangian duality method [62] with a zero duality gap. The details of solving Problem (B.9) can be found in Appendix I of [34], and are thus omitted here.

Appendix C

Characterizations of the Vertex Points in Figs. 3.8 (a) and (b)

In this appendix, we characterize the vertex points on the boundary of the O-E region and R-E region (cf. Fig. 3.8) for both the cases with and without CSIT.

O-E region without CSIT

As shown in Fig. 3.8 (a), $Q_{\max}$ is given by

$$Q_{\max} = E_{\nu}[h(\nu)P + I(\nu)], \tag{C.1}$$

when $\rho(\nu) = 0$, $\forall \nu$, i.e., EH mode is active all the time at Rx and thus the resulting non-outage probability $\delta_{\min} = 0$ (corresponding to the outage probability equal to 1). Moreover, $Q_{\min}$ and $\delta_{\max}$ are given by

$$Q_{\min} = \int\limits_{\nu:\log\left(1+\frac{h(\nu)P}{I(\nu)+\sigma^2}\right)<r_0} \big(h(\nu)P + I(\nu)\big) f_{\nu}(h, I) d\nu, \tag{C.2}$$

$$\delta_{\max} = Pr\left\{\log\left(1 + \frac{h(\nu)P}{I(\nu)+\sigma^2}\right) \geq r_0\right\}. \tag{C.3}$$

Note that $Q_{\min}$ is the minimum average harvested energy at Rx when the maximum non-outage probability (or minimum outage probability) is achieved. Since the set for the outage fading states is non-empty in (C.2), $Q_{\min} \neq 0$ in general.

O-E region with CSIT

As shown in Fig. 3.8 (a), the point $(\delta_{\min}, Q_{\max})$ is achieved when all the fading states are allocated to EH mode, i.e., $\rho(\nu) = 0$, $\forall \nu$. Thus, the resulting non-outage

probability is $\delta_{\min} = 0$. Moreover, the harvested energy can be expressed as $Q = E_\nu[h(\nu)p(\nu)] + E_\nu[I(\nu)]$, where the first term is the energy harvested from the signal, while the second term is due to the interference. To maximize the first term under both the PPC and APC, the optimal power control policy is to transmit at peak power at the fading states with the largest possible h's. Let $\hat{h}_1$ be the threshold that satisfies

$$\int\limits_{\nu:h(\nu)\geq\hat{h}_1} P_{\text{peak}} f_\nu(h, I) d\nu = P_{\text{avg}}. \tag{C.4}$$

Then $Q_{\max}$ can be expressed as

$$Q_{\max} = \int\limits_{\nu:h(\nu)\geq\hat{h}_1} h(\nu) P_{\text{peak}} f_\nu(h, I) d\nu + E_\nu[I(\nu)]. \tag{C.5}$$

To obtain $\delta_{\max}$, we need to minimize the outage probability under both the APC and PPC without presence of the energy harvester. It can be shown that the optimal power allocation to achieve the maximum non-outage probability can be expressed as the well-known truncated channel inversion policy [91], [89]:

$$p^*(\nu) = \begin{cases} \frac{(e^{r_0}-1)(I(\nu)+\sigma^2)}{h(\nu)}, & \text{if } \frac{h(\nu)}{I(\nu)+\sigma^2} \geq \hat{h}_2. \\ 0, & \text{otherwise} \end{cases} \tag{C.6}$$

where $\hat{h}_2 = \max\{\beta(e^{r_0} - 1), \frac{e^{r_0}-1}{P_{\text{peak}}}\}$ with β denoting the optimal dual variable associated with the APC that satisfies $E_\nu[p^*(\nu)] = P_{\text{avg}}$. Then the maximum non-outage can be expressed as

$$\delta_{\max} = Pr\left\{\frac{h(\nu)}{I(\nu) + \sigma^2} \geq \hat{h}_2\right\}. \tag{C.7}$$

On the other hand, $Q_{\min}$ is achieved when Rx harvests energy at all the outage

fading states. Let $\hat{h}_3$ denote the value of h that satisfies

$$P_{\text{avg}} = \int\limits_{\nu:h(\nu)\geq\hat{h}_3,\frac{h(\nu)}{I(\nu)+\sigma^2}\leq\hat{h}_2} P_{\text{peak}} f_\nu(h,I)d\nu + \int\limits_{\frac{h(\nu)}{I(\nu)+\sigma^2}\geq\hat{h}_2} p^*(\nu) f_\nu(h,I)d\nu. \tag{C.8}$$

Then the minimum harvested energy can be expressed as

$$Q_{\min} = \int\limits_{\nu:h(\nu)\geq\hat{h}_3,\frac{h(\nu)}{I(\nu)+\sigma^2}\leq\hat{h}_2} hP_{\text{peak}} f_\nu(h,I)d\nu + \int\limits_{\nu:\frac{h(\nu)}{I(\nu)+\sigma^2}\leq\hat{h}_2} I(\nu) f_\nu(h,I)d\nu. \tag{C.9}$$

Note that if $\int\limits_{\frac{h(\nu)}{I(\nu)+\sigma^2}\geq\hat{h}_2} p^*(\nu) f_\nu(h,I)d\nu \geq P_{\text{avg}}$, then $\hat{h}_3 = \infty$, i.e., no power is available for energy transfer at Tx. Thus, $Q_{\min}$ is only due to the interference power. Since the set for the outage fading states is non-empty, $Q_{\min} \neq 0$ since the receiver can at least harvest energy from the interference in the outage fading states.

R-E region without CSIT

As shown in Fig. 3.8 (b), the maximum harvested energy $Q_{\max}$ is achieved when all the fading states are allocated to EH mode, i.e., $\rho(\nu) = 0$, $\forall\nu$, and thus has the same expression as that given in (C.1). Moreover, $R_{\min} = 0$. On the other hand, the ergodic capacity is maximized when all the fading states are allocated to ID mode, i.e., $\rho(\nu) = 1$, $\forall\nu$. Consequently, $Q_{\min} = 0$ and

$$R_{\max} = E_\nu\left[\log\left(1 + \frac{h(\nu)P}{I(\nu)+\sigma^2}\right)\right]. \tag{C.10}$$

R-E region with CSIT

As shown in Fig. 3.8 (b), similar to the case of O-E region with CSIT, the maximum harvested energy $Q_{\max}$ is given in (C.5), and $R_{\min} = 0$. As for the point $(R_{\max}, Q_{\min})$, to maximize the ergodic capacity under both the APC and PPC, the optimal transmit power policy is the well-known "water-filling" power allocation

given by [89]

$$p^*(\nu) = \left[\frac{1}{\lambda^*} - \frac{I(\nu)+\sigma^2}{h(\nu)}\right]_0^{P_{\text{peak}}}, \tag{C.11}$$

where $[x]_a^b \triangleq \max(\min(x,b),a)$, and λ^* is the optimal dual variable associated with P_{avg} satisfying $E_\nu[p^*(\nu)] = P_{\text{avg}}$. Thus, the maximum rate is given by

$$R_{\max} = E_\nu\left[\log\left(1+\frac{h(\nu)p^*(\nu)}{I(\nu)+\sigma^2}\right)\right]. \tag{C.12}$$

Then, for the fading states satisfying $\frac{h(\nu)}{I(\nu)+\sigma^2} < \lambda^*$, Rx can harvest energy from the interference. Thus the minimum harvested energy is in general non-zero and can be expressed as

$$Q_{\min} = \int\limits_{\nu:\frac{h(\nu)}{I(\nu)+\sigma^2}<\lambda^*} I(\nu) f_\nu(h,I) d\nu. \tag{C.13}$$

Appendix D

Proof of Lemma 4.5.2

Let e^* and $\{\boldsymbol{v}_0^*, \{\boldsymbol{w}_i^*\}\}$ denote the optimal value and its attaining solution to (P8), respectively. According to Lemma 4.5.1, with $\gamma_e^* = \max\limits_{1\le k\le K} \frac{|\boldsymbol{g}_k^H \boldsymbol{v}_0^*|^2}{\sum\limits_{i=1}^{d} |\boldsymbol{g}_k^H \boldsymbol{w}_i^*|^2+\sigma_k^2}$, we have $g_1(\gamma_e^*) = \frac{|\boldsymbol{h}^H \boldsymbol{v}_0^*|^2}{\sum\limits_{i=1}^{d} |\boldsymbol{h}^H \boldsymbol{w}_i^*|^2+\sigma_0^2}$, and it thus follows for (P8.2) that $\log_2\left(\frac{1+g_1(\gamma_e^*)}{1+\gamma_e^*}\right) = e^*$. Thus, we have

$$\max_{\gamma_e>0} \log_2\left(\frac{1+g_1(\gamma_e)}{1+\gamma_e}\right) \ge e^*. \tag{D.1}$$

On the other hand, given any $\bar{\gamma}_e > 0$ in problem (P8.1), let $\bar{\boldsymbol{v}}_0^*$ and $\{\bar{\boldsymbol{w}}_i^*\}$ denote the corresponding optimal solution, and SINR_0^* and SINR_k^* be given in (4.4) and (4.5), respectively, by substituting the above optimal solution. Therefore, we have

$$\begin{aligned} e^* &\overset{(a)}{\ge} \log_2(1+\mathrm{SINR}_0^*) - \max_{1\le k\le K} \log_2(1+\mathrm{SINR}_k^*) \\ &\overset{(b)}{\ge} \log_2(1+g_1(\bar{\gamma}_e)) - \log_2(1+\bar{\gamma}_e),\ \forall \bar{\gamma}_e > 0, \end{aligned} \tag{D.2}$$

where (a) follows since $\bar{\boldsymbol{v}}_0^*$ and $\{\bar{\boldsymbol{w}}_i^*\}$ is a feasible solution to (P8), and (b) is true since $\mathrm{SINR}_0^* = g_1(\bar{\gamma}_e)$ and $\mathrm{SINR}_k^* \le \bar{\gamma}_e$, $\forall k$. From (D.1) and (D.2), it follows that $\max\limits_{\gamma_e>0} \log_2\left(\frac{1+g_1(\gamma_e)}{1+\gamma_e}\right) = e^*$. Lemma 4.5.2 is thus proved.

Appendix E

Proof of Lemma 4.5.4

First, we show that $\lambda^* > 0$. Let $\boldsymbol{A}_1^*$, $\boldsymbol{B}_1^*$, and ξ_1^* be given in (4.18), (4.19), and (4.20), respectively, by substituting the optimal dual solution of problem (P8.1-SDR-Eqv). To ensure that the Lagrangian in (4.17) is bounded from above such that the dual function exists, it follows that

$$\boldsymbol{A}_1^* \preceq \boldsymbol{0}, \quad \boldsymbol{B}_1^* \preceq \boldsymbol{0}, \quad \xi_1^* \leq 0. \tag{E.1}$$

According to (4.17), the dual problem of (P8.1-SDR-Eqv) can be expressed as

$$\begin{aligned} (\text{P8.1} - \text{SDR} - \text{Eqv} - \text{Dual}): \quad & \underset{\lambda,\{\beta_k\},\{\alpha_k\},\theta}{\texttt{Minimize}} \quad \lambda \\ & \texttt{Subject to} \quad \boldsymbol{A}_1 \preceq \boldsymbol{0}, \quad \boldsymbol{B}_1 \preceq \boldsymbol{0}, \quad \xi_1 \leq 0, \\ & \qquad\qquad\quad \beta_k \geq 0, \quad \alpha_k \geq 0, \quad \forall k, \quad \theta \geq 0. \end{aligned}$$

Since the duality gap between (P8.1-SDR-Eqv) and its dual problem (P8.1-SDR-Eqv-Dual) is zero, λ^* is equal to the optimal value of (P8.1-SDR-Eqv). Therefore, we have $\lambda^* > 0$.

Next, we show that $\theta^* > 0$ by contradiction. Define $\phi = \{k|(\beta_k^*)^2 + (\alpha_k^*)^2 > 0,\ k = 1, \cdots, K\}$. In the following, we discuss two cases in each of which we show that (E.1) cannot be true if $\theta^* = 0$.

The case of $\phi = \emptyset$

Suppose that $\theta^* = 0$. In this case, we have $\boldsymbol{A}_1^* = \boldsymbol{H} \succeq \boldsymbol{0}$, which contradicts to (E.1). Thus, in this case, $\theta^* > 0$ must be true.

The case of $\phi \neq \emptyset$

Suppose that $\theta^* = 0$. Then in this case, we have $\boldsymbol{B}_1^* = -\lambda^* \boldsymbol{H}^* + \sum_{k\in\phi}(\beta_k^*\gamma_e + \alpha_k^*\zeta)\boldsymbol{G}_k$. Since $\sum_{k\in\phi}(\beta_k^*\gamma_e + \alpha_k^*\zeta)\boldsymbol{G}_k \succeq \boldsymbol{0}$ and $\lambda^* > 0$, to guarantee that $\boldsymbol{B}_1^* \preceq \boldsymbol{0}$, it requires that any $\boldsymbol{x} \in \mathbb{C}^{M\times 1}$ that lies in the null space of $\boldsymbol{H}$ must also be in the null space of $\boldsymbol{G}_k$, $\forall k \in \phi$; however, this cannot be true since all the channels $\boldsymbol{h}$ and $\boldsymbol{g}_k$'s are assumed to be linearly independent. Thus, in this case, we also conclude that $\theta^* > 0$.

By combining the above two cases, it follows that $\theta^* > 0$. Lemma 4.5.4 is thus proved.

Appendix F

Proof of Proposition 4.5.1

The KKT conditions of problem (P8.1-SDR-Eqv) are expressed as

$$\boldsymbol{A}_1^* \boldsymbol{S}^* = \boldsymbol{0}, \quad \boldsymbol{B}_1^* \boldsymbol{Q}^* = \boldsymbol{0}. \tag{F.1}$$

First, we show that $\text{rank}(\boldsymbol{Q}^*) \leq \min(K, M)$. The proof directly follows if $K \geq M$ since $\text{rank}(\boldsymbol{Q}^*) \leq M = \min(K, M)$. Thus, in the following we focus on the case of $K < M$.

Lemma F.0.1. *Let $\boldsymbol{Y}$ and $\boldsymbol{Z}$ be two matrices of the same dimension. It then holds that* $\text{rank}(\boldsymbol{Y} + \boldsymbol{Z}) \geq \text{rank}(\boldsymbol{Y}) - \text{rank}(\boldsymbol{Z})$.

Proof. It is known that $\text{rank}(\boldsymbol{Y}) + \text{rank}(\boldsymbol{Z}) \geq \text{rank}(\boldsymbol{Y} + \boldsymbol{Z})$ if $\boldsymbol{Y}$ and $\boldsymbol{Z}$ are of the same dimension. Then we have $\text{rank}(\boldsymbol{Y} + \boldsymbol{Z}) + \text{rank}(-\boldsymbol{Z}) \geq \text{rank}(\boldsymbol{Y})$. Since $\text{rank}(\boldsymbol{Z}) = \text{rank}(-\boldsymbol{Z})$, Lemma F.0.1 is proved. □

Define $\boldsymbol{C}_1^* = -\lambda^* \boldsymbol{H} - \theta^* \boldsymbol{I}$. Since according to Lemma 4.5.4 we have $\lambda^* > 0$ and $\theta^* > 0$, it follows that $\boldsymbol{C}_1^* \prec \boldsymbol{0}$ and thus $\text{rank}(\boldsymbol{C}_1^*) = M$. Furthermore, $\boldsymbol{B}_1^*$ can be expressed as $\boldsymbol{B}_1^* = \boldsymbol{C}_1^* + \sum_{k=1}^K (\beta_k^* \gamma_e + \alpha_k^* \zeta) \boldsymbol{G}_k$. As a result, according to Lemma F.0.1 we have

$$\text{rank}(\boldsymbol{B}_1^*) \geq \text{rank}(\boldsymbol{C}_1^*) - \text{rank}\left(\sum_{k=1}^K (\beta_k^* \gamma_e + \alpha_k^* \zeta) \boldsymbol{G}_k \right) \overset{(a)}{\geq} M - K, \tag{F.2}$$

where (a) is due to the fact that $\text{rank}\left(\sum_{k=1}^K (\beta_k^* \gamma_e + \alpha_k^* \zeta) \boldsymbol{G}_k \right) \leq K$. According to (F.1), $\boldsymbol{Q}^*$ must lie in the null space of $\boldsymbol{B}_1^*$. Therefore, if $K < M$, $\text{rank}(\boldsymbol{Q}^*) \leq M - \text{rank}(\boldsymbol{B}_1^*) \leq K$. By combining the above two cases of $K \geq M$ and $K < M$,

it follows that $\text{rank}(\boldsymbol{Q}^*) \leq \min(K, M)$. The first part of Proposition 4.5.1 is thus proved.

Next, we prove the second part of Proposition 4.5.1. Define

$$\boldsymbol{D}_1^* = -\lambda^* \boldsymbol{H} - \sum_{k=1}^{K} \beta_k^* \boldsymbol{G}_k + \sum_{k=1}^{K} \alpha_k^* \zeta \boldsymbol{G}_k - \theta^* \boldsymbol{I} = \boldsymbol{B}_1^* - \sum_{k=1}^{K} (1+\gamma_e)\, \beta_k^* \boldsymbol{G}_k. \tag{F.3}$$

Then we have

$$\boldsymbol{A}_1^* = \boldsymbol{D}_1^* + (1+\lambda^*)\boldsymbol{H}. \tag{F.4}$$

Define $l_1 = \text{rank}(\boldsymbol{D}_1^*)$. If $l_1 = M$, then we can conclude that $\text{rank}(\boldsymbol{A}_1^*) \geq M-1$ according to (F.4) and Lemma F.0.1. However, if $\text{rank}(\boldsymbol{A}_1^*) = M$, then according to (F.1) it follows that $\boldsymbol{S}^* = \boldsymbol{0}$, which cannot be the optimal solution to (P8-SDR-Eqv). Therefore, we have $\text{rank}(\boldsymbol{A}_1^*) = M-1$ and thus $\boldsymbol{S}^* = b\boldsymbol{\tau}_1\boldsymbol{\tau}_1^H$ if $l_1 = M$, where $\boldsymbol{\tau}_1$ spans the null space of $\boldsymbol{A}_1^*$. Next, we consider the case where $\boldsymbol{D}_1^*$ is not full-rank, i.e., $l_1 < M$. In this case, let $\boldsymbol{\Pi}_1 \in \mathbb{C}^{M\times(M-l_1)}$ with $\boldsymbol{\Pi}_1^H\boldsymbol{\Pi}_1 = \boldsymbol{I}$ denote the orthogonal basis for the null space of $\boldsymbol{D}_1^*$, i.e., $\boldsymbol{D}_1^*\boldsymbol{\Pi}_1 = \boldsymbol{0}$. Let $\boldsymbol{\pi}_{1,n}$ denote the nth column of $\boldsymbol{\Pi}_1$, $1 \leq n \leq M-l_1$. Then we have

$$\boldsymbol{\pi}_{1,n}^H \boldsymbol{A}_1^* \boldsymbol{\pi}_{1,n} = \boldsymbol{\pi}_{1,n}^H \left(\boldsymbol{D}_1^* + (1+\lambda^*)\boldsymbol{H}\right)\boldsymbol{\pi}_{1,n} = (1+\lambda^*)|\boldsymbol{h}^H\boldsymbol{\pi}_{1,n}|^2,\ 1 \leq n \leq M-l_1. \tag{F.5}$$

Since $\boldsymbol{A}_1^* \preceq \boldsymbol{0}$ and $1+\lambda^* > 0$, it follows that $|\boldsymbol{h}^H\boldsymbol{\pi}_{1,n}|^2 = 0$, $\forall n$, or

$$\boldsymbol{H}\boldsymbol{\Pi}_1 = \boldsymbol{0}. \tag{F.6}$$

As a result, we have

$$\boldsymbol{A}_1^*\boldsymbol{\Pi}_1 = \left(\boldsymbol{D}_1^* + (1+\lambda^*)\boldsymbol{H}\right)\boldsymbol{\Pi}_1 = \boldsymbol{0}. \tag{F.7}$$

Moreover, according to (F.4) and Lemma F.0.1, we have

$$\text{rank}(\boldsymbol{A}_1^*) \geq \text{rank}(\boldsymbol{D}_1^*) - \text{rank}\left((1+\lambda^*)\boldsymbol{H}\right) = l_1 - 1. \tag{F.8}$$

Let $\boldsymbol{\Omega}_1$ denote the orthogonal basis for the null space of $\boldsymbol{A}_1^*$, it then follows that

$$\text{rank}(\boldsymbol{\Omega}_1) = M - \text{rank}(\boldsymbol{A}_1^*) \leq M - l_1 + 1. \tag{F.9}$$

Next, we show that $\text{rank}(\boldsymbol{\Omega}_1) = M - l_1 + 1$. According to (F.7), $\boldsymbol{\Pi}_1$ spans $M - l_1$ orthogonal dimensions of the null space of $\boldsymbol{A}_1^*$, i.e., $\text{rank}(\boldsymbol{\Omega}_1) \geq M - l_1$. Suppose that $\text{rank}(\boldsymbol{\Omega}_1) = M - l_1$; then we have $\boldsymbol{\Omega}_1 = \boldsymbol{\Pi}_1$. According to (E.1) and (F.1), $\boldsymbol{S}^*$ can be expressed as $\boldsymbol{S}^* = \sum_{n=1}^{M-l_1} a_n \boldsymbol{\pi}_{1,n}\boldsymbol{\pi}_{1,n}^H$, where $a_n \geq 0$, $\forall n$. However, in this case, no information is transferred to IR since according to (F.6), $\boldsymbol{\pi}_{1,n}$'s all lie in the null space of $\boldsymbol{H}$. As a result, according to (F.9) there exists only one single subspace spanned by $\boldsymbol{\tau}_1 \in \mathbb{C}^{M\times 1}$ of unit norm, which lies in the null space of $\boldsymbol{A}_1^*$, i.e., $\boldsymbol{A}_1^*\boldsymbol{\tau}_1 = \boldsymbol{0}$, and is orthogonal to the span of $\boldsymbol{\Pi}_1$, i.e., $\boldsymbol{\Pi}_1^H\boldsymbol{\tau}_1 = \boldsymbol{0}$. To summarize, we have

$$\boldsymbol{\Omega}_1 = [\boldsymbol{\Pi}_1 \ \boldsymbol{\tau}_1], \tag{F.10}$$

and thus $\text{rank}(\boldsymbol{\Omega}_1) = M - l_1 + 1$. Moreover, according to (E.1) and (F.1), any optimal solution $\boldsymbol{S}^*$ to problem (P8.1-SDR-Eqv) can be expressed as $\boldsymbol{S}^* = \sum_{n=1}^{M-l_1} a_n \boldsymbol{\pi}_{1,n}\boldsymbol{\pi}_{1,n}^H + b\boldsymbol{\tau}_1\boldsymbol{\tau}_1^H$, where $a_n \geq 0$, $\forall n$, and $b > 0$. The second part of Proposition 4.5.1 is thus proved.

Last, we prove the third part of Proposition 4.5.1. Suppose that $(\boldsymbol{S}^*, \boldsymbol{Q}^*, t^*)$ is an optimal solution to problem (P8.1-SDR-Eqv), where $\boldsymbol{S}^*$ is given in (4.22) and $\text{rank}(\boldsymbol{S}^*) > 1$. Then consider the new solution $(\bar{\boldsymbol{S}}^*, \bar{\boldsymbol{Q}}^*, \bar{t}^*)$ given in (4.23)-(4.25). It

can be shown that with this new solution we have

$$\mathrm{Tr}(\boldsymbol{H}\bar{\boldsymbol{S}}^*) = \mathrm{Tr}\left(\boldsymbol{H}\left(\boldsymbol{S}^* - \sum_{n=1}^{M-l_1} a_n \boldsymbol{\pi}_{1,n}\boldsymbol{\pi}_{1,n}^H\right)\right) = \mathrm{Tr}(\boldsymbol{H}\boldsymbol{S}^*), \tag{F.11}$$

$$\mathrm{Tr}(\boldsymbol{H}\bar{\boldsymbol{Q}}^*) + \bar{t}^*\sigma_0^2 = \mathrm{Tr}\left(\boldsymbol{H}\left(\boldsymbol{Q}^* + \sum_{n=1}^{M-l_1} a_n \boldsymbol{\pi}_{1,n}\boldsymbol{\pi}_{1,n}^H\right)\right) + t^*\sigma_0^2 = \mathrm{Tr}(\boldsymbol{H}\boldsymbol{Q}^*) + t^*\sigma_0^2 = 1, \tag{F.12}$$

$$\mathrm{Tr}(\boldsymbol{G}_k\bar{\boldsymbol{S}}^*) \leq \mathrm{Tr}(\boldsymbol{G}_k\boldsymbol{S}^*) \leq \gamma_e(\mathrm{Tr}(\boldsymbol{G}_k\boldsymbol{Q}^*) + t^*\sigma_k^2) \leq \gamma_e(\mathrm{Tr}(\boldsymbol{G}_k\bar{\boldsymbol{Q}}^*) + \bar{t}^*\sigma_k^2), \quad \forall k, \tag{F.13}$$

$$\zeta(\mathrm{Tr}(\boldsymbol{G}_k\bar{\boldsymbol{S}}^*) + \mathrm{Tr}(\boldsymbol{G}_k\bar{\boldsymbol{Q}}^*)) = \zeta(\mathrm{Tr}(\boldsymbol{G}_k\boldsymbol{S}^*) + \mathrm{Tr}(\boldsymbol{G}_k\boldsymbol{Q}^*)) \geq \bar{t}^*\bar{E}_k, \quad \forall k, \tag{F.14}$$

$$\mathrm{Tr}(\bar{\boldsymbol{S}}^*) + \mathrm{Tr}(\bar{\boldsymbol{Q}}^*) = \mathrm{Tr}(\boldsymbol{S}^*) + \mathrm{Tr}(\boldsymbol{Q}^*) \leq \bar{t}^*\bar{P}, \tag{F.15}$$

$$\bar{\boldsymbol{S}}^* \succeq \boldsymbol{0}, \quad \bar{\boldsymbol{Q}}^* \succeq \boldsymbol{0}, \quad \bar{t}^* > 0. \tag{F.16}$$

(F.11) indicates that the new solution $(\bar{\boldsymbol{S}}^*, \bar{\boldsymbol{Q}}^*, t^*)$ can achieve the same optimal value of (P8.1-SDR-Eqv), while (F.12)-(F.16) imply that the new solution satisfies all the constraints of (P8.1-SDR-Eqv). Thus, $(\bar{\boldsymbol{S}}^*, \bar{\boldsymbol{Q}}^*, t^*)$ is also an optimal solution to (P8.1-SDR-Eqv), with $\mathrm{rank}(\bar{\boldsymbol{S}}^*) = 1$.

Proposition 4.5.1 is thus proved.

Appendix G

Proof of Proposition 4.5.2

According to Proposition 4.5.1, if $l_1 = \text{rank}(\boldsymbol{D}_1^*) = M$, then $\boldsymbol{S}^* = b\boldsymbol{\tau}_1\boldsymbol{\tau}_1^H$, and it thus follows that $\text{rank}(\boldsymbol{S}^*) = 1$ is always true for (P1.1-SDR-Eqv). Moreover, since $\boldsymbol{B}_1^* \preceq \boldsymbol{0}$ and $-\sum_{k=1}^K (1+\gamma_e)\beta_k^* \boldsymbol{G}_k \preceq \boldsymbol{0}$, we have $\boldsymbol{D}_1^* \preceq \boldsymbol{0}$ according to (F.3). As a result, to show $\text{rank}(\boldsymbol{D}_1^*) = M$, it is sufficient to verify that the maximum eigenvalue of $\boldsymbol{D}_1^*$ is negative, i.e., $\boldsymbol{D}_1^* \prec \boldsymbol{0}$. Therefore, in the following we show by contradict that if there is no non-zero solution to the equations given in (4.28), then the maximum eigenvalue of $\boldsymbol{D}_1^*$ must be negative.

Since $\boldsymbol{D}_1^* \preceq \boldsymbol{0}$, its maximum eigenvalue can be either zero or negative. Suppose that the maximum eigenvalue of $\boldsymbol{D}_1^*$ is zero. Then there exists at least an $\boldsymbol{x} \in \mathbb{C}^{M\times 1} \neq \boldsymbol{0}$ such that $\boldsymbol{x}^H \boldsymbol{D}_1^* \boldsymbol{x} = 0$. Since $\boldsymbol{B}_1^* \preceq \boldsymbol{0}$ and $-\sum_{k=1}^K (1+\gamma_e)\beta_k^* \boldsymbol{G}_k \preceq \boldsymbol{0}$, according to (F.3) we have

$$\boldsymbol{x}^H \boldsymbol{B}_1^* \boldsymbol{x} = 0, \tag{G.1}$$

$$\boldsymbol{x}^H \sum_{k=1}^K (1+\gamma_e)\, \beta_k^* \boldsymbol{G}_k \boldsymbol{x} = 0. \tag{G.2}$$

From (G.2), we have

$$\boldsymbol{x}^H \boldsymbol{G}_k \boldsymbol{x} = 0, \quad \text{if } k \in \bar{\Psi}, \tag{G.3}$$

where $\bar{\Psi}$ is given in (4.27). Note that (G.3) is equivalent to $\boldsymbol{G}_k \boldsymbol{x} = \boldsymbol{0}$, $\forall k \in \bar{\Psi}$, since $\boldsymbol{G}_k \succeq \boldsymbol{0}$. Moreover, since $\boldsymbol{A}_1^* \preceq \boldsymbol{0}$ and $\lambda^* > 0$ according to Lemma 4.5.4, it follows

from (F.4) that

$$\boldsymbol{x}^H \boldsymbol{H} \boldsymbol{x} = 0. \tag{G.4}$$

Note that (G.4) is equivalent to $\boldsymbol{H}\boldsymbol{x} = \boldsymbol{0}$ since $\boldsymbol{H} \succeq \boldsymbol{0}$. Thus, from (G.1)-(G.4), we have

$$\begin{aligned} \boldsymbol{x}^H \boldsymbol{B}_1^* \boldsymbol{x} &= \boldsymbol{x}^H \left(-\lambda^* \boldsymbol{H} + \sum_{k=1}^{K} \beta_k^* \gamma_e \boldsymbol{G}_k + \sum_{k=1}^{K} \alpha_k^* \zeta \boldsymbol{G}_k - \theta^* \boldsymbol{I} \right) \boldsymbol{x} \\ &= \boldsymbol{x}^H \left(\sum_{k \in \Psi} \alpha_k^* \zeta \boldsymbol{G}_k - \theta^* \boldsymbol{I} \right) \boldsymbol{x} = 0. \end{aligned} \tag{G.5}$$

To summarize, if there is no non-zero solution $\boldsymbol{x} \in \mathbb{C}^{M \times 1}$ to the equations given in (4.28), then (G.3), (G.4) and (G.5) cannot be satisfied at the same time, and it thus follows that the maximum eigenvalue of $\boldsymbol{D}_1^*$ cannot be zero, i.e., $\text{rank}(\boldsymbol{D}_1^*) = M$. Then according to Proposition 4.5.1, $\text{rank}(\boldsymbol{S}^*) = 1$ is always true for (P1.1-SDR-Eqv). Proposition 4.5.2 is thus proved.

References

[1] N. Shinohara, "Power without wires," *IEEE Microwave Mag.*, vol. 12, no. 7, pp. 564–573, Dec. 2011.

[2] R. Zhang and C. K. Ho, "MIMO broadcasting for simultaneous wireless information and power transfer," *IEEE Trans. Wireless Commun.*, vol. 12, no. 5, pp. 1989–2001, June 2013.

[3] S. Goel and R. Negi, "Guaranteeing secrecy using artificial noise," *IEEE Trans. Wireless Commun.*, vol. 7, no. 6, pp. 2180–2189, June 2008.

[4] A. Rubinov, H. Tuy, and H. Mays, "An algorithm for monotonic global optimization problems," *Optimization*, vol. 49, pp. 205–221, Sep. 2001.

[5] L. P. Qian, Y. J. Zhang, and J. Huang, "Mapel: achieving global optimality for a non-convex power control problem," *IEEE Trans. Wireless Commun.*, vol. 8, no. 3, pp. 1553–1563, Mar. 2009.

[6] W. Yu and R. Lui, "Dual methods for nonconvex spectrum optimization of multicarrier systems," *IEEE Trans. Commun.*, vol. 54, no. 7, pp. 1310–1322, July 2006.

[7] Z. Q. Luo, W. K. Ma, A. M. C. So, Y. Ye, and S. Zhang, "Semidefinite relaxation of quadratic optimization problems," *IEEE Signal Process. Mag.*, vol. 27, no. 3, pp. 20–34, May 2010.

[8] T. S. Han and K. Kobayashi, "Optimal power control for cognitive radio networks under coupled interference constraints: a cooperative game-theoretic perspective," *IEEE Trans. Inf. Theory*, vol. 21, no. 1, pp. 49–60, Jan. 1981.

[9] R. Etkin, D. Tse, and H. Wang, "Gaussian interference channel capacity to within one bit," *IEEE Trans. Inf. Theory*, vol. 54, no. 12, pp. 5534–5562, Dec. 2008.

[10] A. B. Carleial, "A case where interference does not reduce capacity," *IEEE Trans. Inf. Theory*, vol. 21, no. 5, pp. 569–570, Sep. 1975.

[11] H. Sato, "The capacity of the Gaussian interference channel under strong interference," *IEEE Trans. Inf. Theory*, vol. 27, no. 6, pp. 786–788, Nov. 1981.

[12] A. S. Motahari and A. K. Khandani, "Capacity bounds for the Gaussian interference channel," *IEEE Trans. Inf. Theory*, vol. 55, no. 2, pp. 620–643, Feb. 2009.

[13] X. Shang, G. Kramer, and B. Chen, "A new outer bound and the noisy-interference sum–rate capacity for Gaussian interference channels," *IEEE Trans. Inf. Theory*, vol. 55, no. 2, pp. 689–699, Feb. 2009.

[14] V. S. Annapureddy and V. V. Veeravalli, "Gaussian interference networks: sum capacity in the low-interference regime and new outer bounds on the capacity region," *Information Theory, IEEE Transactions on*, vol. 55, no. 7, pp. 3032–3050, July 2009.

[15] V. R. Cadambe and S. A. Jafar, "Interference alignment and degrees of freedom of the K-user interference channel," *IEEE Trans. Inf. Theory*, vol. 54, no. 8, pp. 3425–3441, Aug. 2008.

[16] C. M. Yetis, T. Gou, S. A. Jafar, and A. H. Kayran, "On feasibility of interference alignment in MIMO interference networks," *IEEE Trans. Signal Process.*, vol. 58, no. 9, pp. 4771–4782, Sep. 2010.

[17] M. Razaviyayn, G. Lyubeznik, and Z. Q. Luo, "On the degrees of freedom achievable through interference alignment in a MIMO interference channel," *IEEE Trans. Signal Process.*, vol. 60, no. 2, pp. 812–821, Feb. 2012.

[18] M. A. Maddah-Ali and D. Tse, "Completely stale transmitter channel state information is still very useful," *IEEE Trans. Info. Theory*, vol. 58, no. 7, pp. 4418–4431, July 2012.

[19] H. Maleki, S. A. Jafar, and S. Shamai, "Retrospective interference alignment," in *Proc. IEEE Int. Symp. Inf. Theory (ISIT)*, July 2011.

[20] ——, "Retrospective interference alignment over interference networks," *IEEE J. Sel. Topics Signal Process.*, vol. 6, no. 3, pp. 228–240, June 2012.

[21] S. A. Jafar, "Exploiting channel correlations-simple interference alignment schemes with no CSIT," in *Proc. Global Commun. Conf. (Globecom)*, Dec. 2010.

[22] ——, "Blind interference alignment," *IEEE J. Sel. Topics Signal Process.*, vol. 6, no. 3, pp. 216–227, June 2012.

[23] V. R. Cadambe, S. A. Jafar, and C. Wang, "Interference alignment with asymmetric complex signalingsettling the Høst-Madsen–Nosratinia conjecture," *IEEE Trans. Inf. Theory*, vol. 56, no. 9, pp. 4552–4565, Sep. 2010.

[24] Y. Zeng, C. Yetis, E. Gunawan, Y. Guan, and R. Zhang, "Transmit optimization with improper Gaussian signaling for interference channels," *IEEE Trans. Signal Process.*, vol. 61, no. 11, pp. 2899–2913, June 2013.

[25] Z. K. M. Ho and E. Jorswieck, "Improper Gaussian signaling on the two-user SISO interference channel," *IEEE Trans. Wireless Commun.*, vol. 11, no. 9, pp. 3194–3203, Sep. 2012.

[26] V. R. Cadambe and S. A. Jafar, "Parallel Gaussian interference channels are not always separable," *IEEE Trans. Inf. Theory*, vol. 55, no. 9, pp. 3983–3990, Sep. 2009.

[27] A. Gjendemsjoe, D. Gesbert, G. Oien, and S. Kiani, "Binary power control for sum rate maximization over multiple interfering links," *IEEE Trans. Wireless Commun.*, vol. 7, no. 8, pp. 3164–3173, Aug. 2008.

[28] J. Huang, R. A. Berry, and M. L. Honig, "Distributed interference compensation for wireless networks," *IEEE J. Select. Areas Commun.*, vol. 24, no. 7, pp. 1074–1084, May 2006.

[29] M. Chiang, C. W. Tan, D. Palomar, D. O'Neill, and D. Julian, "Power control by geometric programming," *IEEE Trans. Wireless Commun.*, vol. 1, no. 7, pp. 2640–2651, July 2007.

[30] W. Yu, G. Ginis, and J. M. Cioffi, "Distributed multiuser power control for digital subscriber lines," *IEEE J. Sel. Area Commun.*, vol. 20, no. 5, pp. 1105–1115, 2002.

[31] J. Papandriopoulos and J. S. Evans, "SCALE: a low-complexity distributed protocol for spectrum balancing in multiuser DSL networks," *IEEE Trans. Inf. Theory*, vol. 55, no. 8, pp. 3711–3724, Aug. 2009.

[32] S. Hayashi and Z. Q. Luo, "Spectrum management for interference-limited multiuser communication systems," *IEEE Trans. Inf. Theory*, vol. 55, no. 3, pp. 1153–1175, Mar. 2009.

[33] Z. Q. Luo and Z. Zhang, "Dynamic spectrum management: complexity and duality," *IEEE J. Sel. Topics Signal Process.*, vol. 2, no. 1, pp. 57–73, Feb. 2008.

[34] R. Zhang and S. Cui, "Cooperative interference management with MISO beamforming," *IEEE Trans. Signal Process.*, vol. 58, no. 10, pp. 5450–5458, Oct. 2010.

[35] X. Shang, B. Chen, and H. V. Poor, "Multiuser MISO interference channels with single-user detection: optimality of beamforming and the achievable rate region," *IEEE Trans. Inf. Theory*, vol. 57, no. 7, pp. 4255–4273, July 2011.

[36] E. Jorswieck and E. G. Larsson, "The MISO interference channel from a game-theoretic perspective: a combination of selfishness and altruism achieves pareto optimality," in *Proc. Int. Conf. Acoustics, Speech, Signal Process. (ICASSP)*, Mar. 2008.

[37] S. Ye and R. S. Blum, "Optimized signaling for MIMO interference systems with feedback," *IEEE Trans. Signal Process.*, vol. 51, no. 11, pp. 2839–2848, Sep. 2003.

[38] S. S. Christensen, R. Agarwal, E. Carvalho, and J. Cioffi, "Weighted sum-rate maximization using weighted MMSE for MIMO-BC beamforming design," *IEEE Trans. Wireless Commun.*, vol. 7, no. 12, pp. 4792–4799, Dec. 2008.

[39] M. Razaviyayn, M. Sanjabi, and Z.-Q. Luo, "Linear transceiver design for interference alignment: complexity and computation," *IEEE Trans. Inf. Theory*, vol. 58, no. 5, pp. 2896–2910, May 2012.

[40] S. J. Kim and G. B. Giannakis, "Optimal resource allocation for mimo ad hoc cognitive radio networks," *IEEE Trans. Inf. Theory*, vol. 57, no. 5, pp. 3117–3131, May 2011.

[41] C. Shi, D. A. Schmidt, R. A. Berry, M. L. Honig, and W. Utschick, "Distributed interference pricing for the MIMO interference channel," in *Proc. IEEE Int. Conf. on Commun. (ICC)*, 2009.

[42] S. Shi, M. Schubert, and H. Boche, "Rate optimization for multiuser mimo systems with linear processing," *IEEE Trans. Signal Process.*, vol. 56, no. 8, pp. 4020–4030, Aug. 2008.

[43] F. Rashid-Farrokhi, K. R. Liu, and L. Tassiulas, "Transmit beamforming and power control for cellular wireless systems," *IEEE J. Select. Areas Commun.*, vol. 16, no. 8, pp. 1437–1450, Oct. 1998.

[44] S. Vishwanath, N. Jindal, and A. Goldsmith, "Duality, achievable rates, and sum-rate capacity of gaussian mimo broadcast channels," *IEEE Trans. Inf. Theory*, vol. 49, no. 10, pp. 2658–2668, Oct. 2003.

[45] W. Yu, "Uplink-downlink duality via minimax duality," *IEEE Trans. Inf. Theory*, vol. 52, no. 2, pp. 361–374, Feb. 2006.

[46] L. Zhang, R. Zhang, Y.-C. Liang, Y. Xin, and H. V. Poor, "On gaussian mimo bc-mac duality with multiple transmit covariance constraints," *Information Theory, IEEE Transactions on*, vol. 58, no. 4, pp. 2064–2078, Apr. 2012.

[47] E. A. Jorswieck and E. G. Larsson, "Monotonic optimization framework for the two-user MISO interference channel," *IEEE Trans. Commun.*, vol. 58, no. 7, pp. 2159–2168, July 2010.

[48] Y. Xu, T. Le-Ngoc, and S. Panigrahi, "Global concave minimization for optimal spectrum balancing in multi-user DSL networks," *IEEE Trans. Signal Process.*, vol. 56, no. 7, pp. 2875–2885, July 2008.

[49] H. Al-Shatri and T. Weber, "Optimizing power allocation in interference channels using D.C. programming," in *Proc. Workshop on Resource Allocat. in Wireless Netw.*, Avignon, France, June 2010.

[50] P. C. Weeraddana, M. Codreanu, M. Latva-aho, and A. Ephremids, "Weighted sum-rate maximization for a set of interfering links via branch and bound," *IEEE Trans. Signal Process.*, vol. 59, no. 8, pp. 3977–3996, Aug. 2011.

[51] J. B. G. Frenk and S. Schaible, *Fractional programming.* Handbook of Generalized Convexity and Generalized Monotonicity, 2006.

[52] E. A. Jorswieck, E. G. Larsson, and D. Danev, "Complete characterization of the Pareto boundary for the MISO interference channel," *IEEE Trans. Signal Process.*, vol. 56, no. 10, pp. 5292–5296, Oct. 2008.

[53] R. Horst, P. Pardolos, and N. Thoai, *Introduction to global optimization.* Norwell, MA: Kluwer Academic, 2000.

[54] E. Bjornson, G. Zheng, M. Bengtsson, and B. Ottersten, "Robust monotonic optimization framework for multicell MISO systems," *IEEE Trans. Singal Process.*, vol. 60, no. 5, pp. 2508–2523, May 2012.

[55] M. A. Charafeddine, A. Sezgin, Z. Han, and A. Paulraj, "Achievable and crystallized rate regions of the interference channel with interference as noise," *IEEE Trans. Wireless Commun.*, vol. 11, no. 3, pp. 1100–1111, Mar. 2012.

[56] R. Mochaourab and E. A. Jorswieck, "Optimal beamforming in interference networks with perfect local channel information," *IEEE Trans. Singnal Process.*, vol. 59, no. 3, pp. 1128–1141, Mar. 2011.

[57] E. Bjornson, M. Bengtsson, and B. Ottersten, "Pareto characterization of the multicell MIMO performance region with simple receivers," *IEEE Trans. Singal Process.*, vol. 60, no. 8, pp. 4464–4469, Aug. 2012.

[58] P. Cao, E. Jorswieck, and S. Shi, "Pareto boundary of the rate region for single-stream MIMO interference channels: linear transceiver design," *IEEE Trans. Signal Process.*, vol. 61, no. 20, pp. 4907–4922, Oct. 2013.

[59] P. Juho and S. Youngchul, "On the Pareto-optimal beam structure and design for multi-user MIMO interference channels," *IEEE Trans. Signal Process.*, vol. 61, no. 23, pp. 5932–5946, Dec. 2013.

[60] M. Mohseni, R. Zhang, and J. M. Cioffi, "Optimized transmission of fading multiple-access and broadcast channels with multiple antennas," *IEEE J. Sel. Areas Commun.*, vol. 24, no. 9, pp. 1627–1639, Aug. 2006.

[61] R. Zhang, Y. C. Liang, C. C. Chai, and S. Cui, "Optimal beamforming for two-way multi-antenna relay channel with analogue network coding," *IEEE J. Sel. Areas Commun.*, vol. 27, no. 5, pp. 699–712, June 2009.

[62] S. Boyd and L. Vandenberghe, *Convex Optimization*. Cambridge, U.K., Cambidge Univ. Press, 2004.

[63] N. Bambos, S. C. Chen, and G. J. Pottie, "Radio link admission algorithm for wireless networks with power control and active link quality protection," in *Proc. IEEE INFOCOM*, Boston, MA, 1995.

[64] J. B. G. Frenk and S. Schaible, "Fractional programming," *Handbook of Generalized Linear Fractional Programming*, pp. 335–386, 2006.

[65] M. Schubert and H. Boche, "Solution of the multiuser downlink beamforming problem with individual SINR constraints," *IEEE Trans. Veh. Technol.*, vol. 53, no. 1, pp. 18–28, Jan. 2004.

[66] R. Horn and C. Johnson, *Matrix Analysis*. Cambridge University Press, 1985.

[67] M. Codreanu, A. Tolli, M. Juntti, and M. Latva-aho, "Joint design of Tx-Rx beamformers in MIMO downlink channels," *IEEE Trans. Signal Process.*, vol. 55, no. 9, pp. 4639–4655, Sep. 2007.

[68] L. Zhang, Y. C. Lian, and Y. Xin, "Joint beamforming and power control for multiple access channels in cognitive radio networks," *IEEE J. Sel. Areas Commun.*, vol. 26, no. 1, pp. 38–51, Jan. 2008.

[69] M. Grant and S. Boyd, "Cvx: Matlab software for disciplined convex programming," 2011. [Online]. Available: available at http://cvxr.com/cvx/

[70] S. Sudevalayam and P. Kulkarni, "Energy harvesting sensor nodes: survey and implications," *IEEE Commun. Surveys Tuts.*, vol. 13, no. 3, pp. 443–461, 2011.

[71] T. Le, K. Mayaram, and T. Fiez, "Efficient far-field radio frequency energy harvesting for passively powered sensor networks," *IEEE J. Solid-State Circuits*, vol. 43, no. 5, pp. 1287–1302, May 2008.

[72] A. M. Zungeru, L.-M. Ang, S. Prabaharan, and K. P. Seng, "Radio frequency energy harvesting and management for wireless sensor networks," *Energy Scavenging and Optimization Techniques for Mobile Devices. V. Hrishikesh, and G-M. Mountean (Eds.) USA*, pp. 341–367, 2012.

[73] R. Vullers, R. van Schaijk, I. Doms, C. Van Hoof, and R. Mertens, "Micropower energy harvesting," *Elsevier Solid-State Electronics*, vol. 53, no. 7, pp. 684–693, July 2009.

[74] D. Bouchouicha, F. Dupont, M. Latrach, and L. Ventura, "Ambient RF energy harvesting," in *IEEE Int. Conf. Renewable Energies Power Quality (ICREPQ10)*, 2010, pp. 486–495.

[75] T. Paing, J. Shin, R. Zane, and Z. Popovic, "Resistor emulation approach to low-power RF energy harvesting," *IEEE Trans. Power Electron.*, vol. 23, no. 3, pp. 1494–1501, May 2008.

[76] H. Jabbar, Y. S. Song, and T. T. Jeong, "RF energy harvesting system and circuits for charging of mobile devices," *IEEE Trans. Compter Electron.*, vol. 56, no. 1, pp. 247–253, Feb. 2010.

[77] C. K. Ho and R. Zhang, "Optimal energy allocation for wireless communications with energy harvesting constraints," *IEEE Trans. Signal Process.*, vol. 60, no. 9, pp. 4808–4818, Sep. 2012.

[78] V. Sharma, U. Mukherji, V. Joseph, and S. Gupta., "Optimal energy management policies for energy harvesting sensor nodes," *IEEE Trans. Wireless Commun.*, vol. 9, no. 4, pp. 1326–1336, Apr. 2010.

[79] O. Ozel, K. Tutuncuoglu, J. Yang, S. Ulukus, and A. Yener, "Transmission with energy harvesting nodes in fading wireless channels: optimal policies," *IEEE J. Sel. Area Commun.*, vol. 29, no. 8, pp. 1732–1743, Sep. 2011.

[80] H. Ju and R. Zhang, "Throughput maximization in wireless powered communication networks," *IEEE Trans. Wireless Commun.*, vol. 13, no. 1, pp. 418–428, Jan. 2014.

[81] L. Liu, R. Zhang, and K. C. Chua, "Multi-antenna wireless powered communication with energy beamforming," submitted to *IEEE Trans. Commun.* (Available online at arXiv: 1312.1450).

[82] G. Yang, C. K. Ho, R. Zhang, and Y. L. Guang, "Throughput optimization for massive mimo systems powered by wireless energy transfer," submitted to *IEEE J. Select. Areas Commun.* (Available online at arXiv:1403.3991).

[83] L. R. Varshney, "Transporting information and energy simultaneously," in *Proc. IEEE Int. Symp. Inf. Theory (ISIT)*, July 2008.

[84] P. Grover and A. Sahai, "Shannon meets Tesla: wireless information and power transfer," in *Proc. IEEE Int. Symp. Inf. Theory (ISIT)*, June 2010.

[85] X. Zhou, R. Zhang, and C. Ho, "Wireless information and power transfer: architecture design and rate-energy tradeoff," *IEEE Trans. Commun.*, vol. 61, no. 11, pp. 4754–4767, Nov. 2013.

[86] Y. Wu, Y. Liu, Q. Xue, S. Li, and C. Yu, "Analytical design method of multiway dual-band planar power dividers with arbitrary power division," *IEEE Trans. Microwave Theory and Techniques*, vol. 58, no. 12, pp. 3832–3841, Dec. 2010.

[87] E. Biglieri, J. Proakis, and S. S. (Shitz), "Fading channels: information-theoretic and communications aspects," *IEEE Trans. Inf. Theory*, vol. 44, no. 6, pp. 2619–2692, Oct. 1998.

[88] R. J. McEliece and W. E. Stark, "Channels with block interference," *IEEE Trans. Inf. Theory*, vol. 30, no. 1, pp. 44–53, Jan. 1984.

[89] A. Goldsmith and P. P. Varaiya, "Capacity of fading channels with channel side information," *IEEE Trans. Inf. Theory*, vol. 43, no. 6, pp. 1986–1992, Nov. 1997.

[90] L. H. Ozarow, S. Shamai, and A. D. Wyner, "Information theoretic considerations for cellular mobile radio," *IEEE Trans. Veh. Technol.*, vol. 43, no. 2, pp. 359–378, May 1994.

[91] G. Caire, G. Taricco, and E. Biglieri, "Optimal power control over fading channels," *IEEE Trans. Inf. Theory*, vol. 45, no. 5, pp. 1468–1489, July 1999.

[92] G. Caire and S. S. (Shitz), "On the capacity of some channels with channel state information," *IEEE Trans. Inf. Theory*, vol. 5, no. 6, pp. 2007–2019, Sep. 1999.

[93] R. T. Rockafellar, *Convex Analysis*. Princeton Univ. Press, 1970.

[94] L. Liu, R. Zhang, and K. C. Chua, "Wireless information and power transfer: a dynamic power splitting approach," *IEEE Trans. Commun.*, vol. 61, no. 9, pp. 3990–4001, Set. 2013.

[95] Z. Xiang and M. Tao, "Robust beamforming for wireless information and power transmission," *IEEE Wireless Commun. Letters*, vol. 1, no. 4, pp. 372–375, Aug. 2012.

[96] H. Ju and R. Zhang, "A novel mode switching scheme utilizing random beamforming for opportunistic energy harvesting," *IEEE Trans. Wireless Commun.*, vol. 13, no. 4, pp. 2150–2162, Apr. 2014.

[97] Q. Shi, L. Liu, W. Xu, , and R. Zhang, "Joint transmit beamforming and receive power splitting for MISO SWIPT systems," to appear in *IEEE Trans. Wireless Commun.* (Available online at arXiv:1304.0062).

[98] S. Timotheou, I. Krikidis, and B. Ottersten, "MISO interference channel with QoS and RF energy harvesting constraints," in *Proc. IEEE Int. Conf. on Commun. (ICC)*, 2013.

[99] C. Shen, W. C. Li, and T. H. Chang, "Simultaneous information and energy transfer: a two-user MISO interference channel case," in *Proc. IEEE Global Commun. Conf. (GLOBECOM)*, Dec. 2012.

[100] J. Park and B. Clerckx, "Joint wireless information and energy transfer in a two-user MIMO interference channel," *IEEE Trans. on Wireless Commun*, vol. 12, no. 8, pp. 4210–4221, Aug. 2013.

[101] B. K. Chalise, Y. D. Zhang, and M. G. Amin, "Energy harvesting in an OSTBC based amplify-and-forward MIMO relay system," in *Proc. IEEE International Conference on Acoustics, Speech, and Signal Processing (ICASSP)*, 2012, pp. 3201–3204.

[102] I. Krikidis, S. Timotheou, and S. Sasaki, "RF energy transfer for cooperative networks: data relaying or energy harvesting?" *IEEE Commun. Letters*, vol. 16, no. 1, pp. 1772–1775, Nov. 2012.

[103] B. K. Chalise, W.-K. Ma, Y. D. Zhang, H. A. Suraweera, and M. G. Amin, "Optimum performance boundaries of OSTBC based AF-MIMO relay system with energy harvesting receiver," *IEEE Trans. Signal Process.*, vol. 61, no. 17, pp. 4199–4213, Sep. 2013.

[104] Z. Ding, S. M. Perlaza, I. Esnaola, and H. V. Poor, "Power allocation strategies in energy harvesting wireless cooperative networks," *IEEE Trans. on Wireless Commun*, vol. 13, no. 2, pp. 846–860, Feb. 2014.

[105] A. A. Nasir, X. Zhou, S. Durrani, and R. A. Kennedy, "Wireless energy harvesting and information relaying: adaptive time-switching protocols and throughput analysis," submitted to *IEEE Trans. on Wireless Commun.* (Available online at arXiv:1310.7648).

[106] I. Krikidis, "Simultaneous information and energy transfer in large-scale networks with/without relaying," submitted to *IEEE Trans. Commun.* (Available online at arXiv:1310.6511).

[107] X. Zhou, R. Zhang, and C. K. Ho, "Wireless information and power transfer in multiuser OFDM systems," *IEEE Trans. Wireless Commun.*, vol. 13, no. 4, pp. 2282–2294, Apr. 2014.

[108] D. W. K. Ng, E. S. Lo, and R. Schober, "Wireless information and power transfer: energy efficiency optimization in OFDMA systems," *IEEE Trans. Wireless Commun.*, vol. 12, no. 12, pp. 6352–6370, Dec. 2013.

[109] P. Popovski, A. Fouladgar, and O. Simeone, "Interactive joint transfer of energy and information," *IEEE Trans. Commun.*, vol. 61, no. 5, pp. 2086–2097, May 2013.

[110] A. M. Fouladgar, O. Simeone, and E. Erkip, "Constrained codes for joint energy and information transfer," to appear in *IEEE Trans. Commun.* (Available online at arXiv:1311.1187).

[111] I. E. Telatar, "Capacity of multi-antenna gaussian channels," *Europ. Trans. Telecommun*, vol. 10, pp. 585–396, Nov.-Dec. 1999.

[112] J. Xu, L. Liu, and R. Zhang, "Multiuser MISO beamforming for simultaneous wireless information and power transfer," in *Proc. IEEE International Conference on Acoustics, Speech, and Signal Processing (ICASSP)*, 2013.

[113] X. Chen, C. Yuen, and Z. Zhang, "Wireless energy and information transfer tradeoff for limited feedback multi-antenna systems with energy beamforming," *IEEE Trans. on Veh. Technol.*, vol. 63, no. 1, pp. 407–412, Jan. 2014.

[114] A. D. Wyner, "The wire-tap channel," *The Bell System Technical J.*, vol. 54, pp. 1355–1387, Oct. 1975.

[115] I. Csiszár and J. Korner, "Broadcast channels with confidential messages," *IEEE Trans. Inf. Theory*, vol. 24, no. 3, pp. 339–348, May 1978.

[116] S. Leung-Yan-Cheong and M. Hellman, "The Gaussian wire-tap channel," *IEEE Trans. Inf. Theory*, vol. 24, no. 4, pp. 451–456, July 1978.

[117] A. Khisti and G. W. Wornell, "Secure transmission with multiple antennas I: the MISOME wiretap channel," *IEEE Trans. Inf. Theory*, vol. 56, no. 7, pp. 3088–3104, July 2010.

[118] ——, "Secure transmission with multiple antennaspart II: the MIMOME wiretap channel," *IEEE Trans. Inf. Theory*, vol. 56, no. 11, pp. 5515–5532, Nov. 2010.

[119] F. Oggier and B. Hassibi, "The secrecy capacity of the MIMO wiretap channel," *IEEE Trans. Inf. Theory*, vol. 57, no. 8, pp. 4961–4972, Aug. 2011.

[120] T. Liu and S. Shamai, "A note on the secrecy capacity of the multiple-antenna wiretap channel," *IEEE Trans. Inf. Theory*, vol. 55, no. 6, pp. 2547–2553, June 2009.

[121] R. Liu, T. Liu, H. V. Poor, and S. Shamai, "Multiple-input multiple-output Gaussian broadcast channels with confidential messages," *IEEE Trans. Inf. Theory*, vol. 56, no. 9, pp. 4215–4227, Sep. 2010.

[122] Y. Liang, H. V. Poor, and S. Shamai, "Secure communication over fading channels," *IEEE Trans. Inf. Theory*, vol. 54, no. 6, pp. 2470–2492, June 2008.

[123] P. K. Gopala, L. Lai, and H. El Gamal, "On the secrecy capacity of fading channels," *IEEE Trans. Inf. Theory*, vol. 54, no. 10, pp. 4687–4698, Oct. 2008.

[124] Y. Liang, H. V. Poor *et al.*, "Information theoretic security," *Foundations and Trends in Communications and Information Theory*, vol. 5, no. 4, pp. 355–580, 2009.

[125] S. Shafiee and S. Ulukus, "Achievable rates in Gaussian MISO channels with secrecy constraints," in *Proc. IEEE Int. Symp. Inf. Theory (ISIT)*, June 2007.

[126] Q. Li, M. Hong, H.-T. Wai, Y.-F. Liu, W.-K. Ma, and Z. Q. Luo, "Transmit solutions for MIMO wiretap channels using alternating optimization," *IEEE J. Select. Areas Commun.*, vol. 31, no. 9, pp. 1714–1727, Sep. 2013.

[127] L. Zhang, R. Zhang, Y. C. Liang, Y. Xin, and S. Cui, "On the relationship between the multi-antenna secrescy communications and cognitive radio communications," *IEEE Trans. Commun.*, vol. 58, no. 6, pp. 1877–1886, June 2010.

[128] R. Zhang and Y.-C. Liang, "Exploiting multi-antennas for opportunistic spectrum sharing in cognitive radio networks," *IEEE J. Select. Topics in Signal Process.*, vol. 2, no. 1, pp. 88–102, Feb. 2008.

[129] Q. Li and W.-K. Ma, "Optimal and robust transmit designs for MISO channel secrecy by semidefinite programming," *IEEE Trans. Signal Process.*, vol. 59, no. 8, pp. 3799–3812, Aug. 2011.

[130] G. Geraci, R. Couillet, J. Yuan, M. Debbah, and I. B. Collings, "Large system analysis of linear precoding in MISO broadcast channels with confidential messages," *IEEE J. Select. Areas Commun.*, vol. 31, no. 9, pp. 1660–1671, Sep. 2013.

[131] S. A. A. Fakoorian and A. L. Swindlehurst, "On the optimality of linear precoding for secrecy in the MIMO broadcast channel," *IEEE J. Select. Areas Commun.*, vol. 31, no. 9, pp. 1701–1713, Sep. 2013.

[132] C.-Y. Wu, P.-C. Lan, P.-C. Yeh, C.-H. Lee, and C.-M. Cheng, "Practical physical layer security schemes for MIMO-OFDM systems using precoding matrix indices," *IEEE J. Select. Areas Commun.*, vol. 31, no. 9, pp. 1687–1700, Sep. 2013.

[133] L. Zhang, L. Y. C, Y. Pei, and R. Zhang, "Robust beamforming design: from cognitive radio MISO channels to secrecy MISO channels," in *Proc. IEEE Global Commun. Conf. (GLOBECOM)*, Dec. 2009.

[134] J. Li and A. P. Petropulu, "On ergodic secrecy rate for Gaussian MISO wiretap channels," *IEEE Trans. Wireless Commun.*, vol. 10, no. 4, pp. 1176–1187, Apr. 2011.

[135] Z. Li, R. Yates, and W. Trappe, "Achieving secret communication for fast rayleigh fading channels," *IEEE Trans. Wireless Commun.*, vol. 9, no. 9, pp. 2792–2799, Sep. 2010.

[136] L. Dong, Z. Han, A. P. Petropulu, and H. V. Poor, "Improving wireless physical layer security via cooperating relays," *IEEE Trans. Signal Process.*, vol. 58, no. 3, pp. 1875–1888, Mar. 2010.

[137] A. Mukherjee and A. L. Swindlehurst, "Fixed-rate power allocation strategies for enhanced secrecy in MIMO wiretap channels," in *Proc. Signal Process. Advances in Wireless Commun. (SPAWC)*, June 2009, pp. 344–348.

[138] A. Wolf and E. A. Jorswieck, "Maximization of worst-case secrecy rates in mimo wiretap channels," in *44th Asilomar Conf. Signals, Syst. Comput.*, Nov. 2010.

[139] A. Khisti, G. Wornell, A. Wiesel, and Y. Eldar, "On the Gaussian MIMO wiretap channel," in *Proc. IEEE Int. Symp. Inf. Theory (ISIT)*, June 2007.

[140] J. Huang and A. L. Swindlehurst, "Robust secure transmission in MISO channels based on worst-case optimization," *IEEE Trans. Signal Process.*, vol. 7, no. 6, pp. 2180–2189, June 2008.

[141] A. Mukherjee and A. L. Swindlehurst, "Robust beamforming for security in MIMO wiretap channels with imperfect CSI," *IEEE Trans. Signal Process.*, vol. 59, no. 1, pp. 351–361, Jan. 2011.

[142] S. Gerbracht, A. Wolf, and E. A. Jorswieck, "Beamforming for fading wiretap channels with partial channel information," in *Proc. Int. ITG Workshop on Smart Antennas (WSA)*, Feb. 2010.

[143] X. Zhou and M. R. McKay, "Secure transmission with artificial noise over fading channels: achievable rate and optimal power allocation," *IEEE Trans. Veh. Technol.*, vol. 59, no. 8, pp. 3831–3842, Oct. 2010.

[144] Q. Li and W. K. Ma, "Spatially selective artificial-noise aided transmit optimization for MISO multi-eves secrecy rate maximization," *IEEE Trans. Signal Process.*, vol. 61, no. 10, pp. 2704–2717, May 2013.

[145] W. C. Liao, T. H. Chang, W. K. Ma, and C. Y. Chi, "QoS-based transmit beamforming in the presence of eavesdroppers: an artificial-noise-aided approach," *IEEE Trans. Signal Process.*, vol. 59, no. 3, pp. 1202–1216, Mar. 2011.

[146] P.-H. Lin, S.-H. Lai, S.-C. Lin, and H.-J. Su, "On secrecy rate of the generalized artificial-noise assisted secure beamforming for wiretap channels," *IEEE J. Select. Areas Commun.*, vol. 31, no. 9, pp. 1728–1740, Sep. 2013.

[147] Y. Liang, G. Kramer, H. V. Poor, and S. S. (Shitz), "Compound wire-tap channels," in *Proc. 45th Ann. Allerton Conf. Commun., Contr., Comput.*, Sep. 2007.

[148] A. Charnes and W. W. Cooper, "Programming with linear fractional functions," *Naval Res. Logist. Quarter.*, vol. 9, pp. 181–186, Dec. 1962.

[149] T. H. Chang, C. W. Hsin, W. K. Ma, and C. Y. Chi, "A linear fractional semidefinite relaxation approach to maximum likelihood detection of higher-order QAM OSTBC in unknown channels," *IEEE Trans. Singal Process.*, vol. 58, no. 4, pp. 2315–2326, Apr. 2010.

[150] Y. Huang and D. P. Palomar, "Rank-constrained separable semidefinite program with applications to optimal beamforming," *IEEE Trans. Singal Process.*, vol. 58, no. 2, pp. 664–678, Feb. 2010.

[151] A. Beck and Y. C. Eldar, "Strong duality in nonconvex quadratic optimization with two quadratic constraints," *SIAM J. Optim.*, vol. 17, no. 3, pp. 884–860, Oct. 2006.

[152] W. Ai, Y. Huang, and S. Zhang, "New results on Hermitian matrix rank-one decomposition," *Math. Program: Ser. A*, vol. 128, no. 1-2, pp. 253–283, June 2011.

[153] E. Karipidis, N. D. Sidiropoulos, and Z. Q. Luo, "Far-field multicast beamforming for uniform linear antenna arrays," *IEEE Trans. Signal Process.*, vol. 55, no. 10, pp. 4916–49 927, Oct. 2007.

[154] W. Yang and G. Xu, "Optimal downlink power assignment for smart antenna systems," in *Proc. Int. Conf. Acoustics, Speech, Signal Process. (ICASSP)*, Seattle, Washington, May 1998.

List of Publications

Journal Publications

1. L. Liu, R. Zhang, and K. C. Chua, "Achieving global optimality for weighted sum-rate maximization in the K-user Gaussian interference channel with multiple antennas," *IEEE Transactions on Wireless Communications*, vol. 11, no. 5, pp. 1933-1945, May 2012.

2. L. Liu, R. Zhang, and K. C. Chua, "Wireless information transfer with opportunistic energy harvesting," *IEEE Transactions on Wireless Communications*, vol. 12, no. 1, pp. 288-300, January, 2013.

3. L. Liu, R. Zhang, and K. C. Chua, "Wireless information and power transfer: a dynamic power splitting approach," *IEEE Transactions on Communications*, vol. 61, no. 9, pp. 3990-4001, September, 2013.

4. L. Liu, R. Zhang, and K. C. Chua, "Secrecy wireless information and power transfer with MISO beamforming," *IEEE Transactions on Signal Processing*, vol. 62, no. 7, pp. 1850-1863, April, 2014.

5. L. Liu, R. Zhang, and K. C. Chua, "Multi-antenna wireless powered communication with energy beamforming," to appear in *IEEE Transactions on Communications*.

Conference Publications

1. L. Liu, R. Zhang, and K. C. Chua, "A new approach to weighted sum-rate maximization for the K-user Gaussian interference channel," in *Proc. International Conference on Wireless Communications and Signal Processing (WCSP)*, Nanjing, China, 2011. (**Best Student Paper Award**)

2. L. Liu, R. Zhang, and K. C. Chua, "Wireless information transfer with opportunistic energy harvesting," in *Proc. IEEE International Symposium on Information Theory (ISIT)*, Cambridge, MA, USA, 2012.

3. L. Liu, R. Zhang, and K. C. Chua, "Secrecy wireless information and power transfer with MISO beamforming," in *Proc. IEEE Global Communications Conference (Globecom)*, Atlanta, GA, USA, 2013.

4. J. Xu, L. Liu, and R. Zhang, "Multiuser MISO beamforming for simultaneous wireless information and power transfer," in *Proc. IEEE International Conference on Acoustics, Speech, and Signal Processing (ICASSP)*, Vancouver, BC, Canada, 2013.

5. H. Xing, L. Liu, and R. Zhang, "Secrecy wireless information and power transfer in fading wiretap channel," in *IEEE International Conference on Communications (ICC)*, Sydney, 2014.